AD_____

Award Number: DAMD17-03-1-0014

TITLE: FGF Signaling and Dietary Factors in the Prostate

PRINCIPAL INVESTIGATOR: Fen Wang, Ph.D.

CONTRACTING ORGANIZATION: Texas A&M University System
Health Science Center
Houston, TX 77030

REPORT DATE: September 2006

TYPE OF REPORT: Final

PREPARED FOR: U.S. Army Medical Research and Materiel Command
Fort Detrick, Maryland 21702-5012

REPORT DOCUMENTATION PAGE

Form Approved
OMB No. 0704-0188

1. REPORT DATE *(DD-MM-YYYY)*	**2. REPORT TYPE**	**3. DATES COVERED** *(From - To)*
01/09/2006	Final	1 Mar 2003 – 31 Aug 2006

4. TITLE AND SUBTITLE

FGF Signaling and Dietary Factors in the Prostate

5a. CONTRACT NUMBER

5b. GRANT NUMBER
DAMD17-03-1-0014

5c. PROGRAM ELEMENT NUMBER

6. AUTHOR(S)

Fen Wang, Ph.D.

E-Mail: fwang@ibt.tmc.edu

5d. PROJECT NUMBER

5e. TASK NUMBER

5f. WORK UNIT NUMBER

7. PERFORMING ORGANIZATION NAME(S) AND ADDRESS(ES)

Texas A&M University System Health Science Center
Houston, TX 77030

8. PERFORMING ORGANIZATION REPORT NUMBER

9. SPONSORING / MONITORING AGENCY NAME(S) AND ADDRESS(ES)
U.S. Army Medical Research and Materiel Command
Fort Detrick, Maryland 21702-5012

10. SPONSOR/MONITOR'S ACRONYM(S)

11. SPONSOR/MONITOR'S REPORT NUMBER(S)

12. DISTRIBUTION / AVAILABILITY STATEMENT
Approved for Public Release; Distribution Unlimited

13. SUPPLEMENTARY NOTES

14. ABSTRACT Purpose: To study the FGF signaling axis in prostate homeostasis and tumorigenesis, to evaluate dietary factors in modulating FGF signals in the prostate. Scope: To develop mouse models resembling human prostate tumor progressions for screening therapeutic strategies for prostate cancers and evaluating dietary factors in prostate cancer prevention. Major Finding: Ectopic expression of the constitutively-active FGFR1 (caFGFR1) in the prostate induces high-grade prostatic intraepithelial neoplasia (PIN) in transgenic mice in an expression level-dependent manner. Repression of the resident FGFR2 in the prostate also disturbs homeostasis in the prostate as well as potentiates the PIN lesions induced by the ectopic caFGFR1. Up-to-date Progress: Establishing mouse colonies with prostate-specific Fgfr2 disruption and caFGFR1 expression for further characterizations of the FGF signaling and dietary factors in prostate lesions. Generation of a conditional expression vector for expressing FGFR1 in the prostate. Characterization of the prostate of FGFR2 conditional null mice. Generation of 4 transgenic lines for conditional expression of caFGFR1 in the prostate. Significance: Together with previous data from the Dunning prostate tumor model, the findings demonstrate that aberrant FGF signals in the prostate strongly disrupt tissue homeostasis and promote prostate tumor development and progression. The model provides a useful tool for evaluating other tumor initiating factors, including those that cause genetic instability and other oncogenic lesions in prostate tumorigenesis.

15. SUBJECT TERMS
growth factors, tyrosine kinase, mouse model, transgenic mouse, nutrition, tumor prevention issue specific gene inactivation

16. SECURITY CLASSIFICATION OF:			**17. LIMITATION OF ABSTRACT**	**18. NUMBER OF PAGES**	**19a. NAME OF RESPONSIBLE PERSON**
a. REPORT	**b. ABSTRACT**	**c. THIS PAGE**			USAMRMC
U	U	U	UU	131	**19b. TELEPHONE NUMBER** *(include area code)*

TABLE OF CONTENTS

INTRODUCTION

The prostate consists of epithelium and stromal compartments separated by a basement membrane. The communications and mutual regulations between the two compartments are critical for growth, develop, and function of the prostate. The fibroblast growth factor (FGF) signaling complex has long been implicated in mediating these regulatory communications, which consists of 22 single polypeptide ligands, 4 transmembrane tyrosine kinase receptors (FGFR), and a pool of highly heterogenic heparan sulfate proteoglycans (HSPG) in the extracellular matrix. Appearances of the FGF signaling complexes are highly temporally and spatially specific; aberrant expression is often correlated with prostate cancer progression in human and experimental animal models. We previously demonstrated that ectopic expression of a constitutively active FGFR1 mutant (caFGFR1) in the prostate epithelium induces age- and expression level-dependent prostatic intraepithelial neoplasia (PIN). Furthermore, depression of FGFR2 signaling in the prostate also disturbs homeostasis in the prostate and induces prostate hyperplasia. The project is to study whether FGFR1 and FGFR2 elicit receptor-specific activity in the prostate, to determine whether ectopic expression of FGFR1 and depression of FGFR2 synergistically induce prostatic lesion, and to evaluate dietary factors in modulating FGF signals in the prostate. The long-term goal is to develop mouse models resembling human prostate tumor progressions for screening therapeutic strategies for prostate cancers and evaluating dietary factors in prostate cancer prevention.

BODY

Task 1. Characterization of the prostate of caFGFR1/KDNR bigenic mice.

a. Generation of enough male caFGFR1/KDNR bigenic mice for the study by crossing caFGFR1 and KDNR transgenic mice.

b. Collecting prostate tissue of bigenic and control mice at different ages, performing serial section of the prostate and characterization of prostate tissue structures.

Progress:

To date, the prostates of the ARR2PBi-caFGFR1/KDNR bigenic mice and the parental transgenic strains have been phenotypically characterized, and the main results are published in Cancer Research (1). The outlines of the main findings are as follows; please refer to the attachments for the details.

i. ARR2PBi-caFGFR1 mice developed high-grade PIN within 8 months.

In general, exposure to the ectopic FGFR1 kinase induces PIN in the caFGFR1 transgenic mice; the development and severity of the PIN lesion is expression level- and time-dependent.

The phenotype includes increase in prostate tissue mass, increase in mitosis in the prostate, and disorganized and atypical luminal epithelial cells in prostate lumens. Furthermore, the expression of cytokeratins is significantly reduced in epithelial foci with high-grade PIN lesions, especially those with cribriform structures. The high-grade PIN foci, particularly those with cribriform structures, often have a disrupted stromal layer indicated by discontinuous and faint staining of smooth muscle cell characteristic α-actin. Frequently, the over proliferating epithelial cells disrupt the basement membrane, invade the stromal compartment, and form small epithelial foci in the space between the basement membrane and stromal cells. This indicates that the epithelial cells in these foci are not just pushed through the stromal layer and form glandule-like structures. Instead, these epithelial cells form microinvasion foci in the stromal compartment, which are more advanced lesions than high-grade PIN.

ii. Cooperation between ectopic expression of FGFR1 and depression of FGFR2 signaling in perturbation of prostate homeostasis.

Depression of the endogenous FGFR2 signaling alone by expression of a kinase inactive mutant (KDNR) only induces low-grade PIN lesions in the prostate. Yet, it synergistically perturbs prostate tissue homeostasis with the ectopic FGFR1 kinase in the prostate of caFGFR1/KDNR bigenic mice. Depression of the endogenous FGFR2 signaling significantly increases the neuroendocrine cell population in the prostate of the caFGFR1 transgenic mice. Furthermore, depression of the FGFR2 signaling in the prostate of the PB-caFGFR1 transgenic mice potentiates PIN lesion development and shortens the dormant period before developing PIN lesions, which expresses caFGFR1 kinase at low levels.

Task 2. Generation of ROSA-caFGFR1/Fgfr2c/c mice, and characterization of the prostates.

a. *Construction of the ROSA-caFGFR1 knock-in vector.*
b. *Introduction of the ROSA-caFGFR1 construct to mouse embryo stem cells.*
c. *Generation of founders bearing the ROSA-caFGFR1 locus.*
d. *Establishing colonies from each positive founder and verifying gemline integration of the ROSA-caFGFR1 locus.*
e. *Collecting prostates from ROSA-caFGFR1/Fgfr2$^{c/c}$ and control mice, performing serial section of the prostate and characterization of the prostate tissue structures.*
f. *Access the impact of dietary factors on the initiation and development of prostate lesions in ROSA-caFGFR1/Fgfr2$^{c/c}$ mice.*

Progress:

i. Generation of the ROSA-caFGFR1 knock-in mice.

The ROSA26 locus encodes an unessential gene that is strongly and ubiquitously expressed, which is ideal for tissue specific expression of a target gene together with the Cre-loxP recombination technology. To knock-in the conditionally expressed caFGFR1 transgene, a ROSA-caFGFR1 knock-in vector was constructed (Fig. 1). Since the caFGFR1 cDNA is inserted downstream of the neo cassette, which has multiple translational stop sites and polyA addition sites, the caFGFR1 cDNA will not be transcribed until the loxP flanked neo cassette is removed by Cre recombinase.

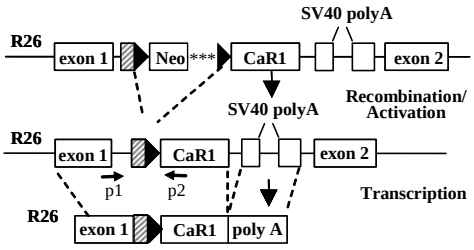

Fig. 1. Scheme for generation of ROSA-caFGFR1 mice. The expression of caFGFR1 is blocked by the loxP flanked neo cassette without the Cre recombinase. Removal of the neo cassette mediated by Cre recombinase activates the transcription of FGFR1 cDNA. After splicing, the matured transcript only encodes caFGFR1. p1 and p2 are the diagnostic primers for detection of the excision of the neo cassette; triangles, loxP sites; hatch box, splice acceptor sequence; neo, neo cassette; *, translational stop codon; caFGFR1, caFGFR1 cDNA; polyA, the splice site and the polyA addition site of SV40 T antigens; exon1, 3, exon1, 3 of the ROSA26 locus.

The ROSA-caFGFR1 DNA was excised from the vector and introduced to AK7 mouse embryo stem (ES) cells by electroporation. Five colonies were identified to have correct recombination. Among them, A76 was selected for the microinjection. Four chimera founders were generated from the injection, and one founder has gemline integration, as demonstrated with the PCR screen of caFGFR1 in the agouti offspring followed by conformation with Southern analysis (Fig. 2A,B). To determine whether the ROSA-caFGFR1 transgene could be activated by Cre recombinase mediated excision of the neo cassette and to assess the expression profile of the caFGFR1, the ROSA-caFGFR1 mouse was crossed with the ARR2PBi-Cre

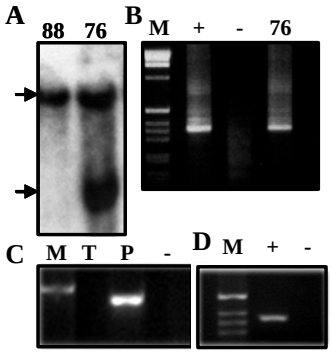

Fig. 2. A. Integration of the caFGFR1 cDNA in the ROSA locus. The indicated ES clones selected from the geneticin resistant cultures were Southern analyzed with the ROSA probe. The upper band represents the wildtype locus, and the bottom band represents the caFGFR1 knock-in locus. **B. PCR detection of ROSA-caFGFR1 mice.** The tail DNAs were purified from ROSA-caFGFR1 and wildtype littermates for PCR analysis as described (1). The 350-bp band representing the caFGFR1 cDNA was detectable in offspring of clone 76. **C. ARR2PBi-Cre driven excision of the neo cassette**. The genomic DNA prepared from the prostate and tail of the ROSA-caFGFR1/ARR2PBi-Cre mouse, as indicated, was PCR amplified with the primer specified in Fig.1. The band representing the activated ROSA-caFGFR1 transgene was detectable only in the prostate. **D. Expression of ROSA-caFGFR1 in the prostate.** The RNA sample prepared from a prostate of a 5-month-old ROSA-caFGFR1/ARR2PBi-Cre mouse was PCR analyzed with (+) and without (-) reverse transcription as described (1). The 350 bp band representing caFGFR1 transcripts was only detectable with the reverse transcription. M, 1 kb molecular weight marker; +, positive control; - negative control; T, tail; 76, clone 76.

transgenic mouse that expressed the Cre recombinase in prostate epithelial cells (3). Prostate tissues of 5-month-old ROSA-caFGFR1/ARR2PBi-Cre bigenic mice were collected for genomic and RNA preparations. PCR analyses with the primers indicated in Fig. 1 show that the neo cassette is excised specifically in prostate, but not tail, DNA (Fig. 2C). To assess whether the ROSA-caFGFR1 transgene is expressed in the prostate, RNA samples from the prostate of 5-month-old bigenic mice were analyzed with Northern blotting with a probe specific for human FGFR1, which does not hybridize with the endogenous mouse FGFR1 transcript. The results in Fig. 2D show that expression of the caFGFR1 transgene is lower than the detection limit, although RT-PCR analyses revealed that the caFGFR1 is expressed in the prostate.

ii. Generation of ROSA-caFGFR1$_{v2}$ knock-in mice.

The most likely reason that the ROSA-caFGFR1 transgene has a low transcription activity is that the transgene has an intron sequence downstream of the stop codon of the caFGFR1 cDNA. According to the nonsense-mediated decay theory, the mRNA is not stable if the stop codon is not in the last exon. To correct this problem, second generation of the ROSA-caFGFR1 transgene was generated (Fig. 3) in which the intronic sequence in the SV40 non-coding region was removed. The ROSA-caFGFR1 fragment was excised from the vector and was introduced to AK7 mouse embryo stem (ES) cells by electroporation. The transfected AK7 cells were selectively grown in the presence of geneticin. About four hundred geneticin resistant clones were selected for Southern analyses with the ROSA probe. Six colonies were identified to have the correct recombination. Among them, H12 and G4 were selected for microinjections. The microinjected blastcysts were transferred to a pseudopregnant foster mother for full-term development. Two high percentage chimeric founders were generated from the injections. Currently, we are testing whether the founder has gemline integration.

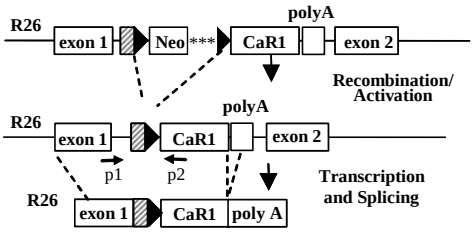

Fig. 3. The ROSA-caFGFR1$_{v2}$ knock-in vector. The intronic sequence of the sv-40 3'-end non-coding region was removed from the original vector sequence shown in Fig. 1. An sv-40 polyA additional site was directly ligated downstream of the stop codon of FGFR1 cDNA to prevent degradation of the transcript due to the nonsense mediated decay. p1 and p2 are the diagnostic primers for detection of the excision of the neo cassette; triangles, loxP sites; hatch box, splice acceptor sequence; neo, neo cassette; *, translational stop codon; caFGFR1, caFGFR1 cDNA; polyA, the splice site and the polyA addition site of SV40 T antigens; exon1, 3, exon1, 3 of the ROSA26 locus

Three chimera founders were generated from the injection, and all founders had gemline integration, as demonstrated with the PCR screen of caFGFR1$_{v2}$ in the agouti offspring followed by conformation with Southern analysis. To determine whether the ROSA-caFGFR1$_{v2}$ transgene could be activated by Cre recombinase, the ROSA-caFGFR1$_{v2}$ mouse was crossed with the ARR2PBi-Cre transgenic mouse as described above (3). Prostate tissues of 5-month-old ROSA-caFGFR1$_{v2}$/ARR2PBi-Cre bigenic mice were collected for genomic and RNA preparations. Northern analyses with a probe specific for human FGFR1 demonstrated that expression of the caFGFR1 transgene was again lower than the detection limit, although RT-PCR analyses revealed that the caFGFR1 was expressed in the line.

iii. Generation of transgenic mice with conditional expression of FGFR1.

Generating genetically engineered mice that express high levels of the constitutively active caFGFR1 in the prostate epithelial cells independent of androgen regulation and differentiation is important to the project. Therefore, we adopted an alternative way to generate mice with conditional expression of caFGFR1 transgene. A conditional expression vector (CXG) was constructed as illustrated in Fig. 4A. A loxP flanked cDNA cassette for the green fluorescence protein (GFP) and three transcriptional termination sites was used to silence the expression of the transgene gene. Excision of the floxed cassette activates expression of the transgenes. An insulator element from chicken β-globin locus was inserted at the 3'-end of the transgene to reduce negative impact imposed by the sequence flanking the transgene. To determine whether the GFP cassette could be excised, a fly luciferase coding cDNA was inserted in the CXG transgenic vector. Transient expression in COS-7 cells showed that the cells transfected with the CXG-luciferase alone only expressed GFP but not the luciferase. Coexpression with the Cre recombinase shut down GFP expression and activated luciferase expression, indicating that expression of the transgene in the CXG vector is Cre-dependent (Fig. 4B, C).

To test whether the CXG conditional expression vector is suitable for expressing FRS2α in mice, we then generated three lines of CXG-FRS2α transgene mice. Heterozygous mutant mice bearing the CXG-*FRS2α* transgene were viable, fertile, normal in size, and did not display any gross physical or behavioral abnormalities. The tail from positive founders exhibited strong green fluorescent activity (data not shown). To determine whether the silenced *Frs2α* transgene could be activated by Cre recombinase, the CXG-*Frs2α* transgenic mice were crossed with CAGG-Cre-Ertm transgenic mice from the Jackson Laboratory, which carried a transgene encoding the Cre/Esr1 fusion protein. The recombinase activity of the Cre-Ertm fusion protein is tamoxifen-inducible. To determine whether the expression of FRS2α was Cre-dependent, two-week-old bigenic mice were injected with 2 mg of 4-hydroxyltamoxifen. Two days after the injection, the kidney and other tissues were collected for evaluation of GFP and FRS2α expression. The results showed that GFP was expressed in the kidney without tamoxifen injection. Activation of Cre-Ertm silenced expression of the GFP (Fig. 4D) and activated FRS2α expression in the kidney, as evaluated with RT-PCR (Fig. 4E). The results showed that expression of the target gene in the CXG vector was Cre-dependent.

To generate transgenic mice that conditionally express caFGFR1 in the prostate, the cDNA encoding caFGFR1 was inserted to the CXG vector for pronuclear injection. Four positive founders were generated. All the transgenic founders exhibited a high level of GFP expression in the tail. Currently, all transgenic founders are crossed with the ARR2PBi-Cre mice for activation of the caFGFR1 transgene in the prostate, and the expression level of the transgene will be determined in the prostate with and without coexpression of the Cre recombinase once the colonies are established, which will take another 4-6 months to finish the characterization.

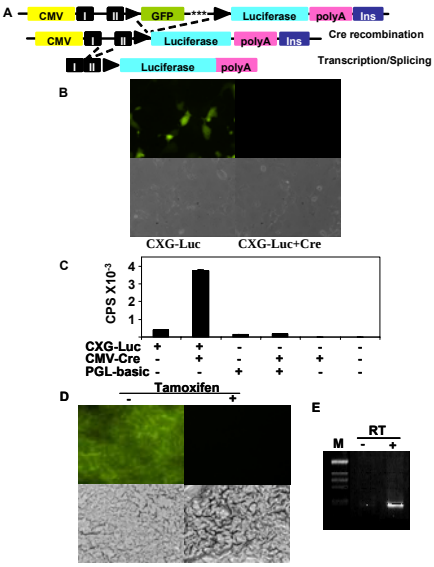

Fig 4. Construction and expression of the CXG conditional expression vector. **A**. Schematic of the CXG-Luc vector. Expression of the target gene is mediated by a hybrid promoter composed of the CMV immediate early enhancer fused to the chicken β-actin promoter. Only when the floxed GFP cassette is excised by Cre recombinase will the downstream luciferase be expressed. Triangles, loxP sites; solid box, exon 1 and 2 of chicken β-actin allele; neo, neo cassette; *, translational stop codon; Luc, luciferase cDNA; polyA, the rabbit globin terminator region. **B**. Expression of GFP. COS-7 cells were transiently transfected with the CXG-Luc vector with or without coexpression of Cre recombinase. The output of fluorescence was observed under a microscope (top panels). Bottom panels, the same cells were observed under a phase contrast microscope. **C**. Expression of the luciferase reporter. COS-7 cells transfected with the indicated plasmids were lysed and the luciferase activity was assessed. **D.** Expression of GFP and FRS2α in transgenic mice before and after Cre-mediated recombination. The CXG-FRS2α/CAGG Cre-Ertm bigenic mice were injected with tamoxifen 3 weeks after the birth to activate the expression of the FRS2α transgene. The kidneys were harvested from the mice with or without the injection as indicated. The fluorescent output from cryosections of the kidney was observed under a fluorescent microscope (top panels), and tissue structures of the same region under a phase contrast microscope (bottom panels). **E**. Expression of FRS2α at the mRNA level. Total RNA from kidneys of the same tamoxifen-injected mouse as in D was extracted for PCR analysis for FRS2α expression with the primers indicated in A with or without reverse transcription. RT, reverse transcription;. M, molecular weight marker.

iv. Ablation of the *Fgfr2* alleles in urogenital sinus during late embryogenesis disrupted development and androgen responsiveness of the prostate.

Development of rodent prostate glands is initiated late in the fetal stage when epithelial buds from the urogenital sinus penetrate into the surrounding urogenital mesenchyme in different direction giving rise to the ventral (VP), dorsal (DP), lateral (LP), and anterior (AP) prostate (4,5). At the time of birth, the mouse prostate is rudimentary, which is consisted of several solid, unbranched epithelial cords. The branching morphogenesis followed by cytological and functional differentiation occurs immediate postnatal period (5).

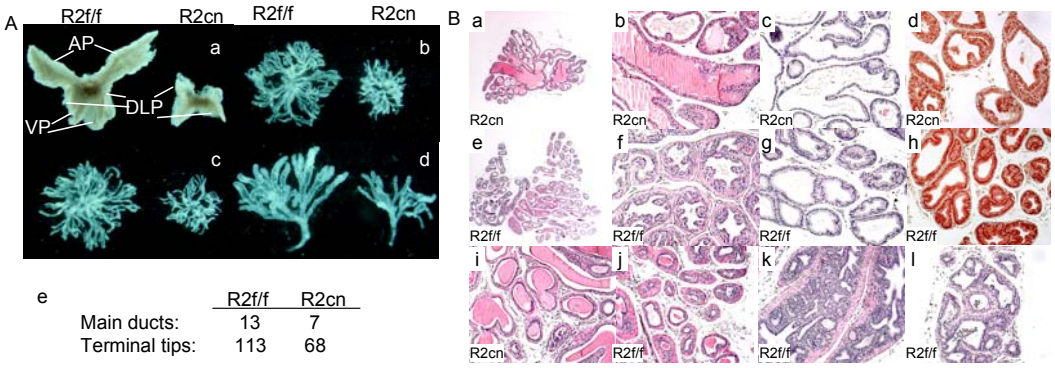

Fig. 5. Ablation of *Fgfr2* alleles disrupted development and androgen responsiveness of the prostate. A. Gross appearance of prostatic tissues dissected from *Fgfr2*$^{f/f}$ (R2f/f) and *Fgfr2* conditional null (R2cn) mice. a. The typical tissue appearance of an R2f/f prostate, which has two ventral, anterior, and dorsal lobes; and an R2cn prostate that only has two underdeveloped dorsal lateral lobes. b-d, Ductal network of DLP of R2f/f and R2cn mice. The DLPs dissected from a 6-week-old R2f/f and R2cn mice were partially digested with collogenase, and the epithelial ductal network was fully separated. b-c, Low magnification view of the whole DLP; d, High magnification of a main duct dissected out from the same prostate lobe. e. The average number of main epithelial ducts and terminal ductal tips in an R2f/f and R2cn DLP. AP, anterior prostate; DLP, dorsolateral prostate; VP, ventral prostate. **B**. Histological characterization of the prostatic tissue. a-d, R2cn prostate. a, dorsolateral lobe; b, high magnification view of a; c, ventral prostate of R2cn mice; d, immunohistochemistry staining of the dorsolateral prostate with the anti-AR antibody. e-h, *Fgfr2*$^{f/f}$ prostate. e, low magnification view of the prostate; f and g, high magnification view of e, showing dorsolateral and ventral prostatic lobes, respectively; h, immunohistochemistry staining with the anti-AR antibody. i-m, H&E staining of prostatic tissue of castrated R2cn (i) prostate (dorsolateral lobe) and *Fgfr2*$^{f/f}$ mice (j-l). j, dorsolateral lobe; k, anterior lobe; l, ventral lobe.

To determine whether the FGFR2 signaling was essential for prostatic development, the *Fgfr2*-floxed mouse was crossed with the NKX3.1-Cre transgenic mouse obtained from Dr. Michael Shen's laboratory to specifically disrupt the floxed *Fgfr2* alleles in the urogenital sinus at late embryonic stages (E17.5-18.5). The prostate glands of mice with homozygous floxed *Fgfr2* alleles had no noticeable difference in gross tissue morphology as well as in histological structures from that of wildtype and heterozygous *Fgfr2* floxed allele, and hereafter are considered as controls. The mice with *Fgfr2* conditional null alleles (*R2cn*) were viable and had a well developed male reproductive system, except having a very small prostate, and low reproductivity in males. Gross tissue inspection showed that the *R2cn* prostate had poorly developed dorsal and lateral lobes, which are thinner and more transparent than that of wildtype prostate. Among the 15 R2cn mice examined at different ages, 12 mice only had dorsolateral prostatic lobes (Fig. 5A, upper panel). One mouse had a very small anterior lobe (data not shown); 1 mouse had a ventral lobe (data not show), and 1 mouse had two small anterior and 1 ventral lobes (Fig. 5). To quantitate the number of epithelial ducts in the DLP lobes, the wildtype and R2cn prostates were digested with collogenase for separation of the ducts (Fig. 5B).

Histological analyses of the R2cn prostate of young adult males showed that only very few branch-points and distal tips were present in dorsal and lateral lobes of the prostate (Fig. 5B, panels a-b), ventral lobe (Fig. 5B, panel b), and anterior lobe (data not shown). The average wet weight of *Fgfr2* null prostate was 15 mg, which is significantly lower than that of mice with floxed *Fgfr2* alleles (~80 mg). H&E staining with paraffin embedded tissue sections showed

that the epithelial ducts were short and small in diameter and lined with simple, low-columnar cells with very few infolding. To determine whether the *R2cn* prostate undergoes morphogenesis during postnatal development, the numbers of proliferating cell nuclear antigen (PCNA) expressing cells were compared between the *R2cn* prostate and controls. The results showed that PCNA was expressed in many cells of the *Fgfr2*-floxed prostate of 4-5-week-old mice, and the *R2cn* prostate only had very few PCNA-expressing cells. In addition, TUNEL assay showed that many cells in the *R2cn* prostate were undergoing apoptosis at the age of 8 weeks. To determine whether the *R2cn* prostate was androgen responsive, the male *R2cn* was castrated at the age of 6-8 weeks. Two weeks after the castration, the mice were implanted with an androgen pellet to restore androgens to normal levels. The prostate of *Fgfr2*-floxed mice dramatically decreased in size two weeks after the castration. Tissue mass of the prostate was restored to regular size 7 days after androgen replenishment. H&E staining show that the epithelial ducts were reduced in every lobe of wildtype prostate, which were lined with low-columnar cells (Fig. 5B, panels j-l). In contrast, the R2cn prostate did not atrophy in castrated mice, nor increase in size after androgen restoration. H&E staining also did not show any obvious change before and after castration (Fig. 5B, panels b and i), and after androgen restoration (data not shown). The results suggested that disruption of the FGFR2 signaling in the prostate abrogated androgen responsiveness in the prostate, and further confirmed that the androgen regulatory function, at lease in part, was mediated by the FGF signaling pathway. One of the main objectives of this project is to investigate the detailed molecular mechanism how FGFR2 mediates regulatory activities of the androgens in the prostate, both in development and in tissue homeostasis, and to determine whether disruption of FGFR2 signaling promotes prostate tumorigenesis.

To determine the expression pattern of the Nkx3.1-Cre transgene, the ROSA-26 reporter mice were crossed with the Nkx3.1-Cre transgenic mice. The lacZ staining of the urogenital sinus of E18.5 bigenic embryos showed that the Nkx3.1-Cre transgene was expressed in all prostate buds (Fig 6). Currently, we do not know why the R2cn mice did not have the anterior and ventral prostate lobes. It is possible that the development of anterior and ventral prostate buds is more FGFR2 kinase-dependent than dorsal-lateral prostate buds. It is also possible that the dorsal and lateral prostate buds, but not the anterior and ventral buds, develop earlier than expression of the Nkx3.1-Cre, and, therefore, earlier than disruption of the $Fgfr2^{f/f}$ alleles. Since the morphogenetic processes and final adult tissue morphologies differ vastly by region within the mouse prostate (4), it is possible that the discrepancy of development of each lobe of prostate resulted from disruption of *Fgfr2* alleles at different times. The results had been summarized in

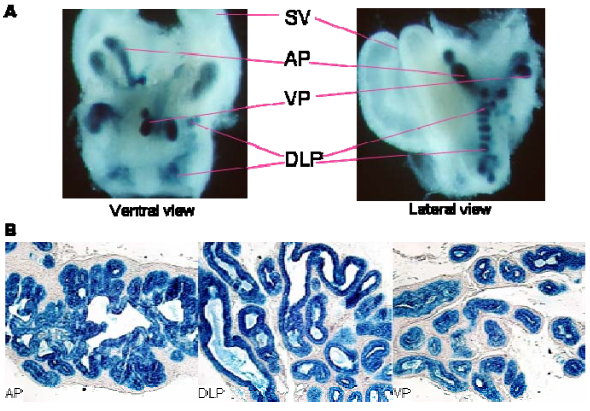

Fig. 6. Expression of the Nkx3.1-Cre transgene in prostatic epithelia. A. Ventral and lateral views of the X-gal stained urogenital sinus dissected from an E18.5 embryo of the Nkx3.1-Cre/ROSA 26 bigenic mice as indicated. The X-gal stained tissues representing anterior (AP), ventral (VP), and dorsolateral (DLP) prostatic lobes were labeled. B. The anterior, dorsolateral, and ventral prostatic lobes of a 6-week-old Nkx3.1-Cre/ROSA 26 bigenic male were cryosectioned and stained with X-gal. Note that only epithelial cells in the lumen were stained, indicating that the Nkx3.1-Cre transgene was only expressed in the epithelial cells.

a manuscript for publication in Development.

v. Characterization of the prostates with disrupted resident FGFR2 signaling axis in matured prostate epithelial cells.

To disrupt the resident FGFR2 in the epithelium of matured prostates, the mice with loxP flanked FGFR2 allele were crossed with the ARR2PBi-Cre transgenic mice. Prostate tissues from 5-month-old FGFR2-floxed and FGFR2 conditional-null mice were harvested for RNA preparations. Results in Fig. 6 showed that the expression of FGFR2 was significantly reduced in the prostate. Preliminary results showed that the disrupted FGFR2 null prostates were significantly larger than the FGFR2 floxed littermates. The average wet weight of the FGFR2 null prostate was 283 mg, which is about 2.5 times larger than that of FGFR2 floxed littermates (Fig. 6). Histochemistry analyses revealed that the FGFR2-null prostate developed high-grade PIN at the age of 12 months or older. Moreover, the expression of cytokeratin 18 that is highly expressed in well-differentiated prostate epithelial cells was significantly reduced in FGFR2 null prostates. On the other hand, the expression of cytokeratin 14 that is expressed in less-differentiated prostate basal cells was increased in FGFR2 null prostate. This suggests that disruption of the resident FGFR2 perturbs tissue homeostasis in the prostate.

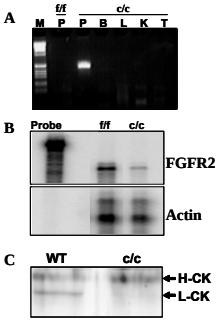

Fig. 7. ***A. Prostate-specific disruption of FGFR2.*** Genomic DNAs from the prostate and indicated tissues from FGFR2 conditional null and floxed mice were extracted, and the 500 bp fragment representing the null allele of FGFR2 was PCR amplified for as described (2). ***B. Reduction of FGFR2 expression in Fgfr2$^{c/c}$*** **prostate.** Total RNAs were extracted from the prostates of indicated mice. The expression of FGFR2 was assessed by the RNase protection assays with probes for FGFR2 (top panel), or β-actin for loading controls (bottom panel). ***C. Disruption of FGFR2 changes cytokeratin expression in the prostate.*** The prostate of FGFR2 condition null mice and wildtype littermates were harvested at the age of 1 year and homogenized in 1% Triton-PBS. The lysates equivalent to 20 μg proteins were separated on SDS-PAGE, and cytokeratins were detected with anti-pan cytokeratin antibodies. M, 1 kb DNA marker; P, prostate; B, bladder; L, liver; K, kidney; T, testis; f/f, Fgfr2$^{f/f}$; c/c, Fgfr2$^{c/c}$; H-CK and L-CK, high molecular weight and low molecular weight cytokeratin, respectively.

vi. To evaluate dietary effects on prostate lesions induced by disruption of the resident FGFR2 signaling.

The ROSA-caFGFR1 knock-in mice have not been fully characterized to date; therefore, it is too early to test the dietary effect on tissue homeostasis in the prostate of ROSA-caFGFR1/FGFR2 null mice. Instead, since the FGFR2 null/ARR2PBi-caFGFR1 prostate has been characterized, we are carrying out the experiments with the FGFR2 condition-null mice with or without expression of the caFGFR1 transgene in the prostate. Forty each of newly weaned mice of FGFR2 condition null and FGFR2 floxed mice were set aside and fed with high fat/cholesterol (40% calories from saturated fat, 2% cholesterol) diet and regular diet. The mice will be sacrificed at the ages of 8, 10, 12, 14, and 16 months. Currently, the preliminary data indicate that a high fat/cholesterol diet might accelerate PIN development in FGFR2 null/ARR2PBi-caFGFR1 mice. Detailed characterization will be needed to fully assess the role

of diet in prostate lesion development and progression. The data gathered in this pilot study had been used to develop a project for soliciting NIH funding.

KEY RESEARCH ACCOMPLISHMENTS

1. Establish a highly efficient prostate specific Cre mouse model for tissue specific disruption and activation of genes in the prostate. The Cre recombinase efficiently excises the loxP-flanked fragment in the FGFR2 locus in the prostate as well as in ROSA-caFGFR1 knock-in mice for conditional expression of the constitutively active FGFR1 (caFGFR1) in the prostate.
2. Characterize the phenotype of the ARR2PBi-caFGFR1 transgenic mice that express caFGFR1 at high levels. The mice develop high-grade prostatic intraepithelial neoplasia (PIN) within one year. The initiation and progression of PIN is caFGFR1 expression level-dependent.
3. Characterize the phenotype of the PB-caFGFR1/KDNR and ARR2PBi-caFGFR1/KDNR bigenic mice. Suppression of the resident FGFR2 signaling and expression of the caFGFR1 synergistically disrupt homeostasis and induce PIN lesions in the prostate.
4. Generation of a line of ROSA-caFGFR1 knock-in mice that carry a silent caFGFR1 coding sequence in the ROSA locus for conditional expression of the caFGFR1 in target tissues. The neo cassette that suppresses expression of the caFGFR1 could be removed in the prostate via Cre-mediated recombination.
5. Generation of a colony of mice with prostate-specific disruption of FGFR2. The average wet weight of FGFR2-null prostate tissues were at least two times larger than that of the FGFR2-floxed mice and had an increased population of basal epithelial cells. The histology characterization of the FGFR2-null prostate is undertaken currently.
6. Construction of a conditional expression transgenic vector for conditional expression of FGFR1. In vitro results showed that the vector had a low background expression of luciferase with a silencing GFP cassette; excision of the GFP cassette activated the luciferase expression. Currently, we are in the process of cloning the caFGFR1 cDNA into the vector for generation of the transgenic mice.
7. Construction and generation of ROSA-caFGFR1v2 knock-in mice. The knock-in vector was constructed; five clones of mouse embryonic stem cells with the predicted recombination were generated. Two clones were injected so far. Two chimeric males were generated. A breeding colony will be set up as soon as the mice are mature.
8. Generation of CXG-caFGFR1 transgenic mice for conditional expression of caFGFR1 in the prostate.
9. Discover that FGFR2 in epithelial cells plays important roles in prostate development. Disruption of FGFR2 in epithelial urogenital cells at embryonic day 17.5 significantly disturbs prostate development.

10. Discover that epithelial resident FGFR2 kinase is important in androgen responsiveness of prostates.
11. Discover that overexpression of Cks1 and Cks2 contributes to prostate tumorigenesis by promoting proliferation and preventing apoptosis, respectively.

REPORTABLE OUTCOMES

1. Publications:

a. Jin, C., K. McKeehan, and F. Wang (2003) Transgenic mouse with high Cre recombinase activity in all prostate lobes, seminal vesicle, and ductus deferens. *The Prostate* **57:**160-164.

b. Jin, C., K. McKeehan, W. Guo, S. Jauma, M. M. Ittmann, B. Foster, N. M. Greenberg, W. L. McKeehan, and F. Wang (2003) Cooperation between ectopic FGFR1 and depression of FGFR2 signaling in induction of prostatic intraepithelial neoplasia in mouse prostate *Cancer Res.* **63:** 8784-8790.

c. Zhang, Y., Y. Lin, C. Bowles, and F. Wang (2004). Direct cell cycle regulation by the fibroblast growth factor receptor (FGFR) kinase through phosphorylation-dependent release of Cks1 from FGFR substrate 2. *J. Biol. Chem.* **279**: 55348-55354.

d. Lin, Y., G. Liu, and **F. Wang** (2006) Generation of an *Fgf9* Conditional Null Allele. Genesis **44**: 150-154.

e. Guo, C., G. Wu, S. S. Taylor, **F. Wang**, Y. Zuo, I. Van Huizen, G. Bauman, J. L. Chin, M. Moussa, J. W. Xuan (2006). Bub1 up-regulation and hyper-phosphorylation are major features Promoting Prostate Cancer Transformation in SV40 Tag -induced Transgenic Mouse Models. Molecular Cancer Res (in press).

f. Zhang, Y., K. McKeehan, and **F. Wang** (2006). Tyrosine phosphorylation on type 1 fibroblast growth factor receptor (FGFR) promotes binding of FGFR substrate 2 alpha to the receptor kinase. J. Biol. Chem. (in revision).

g. Huang, X., C. Yu, C. Jin, C. Yang, R. Xie, D. Cao, **F. Wang,** and W.L. McKeehan. (2006) Dual functions of fibroblast growth factor 21 in chemically-induced hepatocarcinogenesis. Mol Carcinogenesis (in press).

h. Lin, Y., J. Zhang, G. Liu, and **F. Wang** (2006) Generation of an Frs2α Conditional Null Allele. Genesis (submitted).

i. Yongshun Lin, Guoqin Liu, Ya-Ping Hu, Kai Yu, Yongyou Zhang, Chunhong Lin, Kerstin McKeehan, Jim W. Xuan, David Ornitz, Michael M. Shen, Norman Greenberg, Wallace L. McKeehan, and **F. Wang** (2006). Fibroblast growth factor receptor 2 tyrosine kinase is required for prostate epithelial morphogenesis and acquisition of strict androgen dependency. (in revision).

j. Huang, X., C. Yang, C. Jin, **F. Wang,** W.L. McKeehan (2006) Lack of fibroblast growth factor receptor 4 causes hyperlipidemia and insulin resistance but prevents high fat diet-induced fatty liver. Cell Metabolism (submitted)

k. Lin, Y., K. McKeehan, C. Bowles, W. L. McKeehan, and **F. Wang**. (2006). The epithelial-resident fibroblast growth factor receptor tyrosine kinase is

essential for androgen responsiveness of the prostate. Development (in preparation).

l. Lan, Y, Y. Lin, J. Zhang, K. McKeehan, and **F. Wang**. (2006) Generation of a transgenic mouse model for conditional expression of fibroblast growth factor receptor substrate 2 (FRS2). Genesis (in preparation).

m. Kobayashi, M., W-K Chan, C. Jin, X. Huang, Y. Luo, D. Cao, **F. Wang**, T. Okamoto, and W. L. McKeehan (2006), Ectopic FGFR1 abrogates the androgen response by alteration of the androgen receptor in pre-malignant prostate tumor epithelial cells. Cancer Res. (in preparation).

2. Abstract:

1. Kerstin McKeehan, Scot Jauma, and Fen Wang (2004) **Aberrant FGF signaling axis disrupts homeostasis and induces prostatic intraepithelial neoplasia in the prostate of genetically altered mice.** *AACR Annual Meeting Abstract.*

2. Fen Wang. (2004) **The fibroblast growth factor signaling axis and polysaccharides of the extracellular matrix in neuron regeneration.** The Third Symposium on Neuroscience for Young Scholars Worldwide, Guangzhou, China.

3. Yongyou Zhang, Kerstin McKeehan and Fen Wang (2004) **The fibroblast growth factor signaling axis and polysaccharides of the extracellular matrix in neuron regeneration.** The Third Symposium on Neuroscience for Young Scholars Worldwide, Guangzhou, China.

4. Fen Wang (2004) **Characterization of the function of the fibroblast growth factor signaling axis in the prostate of genetically engineered mice**. The 9th International Oncology meeting.

5. Xinqiang Huang, Chundong Yu, Chengliu Jin, Courtney A. Bowles, Fen Wang, and Wallace L. McKeehan (2004) **Forced expression of fibroblast growth factor receptor (FGFR) 1 in hepatocytes accelerates carcinogen-initiated hepatocarcinogenesis**. The American Association for Cancer Research (AACR) Meeting, Orlando, FL., March 27-31, 2004.

6. Jinsheng Weng, Jianhua Wang, Xiaoxiao Hu, Fen Wang, Michael Ittmann, Mingyao Liu (2005). **PSGR2, a novel G-protein coupled receptor, is overexpressed in human prostate cancer**. Annual symposium of the American Association of Cancer Research, Anaheim, CA.

7. Xinqiang Huang, Chundong Yu, Chengliu Jin, Courtney A. Bowles, Fen Wang, and Wallace L. McKeehan (2005). **Ecotopic activity of FGFR1 in hepatocytes accelerates hepatocarcinogenesis by driving proliferation and VEGF-**

induced angiogenesis. Annual Symposium of the American Association of Cancer Research, Anaheim, CA

8. Yongyou Zhang, Yongshun Lin, Courtney Bowles, and Fen Wang (2006) **Phosphorylation-dependent release of Cks1 from FRS2 suggests a new mitogenic pathway of the FGFR kinase.** Gordon Research Conference, Hong Kong, China.

9. **FGFR2 signaling in the prostate.** Mouse Models of Human Cancer Consortium Steering Committee meeting, Washington DC

10. **Jue Zhang, Yongshun Lin, Chunhong Lin, Robert J. Schwartz, and Fen Wang** Conditional ablation of Frs2α alleles in the heart disrupts heart development. 2nd research retreat of the Cardiovascular Research Institute, Texas A&M Health Science Center, College Station, TX

3. Presentations:

a. **The FGF signaling axis in prostate homeostasis and tumorigenesis.** Annual meeting of the Society of Chinese Bioscientists of America, Texas Chapter. Houston, TX (2003).

b. **The FGF signaling axis in prostate homeostasis and tumorigenesis.** Sealy Center for Cancer Cell Biology, University of Texas, Medical Branch. Galveston, TX (2003).

c. **The FGF signaling axis in prostate homeostasis and tumorigenesis.** Department of Molecular and Cellular Biology, Baylor College of Medicine. Houston, TX (2003)

d. **The FGF signaling in the prostate: from molecules to mice.** Meharry Medical College-Vanderbilt University Alliance. Nashville, TN (2004).

e. **The extracellular matrix and the FGF signaling in spinal cord regeneration.** The Spinal Cord Injury Workshop sponsored by The Institute of Rehabilitation and Research (TIRR) in Galveston. (2004).

f. **The FGF signaling in the prostate: from molecules to mice.** The Life Science College, Xiamen University. Xiamen, China. (2004).

g. **Establishing genetically engineered mouse model for cancer research.** The Biotechnology College. Jimei University. Xiamen, China (2004).

h. **The fibroblast growth factor signaling axis and polysaccharides of the extracellular matrix in neuron regeneration.** The Third Symposium on Neuroscience for Young Scholars Worldwide. Guangzhou, China (2004)

i. **The Fibroblast growth factor signaling axis.** The Society of Chinese Bioscientists of America. Texas Chapter. Houston TX (2005).

j. **The fibroblast growth factor signaling axis in the prostate.** The Methodist Hospital Research Institute, Genitourinary Oncology Center Seminar Series. Houston, TX (2005)

k. **The FGF signaling complex in the prostate.** Information Exchange Seminar series, the Institute of Biosciences and Technology, Texas A&M Health Science Center, Houston TX (2006).

l. **FGFR2 signaling in the prostate.** Mouse models of Human Cancer Consortium Steering Committee meeting. Washington DC (January 16-18, 2006).

m. **FGFR2 signaling in prostate development.** Gordon Research Conference (Fibroblast growth factor in development and disease) Ventura, CA (March 12-17, 2006)

4. Requests for mouse models through collaborations:

25

CONCLUSIONS

The prostatic intraepithelial neoplasia (PIN) development and homeostasis perturbation in the prostate of caFGFR1 transgenic mice are caFGFR1 expression level dependent. Repression of the FGFR2 signaling potentiated perturbation of prostate homeostasis induced by the ectopic caFGFR1 kinase. In addition, disruption of FGFR2 during prostate development significantly affected prostate development and diminished androgen responsiveness of the prostate. The results further suggest that aberrant FGF signaling in the prostate is a strong factor in prostate morphogenesis, growth, and tissue homeostasis. Aberrantly activation of the FGF signaling axis is a strong promoter for prostate tumor development and progression. In addition, the ARR2PBi-caFGFR1/FGFR2 conditional null mouse model provides a useful tool for evaluating other tumor initiating factors, including genetic instability and other oncogenic lesions in prostate tumorigenesis.

REFERENCES

1. Jin, C., McKeehan, K., Guo, W., Jauma, S., Ittmann, M. M., Foster, B., Greenberg, N. M., McKeehan, W. L., and Wang, F. (2003) *Cancer Res* **63**, 8784-8790
2. Yu, K., Xu, J., Liu, Z., Sosic, D., Shao, J., Olson, E. N., Towler, D. A., and Ornitz, D. M. (2003) *Development* **130**, 3063-3074
3. Jin, C., McKeehan, K., and Wang, F. (2003) *Prostate* **57**, 160-164
4. Sugimura, Y., Cunha, G. R., and Donjacour, A. A. (1986) *Biol Reprod* **34**, 961-971
5. Hayashi, N., Sugimura, Y., Kawamura, J., Donjacour, A. A., and Cunha, G. R. (1991) *Biol Reprod* **45**, 308-321

APPENDICES LIST:

1. Yongshun Lin, Guoqin Liu, Ya-Ping Hu, Kai Yu, Yongyou Zhang, Chunhong Lin, Kerstin McKeehan, Jim W. Xuan, David Ornitz3 Michael M. Shen, Norman Greenberg, Wallace L. McKeehan, and **Fen Wang** (2006) Fibroblast growth factor receptor 2 tyrosine kinase is required for prostatic morphogenesis and acquisition of strict androgen dependency for adult tissue homeostasis. Development (in revision)
2. Zhang, Y., K. McKeehan, and **F. Wang** (2006). Tyrosine phosphorylation on type 1 fibroblast growth factor receptor (FGFR) promotes binding of FGFR substrate 2 alpha to the receptor kinase. J. Biol. Chem. (submitted).
3. Lin, Y., J. Zhang, G. Liu, and **F. Wang** (2006) Generation of an *Frs2*α Conditional Null Allele. Genesis (submitted).

Fibroblast growth factor receptor 2 tyrosine kinase is required for prostatic morphogenesis and acquisition of strict androgen dependency for adult tissue homeostasis

Yongshun Lin, Guoqin Liu[1], Ya-Ping Hu[2], Kai Yu[3], Yongyou Zhang, Chunhong Lin, Kerstin McKeehan, Jim W. Xuan[4], David Ornitz[3], Michael M. Shen[2], Norman Greenberg[5], Wallace L. McKeehan, and Fen Wang[¶]

Center for Cancer Biology and Nutrition, Institute of Biosciences and Technology, Texas A&M University System Health Science Center, 2121 W. Holcombe Blvd., Houston, TX 77030-3303. [1], State Key Laboratory of Plant Physiology and Biochemistry, College of Biological Sciences, China Agricultural University, Beijing, P.R. China 100094; [2], Center for Advanced Biotechnology and Medicine, UMDNJ-Robert Wood Johnson Medical School, 679 Hoes Lane, Piscataway, NJ 08854; [3], Department of Molecular Biology and Pharmacology, Washington University, School of Medicine, 660 South Euclid Avenue, Saint Louis, MO, 63110; [4], Department of Surgery, University of Western Ontario, London, ON, N6A 4G5, Canada; [5], Clinical Research Division, Fred Hutchinson Cancer Research Center, 1100 Fairview Ave. Seattle, WA 98109-1024

¶Corresponding Author

Address: Center for Cancer Biology and Nutrition, Institute of Biosciences and Technology, Texas A&M University System Health Science Center, 2121 W. Holcombe Blvd., Houston, TX 77030-3303.

Phone: 713-677-7520, Fax: 713-677-7512, e-mail: fwang@ibt.tmc.edu

Running title: FGFR2 in prostate development

Summary

The fibroblast growth factor (FGF) family consists of products of 22 homologous genes and regulates a broad spectrum of biological activities by activating diverse isotypes of FGF receptor tyrosine kinases (FGFR). Among the FGFs, FGF7 and FGF10 have been implicated in the regulation of prostate development and prostate tissue homeostasis by signaling through the FGFR2 isoform. Using conditional gene ablation with the Cre/LoxP system in mice, we demonstrate a tissue-specific requirement for FGFR2 in urogenital epithelial cells, the precursors of prostatic epithelial cells, for prostatic branching morphogenesis and growth. Most *Fgfr2* conditional null (*Fgfr2*^{cn}) embryos developed only two dorsal (dp) and two lateral prostatic lobes (lp), which contrasts to wildtype (WT) prostate that has two anterior (ap), two dp, two lp, and two ventral (vp) lobes. Unlike WT prostates that are composed of well developed epithelial ductal networks, the *Fgfr2*^{cn} prostates, despite retaining a compartmented tissue structure, exhibited a primitive epithelial architecture. Moreover, although *Fgfr2*^{cn} prostates continued to produce secretory proteins in an androgen-dependent manner, they responded poorly to androgen with respect to tissue homeostasis. The results demonstrate that FGFR2 is important for prostate organogenesis and for the prostate to be developed to a strictly androgen-dependent organ with respect to tissue homeostasis but not the secretory function, implying that androgens may regulate tissue homeostasis and function through different pathways. Therefore, *Fgfr2*^{cn} prostates provide a useful animal model for scrutinizing the molecular mechanisms by which androgens regulate prostate growth, homeostasis, and function, and may yield clues as to how advanced prostate tumor cells escape strict androgen regulations.

Introduction

Development of mouse prostates is initiated at embryonic day 17 (E17), when a group of urogenital sinus epithelial cells derived from the hind gut endoderm grow out into the surrounding urogenital sinus mesenchyme in anterior, ventral, dorsal, and lateral directions. These buds subsequently form the anterior, ventral, dorsal, and lateral prostate lobes, respectively (Cunha et al., 2004; Thomson, 2001). At postnatal day 1 (P1), solid prostatic buds are formed surrounding the urethra, which already exhibit secondary and tertiary ductal branches. The ducts then undergo extensive branching morphogenesis, elongate from distal points, and form intraductal mucosal infolding. About 80% of ductal branching is completed by day 10 of neonatal life in mice, and the process is normally completed in 60-90 days. During this stage, the epithelial cells differentiate into luminal secretory epithelial cells, basal epithelial cells, and neuroendocrine cells, concurrent with the differentiation of mesenchyme into smooth muscle cells and fibroblasts (Cunha et al., 2004; Hayward et al., 1997).

Adult prostates are androgen dependent organs with respect to growth, tissue homeostasis, and function. Normally, the epithelium rapidly regresses to an atrophic state upon depletion of androgens. About 35% of the ductal tips and branch-points are lost in distal regions within two weeks after orchiectomy. Androgen replenishment induces active cellular proliferation in the epithelium of atrophied prostate within 2 days, and the epithelial ducts completely regenerate within 14 days (Sugimura et al., 1986b). Since tissue recombination experiments showed that the androgen receptor (AR) in epithelial cells is not essential for prostates to respond to androgens, it is proposed that paracrinal growth factors between stromal and epithelial compartments mediate at least

some of the regulatory functions of androgen and are critical for androgens to instruct epithelial cells undergoing proliferation and differentiation (Cunha, 1996; Cunha et al., 2004; McKeehan et al., 1998; Thomson, 2001). Reciprocal communication from epithelia to mesenchymes may also play similar roles in stroma development, particularly in the differentiation to smooth muscle cells (Cunha, 1994; Cunha et al., 1996; Cunha et al., 2004; Hayward et al., 1998; Jin et al., 2004). It remains unresolved whether androgens regulate growth, tissue homeostasis, and functions via similar signaling mechanisms, although the FGF signaling axis has been implicated to be important for androgen signaling in prostates.

The mammalian FGF family consists of at least 22 gene products that control a wide spectrum of cellular processes. Most FGFs bind and activate transmembrane tyrosine kinases receptors (FGFRs) encoded by four highly conserved genes that exhibit a variety of splice variants (McKeehan et al., 1998; Powers et al., 2000; Wang and McKeehan, 2003). Expression of FGFs and FGFRs is spatiotemporally-specific in embryos and tissue- and cell type-specific in adults. Aberrant activations of FGF signaling pathways are found in developmental disorders and in diverse adult tissue-specific pathologies, including malignant cancer (McIntosh et al., 2000; McKeehan et al., 1998; Ornitz, 2000; Wang and McKeehan, 2003).

In prostate, members of the FGF family and alternative splice forms of FGFRs are partitioned in the epithelium and mesenchyme (stroma), mediating directional and reciprocal communications between the two compartments. Ablation of this two-way communication in mature prostates perturbs tissue homeostasis and leads to prostatic intraepithelial neoplasia (PIN) and progressively more severe lesions (Jin et al., 2003a;

McKeehan et al., 1998). In addition, a series of stepwise changes in FGF signaling contributes to the progression of prostate lesions, including reduction in resident FGFR2 expression accompanied by expression of ectopic epithelial FGFR1 expression (Jin et al., 2003a; Kwabi-Addo et al., 2001; Lu et al., 1999; McKeehan et al., 1998; Pirtskhalaishvili and Nelson, 2000). Additionally, changes in the expression of FGF1, FGF2 (Ropiquet et al., 1999), FGF6 (Ropiquet et al., 2000), FGF8 (Dorkin et al., 1999; Gnanapragasam et al., 2002; Song et al., 2002; Wang et al., 1999), FGF9 (Giri et al., 1999b), and FGF17 (Polnaszek et al., 2004) have been observed to be associated with prostatic lesions.

During prostatic organogenesis, messenger mRNAs for both FGF7 and FGF10 are localized in the mesenchyme, and the receptors for FGF7/10 are found in the epithelium of the urogenital sinus in embryos and the distal signaling center of elongating and branching ducts in postnatal prostates (Huang et al., 2005; Thomson and Cunha, 1999). Both FGF7 and FGF10 can substitute for androgens in organ culture of neonatal prostates, supporting extensive epithelial growth and ductal branching morphogenesis. Ablation of *Fgf10* alleles abrogates prostate development and diminishes androgen responsiveness of prostatic rudiments in organ culture and tissue recombination experiments (Donjacour et al., 2003). This suggests that FGF10 signaling is essential for prostate development. Although it is generally accepted that the FGFR2IIIb isoform is the primary receptor for FGF10, the inability of mice deficient in FGFR2 to survive has prevented a direct analysis of the function of FGFR2 in prostate development, maintenance of homeostasis, and androgen dependency.

To overcome this limitation, we specifically disrupted *Fgfr2* alleles in prostate precursor cells at E17.5. Unlike normal prostates composed of 2 anterior, 2 dorsal, 2 lateral, and 2 ventral lobes, most young adult *Fgfr2*^{cn} mice developed a small prostate that was frequently limited to 2 dorsal and 2 lateral lobes. Development of the epithelial compartment *in Fgfr2*^{cn} prostates was impaired, which could be characterized by deficient in intralumenal infolding. In contrast to WT prostates, maintenance of mature *Fgfr2*^{cn} prostates was not strictly androgen-dependent. No significant prostatic atrophy was observed two weeks after castration in adult *Fgfr2*^{cn} mice. Similarly, androgen replenishment to the castrated males also failed to induce cell proliferation in *Fgfr2*^{cn} prostates. The results showed that FGFR2 signals were essential for strict androgen dependency in adult prostates with respect to tissue homeostasis. Interestingly, as in control prostates, production of secretory proteins in *Fgfr2*^{cn} prostate was dramatically reduced by androgen deprivation, suggesting that the secretory function of *Fgfr2*^{cn} prostates remained androgen regulated. Together, the data suggest that androgens may elicit regulatory functions in the prostate via multiple pathways. Thus, *Fgfr2*^{cn} prostates provide a useful animal model for scrutinizing the molecular mechanisms by which androgens regulate prostate growth, homeostasis, and function, and may yield clues as to how advanced prostate tumor cells escape strict androgen regulation.

MATERIALS AND METHODS

Animals.

All animals were housed in the Program of Animal Resources of the Institute of Biosciences and Technology, and were handled in accordance with the principles and procedure of the *Guide for the Care and Use of Laboratory Animals*. All experimental procedures were approved by the Institutional Animal Care and Use Committee. The mice carrying LoxP-flanked *Fgfr2* alleles, the ROSA26 reporter, and the Nkx3.1-Cre knock-in alleles were bred and genotyped as described (Jin et al., 2003b; Soriano, 1999; Yu et al., 2003). Orchiectomy and prostate regeneration were carried out as described previously (Donjacour and Cunha, 1988; Jin et al., 2003a; Wang et al., 2004). Serum levels of androgens in $Fgfr2^{cn}$ and control littermates were measured with the DSL-400 Androgen Assessment Kit (Diagnostic Systems Laboratories, Webster, TX), according to the manufacturer's suggested procedure.

Collection of prostate tissues and histology analysis.

The urogenital complex was excised from the $Fgfr2^{cn}$ and $Fgfr2^{flox}$ mice at the ages indicated in the text and fixed with 4% paraformaldehyde-PBS solution for 30 min. The prostate tissues were then dissected from the urogenital tracks under a stereo microscope, weighted, and further fixed for an additional 4 hours as described (Jin et al., 2003a; Wang et al., 2004). In some cases, each individual lobe was dissected and fixed separately. Fixed tissues were serially dehydrated with ethanol, embedded in paraffin, and completely sectioned according to standard procedures. One out of every five slides were re-hydrated and stained with hematoxylin and eosin (H&E) for scanning of general tissue structures. Immunohistochemical analyses were performed on 7 μm

paraffin sections mounted on Superfrost/Plus slides (Fisher Scientific, Pittsburgh, PA). The antigens were retrieved by autoclaving in Tris-HCl buffer (pH 10.0) for 5 minutes or as suggested by manufacturers of the antibodies. The source and concentration of primary antibodies are: mouse anti-cytokeratin 8 (1:15 dilution) from Fitzgerald (Concord, MA); mouse anti-smooth muscle α-actin (1:1 dilution) and mouse anti-PCNA (1:1000 dilution) from Sigma Co (Saint Louis, MO); mouse anti-P63 (1:150 dilution) and mouse anti-AR (1:150 dilution) from Santa Cruz (Santa Cruz, CA); rabbit anti-probasin (1:3000 dilution) from the Greenberg laboratory; and rabbit anti-PSP94 (1:2000 dilution) from the Xuan laboratory. To quantitate numbers of stained cells, total numbers of stained cells from at least 3 sections per prostate, and 3 prostates per genotype were scored for statistical analyses.

For wholemount lacZ staining, the urogenital sinuses were lightly fixed with 0.2% glutaraldehyde for 30 minutes, and the lacZ activity was analyzed by incubation with 1 mg/ml X-Gal at room temperature overnight as described (Liu et al., 2005). For TUNEL assay, tissues were fixed and sectioned as described above, and the apoptotic cells were detected with the ApopTag Peroxidase In Situ Kit from Chemicon, Inc, (Temecula, CA).

Microdissection of prostate ducts.

Microdissections of dorsolateral lobes of the prostate were performed according to Sugimura (Sugimura et al., 1986a). Briefly, individual ductal networks of the prostate gland were microdissected after incubation in 1% collogenase-PBS at 4 °C overnight. All microdissections were performed under a dissection microscope. Numbers of the main ducts and distal ductal tips were scored for statistical analyses.

Secreted protein analyses.

The urogenital complex was excised from the mice as described above, and the prostate was dissected from the urogenital complex in PBS. After being dried with paper towels to remove excessive PBS, the prostate was diced with scissors in 100 μl PBS containing 1 mM PMDF. The PBS-extracted secretory proteins were collected by centrifugation as described (Bhatia-Gaur et al., 1999). The protein concentration of the collected sample was normalized with PBS to a final concentration of 1 mg/ml. Samples equivalent to 25 μg proteins were separated on 5-20% gradient SDS PAGE, and the secretory proteins were visualized with Coomassie Brilliant Blue staining.

In situ hybridization and RT-PCR.

For in situ hybridization, paraffin embedded tissue sections were rehydrated and digested with protease K for 7 minutes at room temperature. After prehybridization at 70 °C for 2 hours, the hybridization was carried out by overnight incubation at 70 °C with 0.5 μg/ml digoxigenin-labeled RNA probes specific for FGFR2IIIB isoform. After being washed with 0.1X DIG washing buffer at 65 °C for 30 minutes for 4 times, specifically bound probes were detected by the alkaline phosphatase conjugated anti-digoxigenin antibody (Roche, Indianapolis, IN). For RT-PCR analyses, total RNA was extracted from dorsolateral prostates with the RNeasy Mini Kit (QIAGEN, Valencia, CA). Reverse transcriptions (RT) were carried out with SuperScript II (GIBCO/BRL, Life Technologies, Grand Island, NY) and random primers according to protocols provided by the manufacturer. The RT-PCR was carried out for 30 and 35 cycles, as indicated, at 94 °C for 1 minute, 55 °C for 1 minute and 72 °C for 1 minute with Taq DNA Polymerase (Promega, Madison, WI) and specific primers listed in Supplemental Table 1. RT-PCR

products were analyzed on 2% agarose gels, and the representing data from at least three repetitive experiments were shown. Real-time RT-PCR analyses were carried out with the SYBR Green JumpStart Taq Ready Mix (Sigma, St. Louis, Missouri) as suggested by the manufacture. Relative abundances of mRNA were calculated using the comparative threshold (CT) cycle method and normalized with the β-actin as internal controls. Data were means of three individual experiments.

RESULTS

Tissue-specific disruption of *Fgfr2* in the prostatic epithelium.

To determine whether FGFR2 was essential for prostatic development, the LoxP/Cre recombination system was used to conditionally inactivate the *Fgfr2* alleles in epithelial cells of the urogenital sinus at late embryonic stages (E17.5) by crossing the mice carrying LoxP flanked *Fgfr2* (*Fgfr2*^{flox}) alleles (Fig. 1A) (Yu et al., 2003) and an NKX3.1-Cre knock-in allele (Hu et al., 2006). Deletion of the sequence for exon 8-10 generated a defective allele encoding a truncated FGFR2 ectodomain as illustrated in Fig. 1B. These epithelial cells later gave rise to prostate epithelial cells. Mice carrying homozygous *Fgfr2*^{flox} and Nkx3.1-Cre alleles were viable, fertile, and had no apparent pathology. The prostates of mice carrying homozygous *Fgfr2*^{flox} alleles, or heterozygous *Fgfr2*^{flox} allele with or without the Nkx3.1 knock-in allele, had no noticeable differences in gross tissue morphology and histological structures from that of WT mice, and therefore were considered as control prostates, although only homozygous *Fgfr2*^{flox} mice were used as controls in most of the study.

Disruption of the *Fgfr2* in the prostate of 3-week-old males was confirmed in by PCR for the absence of the LoxP flanked exons (Fig. 1C). RT-PCR analyses of prostates in 7-day-old *Fgfr2*^{cn} mice with FGFR2IIIB-specific primers showed that expression of FGFR2IIIB was below the detection limit (Fig. 1D), same experiments with IIIc-specific primers or common primers for both IIIb and IIIc isoforms showed that expression of FGFR2 was significantly reduced in *Fgfr2*^{cn} prostates (Fig. 1D); indicating the residual FGFR2 expression was due to expression of FGFR2IIIC isoform in stromal cells or other minor cell populations. Similar results were derived from 3-week old prostates (data not

shown). Furthermore, in situ hybridization with FGFR2IIIB-specific probes showed that the expression of FGFR2 was diminished in the prostate epithelium (Fig. 1E). Morphological examination revealed that the *Fgfr2*^{cn} mice had a notably smaller prostate compared to WT mice. Only small and thin dp and lp lobes were apparent in the *Fgfr2*^{cn} prostates, which were also more transparent than control prostates. Since *Fgfr2*^{cn} dp and lp were small and closely connected, rendering them difficult to separate, the dp and lp were collectively referred to as dorsolateral prostates (dlp). Among the 45 *Fgfr2*^{cn} prostates examined at different ages, 42 exhibited only two dlp lobes. As for the remaining three mice, in addition to the 2 dlp lobes, one mouse also had a very small anterior lobe, one had a ventral lobe, and one had two small anterior and one ventral lobes. Subsequent analyses were mostly performed with the dlp.

Disruption of *Fgfr2* alleles in the prostate epithelium inhibited prostatic bud branching morphogenesis.

To better visualize the defects in prostatic development in *Fgfr2*^{cn} mice, the ROSA26 reporter allele (Soriano, 1999) was bred into the *Fgfr2*^{flox}/Nkx3.1-Cre mice. The disruption of *Fgfr2*^{flox} alleles should occur concurrently with activation of the lacZ reporter by excision of the floxed cassette in ROSA26 alleles. The lower urogenital track was then dissected from embryos and newborn pups for wholemount staining with X-Gal (Fig. 2A). Since the expression of Nkx3.1-Cre is initiated in urogenital sinus epithelial cells that give rise to prostate epitheliums between E17-17.5 days (Hu et al., 2006), X-Gal staining was not visible prior to E17.0 day, and was only weakly visible at E17.25 in a group of cells surrounding the urethra (data not shown). The staining became more prominent at E17.5 day in cells protruding in different directions, which

represent cells giving rise to the prostatic epithelium (Fig. 2A). At this stage, both *Fgfr2*^{cn} and control embryos developed well-defined ap, dlp, and vp buds; no significant difference in X-Gal staining patterns was observed between *Fgfr2*^{cn} and control animals. At E18.5, the X-Gal stained cells in control mice expanded in anterior, dorsolateral, and ventral directions (Fig. 2A, panel E18.5). In contrast, the same cells in *Fgfr2*^{cn} mice failed to expand in both anterior and ventral directions, so that the ap and vp buds remained to be similar to those in E17.5 embryos. Only the cells in dorsal and lateral directions expanded and developed into the dorsal and lateral lobes, respectively. The discrepancy in ap and vp bud formation in *Fgfr2*^{cn} and control mice became more significant at newborn stages. Only the expanding dlp lobes were visible at postnatal day 5 (Fig. 2A, panel P5). To further study the Cre expression pattern, the X-Gal stained tissues were paraffin embedded and sectioned (Fig. 2A, insert and data not shown). The result showed that expression of lacZ was activated homogenously in epithelia compartment in every lobe of *Fgfr2*^{cn} and control prostate, indicating that Nkx3.1 Cre efficiently and uniformly excised the silencing cassette in the ROSA26 locus in epithelial cells in every prostatic bud (Fig 2A). It is expected that the floxed *Fgfr2* alleles were similarly inactivated in all prostatic buds in the same time. Thus, the results implied that FGFR2 signals are more critical for branching morphogenesis for ap and vp than for dlp, although the underlying molecular mechanism is not clear.

Disruption of *Fgfr2* alleles in the prostate epithelium inhibited branching morphogenesis and growth of epithelial ducts.

To continue tracking prostate development in *Fgfr2*^{cn} mice, prostate tissues and the adjacent urethra were dissected from the mice at 2, 4, and 6 weeks. Although they are

always smaller and more transparent than that of normal prostates, *Fgfr2*^{cn} prostates substantially increased in size during pubertal development (Fig. 2B). The prostate is mainly composed of epithelial ducts packed tightly into a lobular structure. To determine whether the *Fgfr2*^{cn} prostates had fewer or smaller ducts than control prostates, the dorsolateral lobes of both *Fgfr2*^{cn} and control prostates were treated with collagenase and the epithelial ducts were subsequently separated (Fig. 2B, bottom panels a and b). The number of main ducts and total number of distal ductal tips were then quantified. The results revealed that the *Fgfr2*^{cn} prostates had fewer ducts than control prostates. The average number of main ducts in the *Fgfr2*^{cn} dorsolateral prostates was 7.2, compared to 12.5 in control prostates ($p<0.05$). The average number of distal ductal tips in *Fgfr2*^{cn} prostate was 58, compared to 113 in control prostates ($p<0.01$). Furthermore, the *Fgfr2*^{cn} ducts were shorter in length and smaller in diameter than those of the control prostates. This indicated that the disruption of the FGFR2 in prostatic bud epithelial cells inhibited both ductal branching morphogenesis and growth of epithelial ducts.

To investigate whether the FGFR2 kinase was required for rapid growth of prostate cells during pubertal development, proliferating cells in *Fgfr2*^{cn} and control prostates at the ages of 2, 4, and 6 weeks were assessed by immunostaining of proliferating cell nuclear antigen (PCNA). At the prepubertal age (2 weeks), the proliferating cells were mainly localized at the distal tips in both *Fgfr2*^{cn} and control prostates (Fig 2C). Data from 3 individual prostates showed that about 34.2±5.0% epithelial cells in *Fgfr2*^{cn} prostates and 36.2±4.4% in control prostates were actively engaged in proliferation. No significant difference was observed at this stage ($p>0.05$). At the age of 4 weeks when

the mice were undergoing rapid pubertal growth, the proliferating cells were widely distributed in the whole prostate. At this stage, the population of proliferating cells in *Fgfr2*^{cn} prostates was significantly smaller than that in control prostates (17.8±1.2% in *Fgfr2*^{cn} prostate, and 35.4±3.5% in control prostate, $p<0.01$). At the post pubertal age (6 weeks), the proliferating cell population in both *Fgfr2*^{cn} and control prostates was dramatically reduced (2.0±0.01% in *Fgfr2*^{cn} prostate, and 2.2±0.05% in control prostate, $p>0.05$), indicating that both *Fgfr2*^{cn} and control prostates were mature at this stage. Together, the result demonstrates that ablation of *Fgfr2* in prostate epithelium impaired cellular proliferation during pubertal growth.

Fgfr2^{cn} prostates had an underdeveloped epithelium compartment with reduced basal cell population.

Epithelial cells in each prostatic lobe normally exhibit a lobe-specific infolding and cellular morphology. Histological analyses showed that *Fgfr2*^{cn} prostate had less epithelial infolding compared to control prostates, especially in the anterior and dorsolateral lobes (Fig. 3A). The epithelial cells were less polarized with reduced columnarization, suggesting that deficient in resident FGFR2 disrupted completion of terminal differentiation in the epithelium. Notably, among the two adult *Fgfr2*^{cn} males having poorly developed ap prostates (out of 45 *Fgfr2*^{cn} mice examined), one had 2 ap lobes that exhibited a tissue structure similar to that of seminal vesicles (Fig. 3 and supplemental Fig. 1); the other one only had 1 lobe that had a tissue structure similar to the prostatic bud of newborn mice (data not shown). Nevertheless, semiquantitative RT-PCR (Fig. 3B) and real-time RT-PCR analyses of total RNA samples extracted from 3-week-old dorsolateral prostates revealed that ablation of *Fgfr2* in the prostate

epithelium did not significantly alter expression of key regulatory molecules for prostate organogenesis and growth, however, the expression of BMP4, TGF-β, and HoxD13 was somewhat reduced in *Fgfr2*^{cn} prostates. Data from real-time RT-PCR confirmed that the expression of BMP4 in *Fgfr2*^{cn} prostates was reduced by 55% ($p<0.001$); TGF-β by 53% ($p<0.001$), and HoxD13 by 58% ($p<0.001$). Similar to the data in Fig. 3B, real-time RT-PCR data also showed no significant difference in expression levels of all other tested molecules between *Fgfr2*^{cn} and control prostates (data not shown).

The epithelial compartment of mature prostates mainly consists of well-differentiated luminal epithelial cells that express cytokeratin 8 and basal epithelial cells that express p63 (Cunha et al., 2004; Kurita et al., 2004). The stromal compartment largely consists of smooth muscle cells that express α-actin and are keratin-deficient. To determine whether *Fgfr2*^{cn} prostates also expressed these characteristic markers, tissue sections were immunochemically analyzed with antibodies against cytokeratin 8, α-actin, and p63. The epithelial and stromal cells in *Fgfr2*^{cn} prostates expressed cytokeratin 8 and α-actin, respectively, at levels similar to that seen in control prostates (Fig. 4A). In contrast, the population of p63 positive basal cells in *Fgfr2*^{cn} prostates was significantly reduced compared to controls, both in growing and mature prostates (Fig. 4B,C). To quantitate the ratio of basal/luminal cells, P63 positive cells in the 3 sections per prostate were scored. Data from three individual experiments showed that the averages ratios of basal/luminal epithelial cells were 0.48 and 0.67 ($p<0.001$) in 2-week-old, 0.24 and 0.48 ($p<0.001$) in 4-week-old, and 0.20 and 0.34 ($p<0.001$) in 6-week-old *Fgfr2*^{cn} and control prostates, respectively, which validated the observation that the basal cells were reduced in *Fgfr2*^{cn} prostates.

Ablation of *Fgfr2* diminished androgen dependency with respect to maintenance of tissue homeostasis, but not production of the secretory proteins in prostates.

Androgens are critical for prostate development, tissue homeostasis, and production of secretory proteins. To ascertain that *Fgfr2*^{cn} mice were not deficient in androgens, serum androgen levels in *Fgfr2*^{cn} and control littermates were determined. No significant difference in serum androgens was observed. The average androgen concentration in *Fgfr2*^{cn} serum was 7.35 ± 8.0 ng/ml (n=12), and that of control was 8.9 ± 9.1 ng/ml (n=12). Thus, the defect in *Fgfr2*^{cn} prostate development was not a result of androgen insufficiency. To determine whether androgen was required for maintaining tissue homeostasis in *Fgfr2*^{cn} prostates, mice at the age of 6 weeks were orchiectomized to deprive androgens. Apoptotic cells in the prostates were subsequently assessed with TUNEL analyses (Fig. 5A). The results showed that apoptotic cells were seldom observed in *Fgfr2*^{cn} and control prostates prior to the castration. The apoptotic figures appeared in the epithelial compartment of control prostates within 1 day after castration, and became more abundant in day 2-4 after castration. In sharp contrast, only a limited number of apoptotic figures were detected in the epithelial compartment of *Fgfr2*^{cn} prostates, indicating that maintenance of cellular homeostasis in *Fgfr2*^{cn} prostates did not as stringently depend on androgen as in control prostates. H&E staining further demonstrated that significant tissue atrophy in the prostate of castrated control, but not the *Fgfr2*^{cn} males (Fig. 5B).

To investigate whether *Fgfr2*^{cn} prostates expressed AR similarly as in control prostates, immunostaining with anti-AR antibodies was carried out. The results revealed that both stromal and epithelial cells in *Fgfr2*^{cn} prostates expressed AR at levels

comparable to that detected in control prostates. As in control prostates, the majority of the AR was located in the nucleus of *Fgfr2*^{cn} prostate epithelial cells, indicating no abnormality in AR expression and nuclear translocation (Fig. 6, 0 day). To further investigate whether *Fgfr2*^{cn} prostates had defects in the AR subcellular localization after androgen deprivation, prostate sections from castrated control and *Fgfr2*^{cn} mice were immunostained with anti-AR antibodies. The results showed that 14 days after androgen deprivation, most of the AR in control prostates could only be found in cytoplasm (Fig. 6, 14 days), which was similar as reported earlier (Lee and Chang, 2003). Yet, even 14 days after the castration, a significant amount of AR was still localized in the nucleus of *Fgfr2*-deficient epithelial cells (Fig. 6, 14 days), which was in sharp contrast to control prostates where exhibited no nuclear localized AR at this time point. The prolonged nuclear localization of the AR in *Fgfr2*^{cn} prostates may explain why the mutant prostates were less androgen dependent, although the detailed molecular mechanism underlying this phenotype remains to be elucidated.

Two weeks after orchiectomy, control prostates underwent tissue atrophy and had a significant change in gross tissue appearance. Consistent with failing to induce apoptosis, the androgen deprivation also failed to induce significant tissue morphological changes in *Fgfr2*^{cn} prostates (Fig. 7A). H&E staining of tissue sections verified that no obvious changes in tissue morphology of *Fgfr2*^{cn} prostates were observed 14 days after the orchiectomy (Fig. 7B, 0 day). To further examine androgen effects in *Fgfr2*^{cn} prostates, time-release testosterone pellets were implanted into mice two weeks after orchiectomy. The prostates were then harvested from day 1 to 14 days after androgen replenishment for histological analyses. Results showed that androgen-replenishment

induced massive cellular proliferation in control prostates within two days (Fig. 7C,D), and the tissue architecture was restored by two weeks after the androgen therapy as reported elsewhere (Fig. 7B) (Sugimura et al., 1986b). In contrast, androgen treatments failed to induce significant proliferation in *Fgfr2*^{cn} prostates, (Fig. 7C,D), a marked contrast to control prostates in which over 90% of luminal epithelial cells were undergoing mitosis at day 2 after androgen treatment. Accordingly, the androgen replenishment also failed to induce significant histological changes in *Fgfr2*^{cn} prostates (Fig 7B).

Although budding of the prostate is androgen dependent, prostatic ductal morphogenesis in prenatal and neonatal stages is likely controlled by a combination of chronic androgen stimulation and an intrinsic “program” that is not well defined since neonatal castration only impairs about 60% of prostatic ductal branching (Donjacour and Cunha, 1988). To test whether ablation of FGFR2 signaling altered androgen dependency of neonatal prostatic morphogenesis, neonatal castration was carried out on *Fgfr2*^{cn} and control mice within 24 hours after birth. Results from 2- and 4-week-old neonatally castrated mice showed that the prostate continued to development in both *Fgfr2*^{cn} and control mice as reported earlier, although the dlp sizes were significantly smaller than those from uncastrated counterparts (Fig 8A). Microdissection analyses showed that the differences in complexity of the epithelial ductal network between *Fgfr2*^{cn} and control prostates were not curtailed. Thus, the results indicated that disruption of the FGFR2 signaling axis in the prostatic epithelium did not diminish androgen dependency for neonatal branching morphogenesis and pubertal growth of prostates. Together with adult tissue homeostasis data, the result implied divergence in

androgen controlling prostatic branching morphogenesis and growth and adult prostate tissue homeostasis.

A major function of prostates is to produce secretory proteins for semen. H&E staining showed that dp and lp lumens of *Fgfr2*^{cn} prostates had abundant eosinphilic substances (Fig. 3A), which likely represented prostatic secretory proteins. SDS-PAGE analyses of PBS-extracts from dlp lumens showed that as in control prostates, *Fgfr2*^{cn} prostates produced abundant secretory proteins (Fig 9A). Western blot and real-time RT-PCR showed that *Fgfr2*^{cn} prostates also produce probasin and PSP94 (prostatic secretory protein of 94 amino acids) although at reduced levels (Fig 9B, C). Both probasin and PSP94 are androgen-regulated characteristics secretory proteins of dorsolateral prostates in rodents (Huizen et al., 2005; Imasato et al., 2001; Johnson et al., 2000; Kasper and Matusik, 2000).

To clarify whether the secretory function of *Fgfr2*^{cn} prostates was androgen-regulated, prostate secretory proteins were extracted from adult *Fgfr2*^{cn} and control prostates two weeks after castration and analyzed as above. Results showed that the abundance of total soluble proteins (Fig. 9A), and of probasin and PSP94 (Fig. 9B), were significantly reduced in both *Fgfr2*^{cn} and control prostates two weeks after castration, even though H&E staining showed that lumen of *Fgfr2*^{cn} prostates was packed with a highly eosinphilic substance. The results suggest that the eosinphilic substances in prostate of castrated *Fgfr2*^{cn} mice were not PBS-extractable, and therefore, were not normal prostatic secretory proteins. The results showed that productions of probasin and PSP94, as well as other soluble secretory proteins, in *Fgfr2*^{cn} prostates remained to be controlled by the androgens as in control prostates.

Together, the data indicated that while ablation of the FGFR2 signaling axis in the prostatic epithelium diminished androgen activity in the regulation of homeostasis, it did not abrogate androgen activity in the regulation of secretory proteins production in prostates.

Discussion

***Disruption of Fgfr2 in prostate epithelium impaired prostatic morphogenesis*.** Despite a large body of indirect evidence, direct demonstration of FGFR2 kinase function in regulating prostatic development, as well as insight into how FGFR2 crosstalks with the androgen signaling axis has been hampered by its essential role in early embryonic development (De Moerlooze et al., 2000; Xu et al., 1998; Yu et al., 2003). Here we report that tissue-specific disruption of FGFR2 in prostate epithelium at E17.5 significantly impaired prostatic development. Most *Fgfr2*^{cn} mice developed only two dorsal and two lateral lobes of the prostate instead of the normal eight lobes (two anterior, two dorsal, two lateral, and two ventral). Although prostates devoid of FGFR2 in the epithelium retained general prostate tissue architecture and were active in generating secretory proteins, the epithelial compartment of *Fgfr2*^{cn} prostates had a poorly developed ductal structure characterized by less extensive intra-ductal infolding, suggesting that disruption of FGFR2 in the epithelium impaired branching morphogenesis.

The FGF10/FGFR2 signaling axis is important for prostate branching morphogenesis. The finding that ablation of FGFR2 in prostate epithelia significantly inhibits prostate branching morphogenesis is consistent with the notion that FGF10 functions as a mesenchymal paracrine regulator of epithelial growth in the prostate (Thomson and Cunha, 1999). Yet, prostatic phenotypes in *Fgfr2*^{cn} mice were generally less severe than in *Fgf10* null mice since most of *Fgf10* null embryos do not have prostatic buds with a few exceptions exhibiting poorly developed rudimentary prostatic buds (Donjacour et al., 2003). Furthermore, ex-vivo cultures of *Fgf10* null urogenital

sinus show that *Fgf10* null phenotypes can not be rescued by FGF10 alone, and can only be partially rescued by FGF10 together with testosterone, suggesting that deficient of FGF10 may not only cause defects in the epithelial compartment. Thus, the mechanism underlying *Fgf10*-null phenotypes in prostates is not simple. Here we showed that Nkx3.1 Cre only efficiently excised floxed sequences in epithelial cells in prostatic rudiments in the urogenital sinus, therefore, the defects in *Fgfr2*^{cn} prostates were likely direct phenotypes of deficiency in FGF10/FGFR2 signals. Thus, *Fgfr2*^{cn} prostates provide a good model to assess FGF10/FGFR2 signaling axis in prostate development and function.

Ablation of the Fgfr2 diminished androgen dependency with respect to tissue homeostasis but not secretory function. In contrast to adult WT prostates that were stringently androgen-dependent, tissue homeostasis in adult *Fgfr2*^{cn} prostates was less androgen dependent since androgen deprivation failed to induce tissue degeneration in adult *Fgfr2*^{cn} prostates within 2 weeks. Neonatal prostatic morphogenesis is controlled by both androgen dependent and independent mechanisms (Donjacour and Cunha, 1988). The androgen independent regulation is likely diminished during development because adult prostates is strictly androgen dependent. Interestingly, ablation of FGFR2 did not alter androgen dependency for neonatal branching morphogenesis and pubertal growth of the prostate. Together, the results suggest that FGFR2 signaling is important not only for prostate organogenesis and growth, but is also for the prostate to be developed into a strict androgen dependent organ with respect to tissue homeostasis. Interestingly, AR expression remained intact in both the epithelial and stromal compartments of *Fgfr2*^{cn} prostates, and the androgen signaling axis remained active in

controlling secretory protein production in mutant prostates. Thus, it appears that the androgen signaling axis regulates tissue homeostasis and function through different pathways.

The AR in mesenchymal cells is both essential and sufficient for promoting epithelial branching morphogenesis and growth during prostate development (Cunha et al., 2004). Function of the epithelial AR is not understood, although it has been reported to be required for stromal cell differentiation (Thomson, 2001). Data from this study suggest that the androgen may regulate tissue homeostasis and production of secretory protein through different mechanisms; it is also androgens regulate the secretory function of epithelial cells directly through the AR signaling pathways within the cells and regulate tissue homeostasis through bidirectional communication between the stromal and epithelial compartments. The stromal AR-mediated signals for prostate development and homeostasis have been proposed to be mediated by paracrine growth factors that have been referred to as andromedins. Although FGF7 and FGF10 are proposed to be candidate andromedins in rat prostate tumor models (Lu et al., 1999; Yan et al., 1992), and ablation of FGF10 disrupts development of male secondary sex organs, including the prostate (Donjacour et al., 2003), no evidence showed that expression of FGF10 is androgen regulated in normal prostates (Thomson, 2001; Thomson and Cunha, 1999). Thus, whether FGF10 functions as an andromedin for prostate development remains to be a question. Although this study did not address the andromedin issue, the data here demonstrated that FGFR2 signals were important for prostate to develop into a strictly androgen dependent organ.

Reduced p63-positive basal cells in the Fgfr2^{cn} prostate. The p63-expressing basal cells are a small population of epithelial cells localized as a discontinuous layer between the luminal epithelial cells and the basement membrane, and which account for about 10% of cells in mature prostate epithelium. The prostatic basal compartment has been proposed to consist of a pool of cellular subtypes that include tissue stem cells and transient/amplifying progenitor cells that give rise to terminally differentiated cells (Lam and Reiter, 2006; Rizzo et al., 2005; Tokar et al., 2005). However, the cell lineage relationship between luminal and basal cells is unclear since the elimination of basal cells by p63 ablation does not affect neuroendocrine (NE) and luminal epithelial cell populations (Kurita et al., 2004). Here we show that prostate rudiments and growing prostates exhibit a higher ratio of basal/luminal epithelial cells, the population of which was gradually reduced as prostates matured (Fig. 4B). Disruption of the FGFR2 signaling axis in prostates significantly reduced the basal cell population, especially in mature prostates. FGF7 has been suggested to have a negative effect on maintenance of basal cell properties in cell culture by promoting differentiation (Heer et al., 2006). Yet, our results suggest that the FGFR2 signaling is most likely essential for maintaining basal cell populations in the prostate. Since Nkx3.1-Cre was expressed in both basal and luminal epithelial cells, it is possible that FGFR2 either directly controls the basal cell population and their fate determination within the cells, or indirectly through regulatory communications between luminal and basal epithelial cells. Further efforts are needed to address this issue.

Development of dlp is less FGFR2 signaling dependent. Experiments with the ROSA26 reporter indicated that the Nkx3.1-Cre was expressed in all buds concomitantly

between E17.25 and E17.5, indicative that the *Fgfr2* alleles were ablated in all prostatic buds at the same time. Similar to previous reports (Cunha et al., 2004; Thomson, 2001), data in Fig 2A showed that the buds for each prostatic lobe appeared at E17.5. No significant difference was noticeable between *Fgfr2*^{cn} and control prostates at this stage. The defects in ap and vp development in *Fgfr2*^{cn} mice apparently occurred between E17.5 and E18.5. Together with the notion that FGFR2IIIB is expressed in the central to distal tips of the elongating ducts in every prostatic bud during branching morphogenesis (Huang et al., 2005), the results indicate that the development of ap and vp buds is more FGFR2 signal dependent, and that the function of FGFR2 in rodent prostates is lobe-specific. Future experiments with FGFR2IIIB isoform null will be carried out to validate this finding. Differential responses to regulatory signals among the prostatic lobes are not uncommon in rodent. For example, treating pregnant females with ligands for aryl hydrocarbon receptors also exhibits a lobe-specific inhibition of prostate branching morphogenesis in mouse (Ko et al., 2002), ablation of Hoxa10 in mice causes partial ap-dlp transformation (Marker et al., 2001; Podlasek et al., 1999) .

It appears that, relative to other prostatic lobes, the dlp has more potential to escape from strict regulation by the FGFR2 and androgen signaling axes with respect to growth and tissue homeostasis. The dlp in rodents is the most similar to the peripheral zone of human prostates in regards to tissue structure, where most prostate cancer arises. Together with the fact that the majority of malignant prostate cancers lose FGFR2 expression and are not androgen responsive (Giri et al., 1999a; Kwabi-Addo et al., 2001; McKeehan et al., 1998; Wang and McKeehan, 2003), and that disruption of the FGFR2 signaling axis has been associated with the progression of prostate lesions in mouse

models (Jin et al., 2003a; Polnaszek et al., 2003), the results support a model in which loss of FGFR2 signaling contributes to the escape from androgen regulation in prostate cancer cells.

Prostate development is orchestrated by multiple signaling pathways that include Shh, Notch, BMPs, and FGFs. FGF10 has been shown to regulate expression of multiple morphoregulatory genes, including Shh, BMP4, BMP7, Hoxb13, and Nkx3.1 (Huang et al., 2005). Here we demonstrated that expression of Shh, BMP7, Nkx3.1, Notch, HoxB13, β-catenin, Foxa1, FGF7, and FGF10 in *Fgfr2*^{cn} prostates at the mRNA level was similar to that seen in control prostates, although expression of TGF-β, BMP4, and Hox D13 was reduced in *Fgfr2*^{cn} prostates. The Nkx3.1-Cre mice carry a Cre knock-in allele that is also null for Nkx3.1, which causes slight changes in prostate ductal morphogenesis, as well as in secretory protein expression in ap and vp (Hu et al., 2006). Quantitative RT-PCR results showed no significant changes in Nkx3.1 expression in the dlp of *Fgfr2*^{cn} mice, indicating that the abnormalities in prostate organogenesis and androgen dependency were independent of Nkx3.1 heterozygosity.

In summary, we established that the FGFR2 tyrosine kinase plays a major role in tissue organogenesis and androgen regulation in the prostate. The prostate devoid of resident epithelial FGFR2 kinase responded poorly to androgens with respect to cellular homeostasis. This may provide a useful animal model for scrutinizing not only the molecular mechanisms behind the regulation of prostate growth, homeostasis, and function by androgens, but also the means by which advanced prostate cancer escapes strict regulation by androgens.

models (Jin et al., 2003a; Polnaszek et al., 2003), the results support a model in which loss of FGFR2 signaling contributes to the escape from androgen regulation in prostate cancer cells.

Prostate development is orchestrated by multiple signaling pathways that include Shh, Notch, BMPs, and FGFs. FGF10 has been shown to regulate expression of multiple morphoregulatory genes, including Shh, BMP4, BMP7, Hoxb13, and Nkx3.1 (Huang et al., 2005). Here we demonstrated that expression of Shh, BMP7, Nkx3.1, Notch, HoxB13, β-catenin, Foxa1, FGF7, and FGF10 in *Fgfr2*^{cn} prostates at the mRNA level was similar to that seen in control prostates, although expression of TGF-β, BMP4, and Hox D13 was reduced in *Fgfr2*^{cn} prostates. The Nkx3.1-Cre mice carry a Cre knock-in allele that is also null for Nkx3.1, which causes slight changes in prostate ductal morphogenesis, as well as in secretory protein expression in ap and vp (Hu et al., 2006). Quantitative RT-PCR results showed no significant changes in Nkx3.1 expression in the dlp of *Fgfr2*^{cn} mice, indicating that the abnormalities in prostate organogenesis and androgen dependency were independent of Nkx3.1 heterozygosity.

In summary, we established that the FGFR2 tyrosine kinase plays a major role in tissue organogenesis and androgen regulation in the prostate. The prostate devoid of resident epithelial FGFR2 kinase responded poorly to androgens with respect to cellular homeostasis. This may provide a useful animal model for scrutinizing not only the molecular mechanisms behind the regulation of prostate growth, homeostasis, and function by androgens, but also the means by which advanced prostate cancer escapes strict regulation by androgens.

Donjacour, A. A., Thomson, A. A. and Cunha, G. R. (2003). FGF-10 plays an essential role in the growth of the fetal prostate. *Dev Biol* **261**, 39-54.

Dorkin, T. J., Robinson, M. C., Marsh, C., Bjartell, A., Neal, D. E. and Leung, H. Y. (1999). FGF8 over-expression in prostate cancer is associated with decreased patient survival and persists in androgen independent disease. *Oncogene* **18**, 2755-61.

Giri, D., Ropiquet, F. and Ittmann, M. (1999a). Alterations in expression of basic fibroblast growth factor (FGF) 2 and its receptor FGFR-1 in human prostate cancer. *Clin Cancer Res* **5**, 1063-71.

Giri, D., Ropiquet, F. and Ittmann, M. (1999b). FGF9 is an autocrine and paracrine prostatic growth factor expressed by prostatic stromal cells. *J Cell Physiol* **180**, 53-60.

Gnanapragasam, V. J., Robson, C. N., Neal, D. E. and Leung, H. Y. (2002). Regulation of FGF8 expression by the androgen receptor in human prostate cancer. *Oncogene* **21**, 5069-80.

Hayward, S. W., Haughney, P. C., Rosen, M. A., Greulich, K. M., Weier, H. U., Dahiya, R. and Cunha, G. R. (1998). Interactions between adult human prostatic epithelium and rat urogenital sinus mesenchyme in a tissue recombination model. *Differentiation* **63**, 131-40.

Hayward, S. W., Rosen, M. A. and Cunha, G. R. (1997). Stromal-epithelial interactions in the normal and neoplastic prostate. *Br J Urol* **79 Suppl 2**, 18-26.

Heer, R., Collins, A. T., Robson, C. N., Shenton, B. K. and Leung, H. Y. (2006). KGF suppresses {alpha}2{beta}1 integrin function and promotes differentiation of the transient amplifying population in human prostatic epithelium. *J Cell Sci* **119**, 1416-24.

Hu, Y. P., Price, S. M., Chen, Z., Banach-Petrosky, W. A., Abate-Shen, C. and Shen, M. M. (2006). (manuscript in preperation).

Huang, L., Pu, Y., Alam, S., Birch, L. and Prins, G. S. (2005). The role of Fgf10 signaling in branching morphogenesis and gene expression of the rat prostate gland: lobe-specific suppression by neonatal estrogens. *Dev Biol* **278**, 396-414.

Huizen, I. V., Wu, G., Moussa, M., Chin, J. L., Fenster, A., Lacefield, J. C., Sakai, H., Greenberg, N. M. and Xuan, J. W. (2005). Establishment of a serum tumor marker for preclinical trials of mouse prostate cancer models. *Clin Cancer Res* **11**, 7911-9.

Imasato, Y., Onita, T., Moussa, M., Sakai, H., Chan, F. L., Koropatnick, J., Chin, J. L. and Xuan, J. W. (2001). Rodent PSP94 gene expression is more specific to the dorsolateral prostate and less sensitive to androgen ablation than probasin. *Endocrinology* **142**, 2138-46.

Jin, C., McKeehan, K., Guo, W., Jauma, S., Ittmann, M. M., Foster, B., Greenberg, N. M., McKeehan, W. L. and Wang, F. (2003a). Cooperation between ectopic FGFR1 and depression of FGFR2 in induction of prostatic intraepithelial neoplasia in the mouse prostate. *Cancer Res* **63**, 8784-8790.

Jin, C., McKeehan, K. and Wang, F. (2003b). Transgenic mouse with high Cre recombinase activity in all prostate lobes, seminal vesicle, and ductus deferens. *Prostate* **57**, 160-4.

Jin, C., Wang, F., Wu, X., Yu, C., Luo, Y. and McKeehan, W. L. (2004). Directionally specific paracrine communication mediated by epithelial FGF9 to stromal FGFR3 in two-compartment premalignant prostate tumors. *Cancer Res* **64**, 4555-62.

Johnson, M. A., Hernandez, I., Wei, Y. and Greenberg, N. (2000). Isolation and characterization of mouse probasin: An androgen-regulated protein specifically expressed in the differentiated prostate. *Prostate* **43**, 255-62.

Kasper, S. and Matusik, R. J. (2000). Rat probasin: structure and function of an outlier lipocalin. *Biochim Biophys Acta* **1482**, 249-58.

Ko, K., Theobald, H. M. and Peterson, R. E. (2002). In utero and lactational exposure to 2,3,7,8-tetrachlorodibenzo-p-dioxin in the C57BL/6J mouse prostate: lobe-specific effects on branching morphogenesis. *Toxicol Sci* **70**, 227-37.

Kurita, T., Medina, R. T., Mills, A. A. and Cunha, G. R. (2004). Role of p63 and basal cells in the prostate. *Development* **131**, 4955-64.

Kwabi-Addo, B., Ropiquet, F., Giri, D. and Ittmann, M. (2001). Alternative splicing of fibroblast growth factor receptors in human prostate cancer. *Prostate* **46**, 163-72.

Lam, J. S. and Reiter, R. E. (2006). Stem cells in prostate and prostate cancer development. *Urol Oncol* **24**, 131-40.

Lee, D. K. and Chang, C. (2003). Endocrine mechanisms of disease: Expression and degradation of androgen receptor: mechanism and clinical implication. *J Clin Endocrinol Metab* **88**, 4043-54.

Liu, W., Selever, J., Murali, D., Sun, X., Brugger, S. M., Ma, L., Schwartz, R. J., Maxson, R., Furuta, Y. and Martin, J. F. (2005). Threshold-specific requirements for Bmp4 in mandibular development. *Dev Biol* **283**, 282-93.

Lu, W., Luo, Y., Kan, M. and McKeehan, W. L. (1999). Fibroblast growth factor-10. A second candidate stromal to epithelial cell andromedin in prostate. *J Biol Chem* **274**, 12827-34.

Marker, P. C., Stephan, J. P., Lee, J., Bald, L., Mather, J. P. and Cunha, G. R. (2001). fucosyltransferase1 and H-type complex carbohydrates modulate epithelial cell proliferation during prostatic branching morphogenesis. *Dev Biol* **233**, 95-108.

McIntosh, I., Bellus, G. A. and Jab, E. W. (2000). The pleiotropic effects of fibroblast growth factor receptors in mammalian development. *Cell Struct Funct* **25**, 85-96.

McKeehan, W. L., Wang, F. and Kan, M. (1998). The heparan sulfate-fibroblast growth factor family: diversity of structure and function. *Prog Nucleic Acid Res Mol Biol* **59**, 135-76.

Ornitz, D. M. (2000). FGFs, heparan sulfate and FGFRs: complex interactions essential for development. *Bioessays* **22**, 108-12.

Pirtskhalaishvili, G. and Nelson, J. B. (2000). Endothelium-derived factors as paracrine mediators of prostate cancer progression. *Prostate* **44**, 77-87.

Podlasek, C. A., Seo, R. M., Clemens, J. Q., Ma, L., Maas, R. L. and Bushman, W. (1999). Hoxa-10 deficient male mice exhibit abnormal development of the accessory sex organs. *Dev Dyn* **214**, 1-12.

Polnaszek, N., Kwabi-Addo, B., Peterson, L. E., Ozen, M., Greenberg, N. M., Ortega, S., Basilico, C. and Ittmann, M. (2003). Fibroblast growth factor 2 promotes tumor progression in an autochthonous mouse model of prostate cancer. *Cancer Res* **63**, 5754-60.

Polnaszek, N., Kwabi-Addo, B., Wang, J. and Ittmann, M. (2004). FGF17 is an autocrine prostatic epithelial growth factor and is upregulated in benign prostatic hyperplasia. *Prostate* **60**, 18-24.

Powers, C. J., McLeskey, S. W. and Wellstein, A. (2000). Fibroblast growth factors, their receptors and signaling. *Endocr Relat Cancer* **7**, 165-97.

Rizzo, S., Attard, G. and Hudson, D. L. (2005). Prostate epithelial stem cells. *Cell Prolif* **38**, 363-74.

Ropiquet, F., Giri, D., Kwabi-Addo, B., Mansukhani, A. and Ittmann, M. (2000). Increased expression of fibroblast growth factor 6 in human prostatic intraepithelial neoplasia and prostate cancer. *Cancer Res* **60**, 4245-50.

Ropiquet, F., Giri, D., Lamb, D. J. and Ittmann, M. (1999). FGF7 and FGF2 are increased in benign prostatic hyperplasia and are associated with increased proliferation. *J Urol* **162**, 595-9.

Song, Z., Wu, X., Powell, W. C., Cardiff, R. D., Cohen, M. B., Tin, R. T., Matusik, R. J., Miller, G. J. and Roy-Burman, P. (2002). Fibroblast Growth Factor 8 Isoform b Overexpression in Prostate Epithelium: A New Mouse Model for Prostatic Intraepithelial Neoplasia. *Cancer Res.* **62**, 5096-5105.

Soriano, P. (1999). Generalized lacZ expression with the ROSA26 Cre reporter strain. *Nat Genet* **21**, 70-1.

Sugimura, Y., Cunha, G. R. and Donjacour, A. A. (1986a). Morphogenesis of ductal networks in the mouse prostate. *Biol Reprod* **34**, 961-71.

Sugimura, Y., Cunha, G. R. and Donjacour, A. A. (1986b). Morphological and histological study of castration-induced degeneration and androgen-induced regeneration in the mouse prostate. *Biol Reprod* **34**, 973-83.

Thomson, A. A. (2001). Role of androgens and fibroblast growth factors in prostatic development. *Reproduction* **121**, 187-95.

Thomson, A. A. and Cunha, G. R. (1999). Prostatic growth and development are regulated by FGF10. *Development* **126**, 3693-701.

Tokar, E. J., Ancrile, B. B., Cunha, G. R. and Webber, M. M. (2005). Stem/progenitor and intermediate cell types and the origin of human prostate cancer. *Differentiation* **73**, 463-73.

Wang, F., McKeehan, K., Yu, C., Ittmann, M. and McKeehan, W. L. (2004). Chronic activity of ectopic type 1 fibroblast growth factor receptor tyrosine kinase in prostate epithelium results in hyperplasia accompanied by intraepithelial neoplasia. *Prostate* **58**, 1-12.

Wang, F. and McKeehan, W. L. (2003). The fibroblast growth factor (FGF) signaling complex. Handbook of Cell Signaling. New York: Academic/Elsevier Press.

Wang, Q., Stamp, G. W., Powell, S., Abel, P., Laniado, M., Mahony, C., Lalani, E. N. and Waxman, J. (1999). Correlation between androgen receptor expression and FGF8 mRNA levels in patients with prostate cancer and benign prostatic hypertrophy. *J Clin Pathol* **52**, 29-34.

Xu, X., Weinstein, M., Li, C., Naski, M., Cohen, R. I., Ornitz, D. M., Leder, P. and Deng, C. (1998). Fibroblast growth factor receptor 2 (FGFR2)-mediated reciprocal regulation loop between FGF8 and FGF10 is essential for limb induction. *Development* **125**, 753-65.

Yan, G., Fukabori, Y., Nikolaropoulos, S., Wang, F. and McKeehan, W. L. (1992). Heparin-binding keratinocyte growth factor is a candidate stromal-to- epithelial-cell andromedin. *Mol Endocrinol* **6**, 2123-8.

Yu, K., Xu, J., Liu, Z., Sosic, D., Shao, J., Olson, E. N., Towler, D. A. and Ornitz, D. M. (2003). Conditional inactivation of FGF receptor 2 reveals an essential role for FGF signaling in the regulation of osteoblast function and bone growth. *Development* **130**, 3063-74.

Figure Legends

Fig. 1. Disruption of the *Fgfr2* alleles in prostate epithelium. A. Schematic of the floxed *Fgfr2* alleles for conditional disruption. The genomic DNA containing exons 6-10 and adjacent introns was shown. Excision of exons 8, 9, and 10 with Cre recombinase deletes the coding sequence of immunoglobulin-like (Ig)-loop III and the transmembrane domain and inactivates the *Fgfr2* alleles. The primers for PCR genotyping and FGFR2 expression analyses were indicated with arrows. **B.** The $Fgfr2^{cn}$ alleles only encode a truncated FGFR2 ectodomain that consist of 2½ Ig-loops. **C.** PCR genotyping for the *Fgfr2 conditional null* alleles. Genomic DNAs extracted from different lobes of $Fgfr2^{cn}$ and control prostates of 4-week-old mice were PCR analyzed with the indicated primers. Primers f1 and f2 amplify fragments of 142 bps from the *WT and 207 bps from the floxed Fgfr2* alleles. Primer f1 and f3 amplify a fragment of 471 bps from the *Fgfr2* null allele, no amplification for the WT *Fgfr2* or $Fgfr2^{flox}$ alleles. **D, E**. Diminished FGFR2 expression in the epithelium of $Fgfr2^{cn}$ prostates. The expression of FGFR2 at the mRNA level assessed with RT-PCR (**D**) and in situ hybridization (**E**). Primers R2f and R2r amplify both IIIb and IIIc isoforms; b and t only amplify IIIb isoform and c and to only amplify IIIc isoform. -, negative control without cDNA templates; ap, anterior prostate; dlp, dorsolateral prostate; vp, ventral prostate; S, signal peptide; I, II, III, immunoglobulin loop I, II, III domains of FGFR2, respectively; TM, the transmembrane domain of FGFR2; F/F, homozygous $Fgfr2^{flox}$ mice; CN, $Fgfr2^{cn}$ mice.

Fig. 2. Disruption of *Fgfr2* alleles in prostate perturbed prostate morphogenesis. A. The urogenital sinuses were dissected from embryos or postnatal pups carrying

ROSA26 reporter/Nkx3.1 Cre, and *Fgfr2*^{flox} or wildtype *Fgfr2* alleles at the indicated days. The tissues were lightly fixed and stained with X-Gal as described. The stained tissues representing each prostatic lobe were indicated. Note that no significant difference was shown in prostatic buds on E17.5 days between *Fgfr2*^{cn} and wildtype controls. Insert, section from the same tissue showing that Nkx3.1 Cre efficiently excised the silencing cassette of the ROSA26 allele. **B.** The prostate and urethra were dissected from 2-, 4-, and 6-week-old mice with the indicated genotypes (left panels). Right panels, dorsolateral prostate lobes dissected from tissues showed in left panels. a, b, the epithelial ducts were dissected from dorsolateral prostates of 6-week-old mice with the indicated genotypes. **C.** Disruption of FGFR2 in epithelium reduced prostatic cell proliferation in adolescent mice. The prostate tissues were collected from *Fgfr2*^{cn} and control mice at the indicated ages, and proliferating cells were identified immunohistochemically by expression of PCNA. Inserts, high magnification views from the same sections. ap, anterior prostate; dlp, dorsolateral prostate; vp, ventral prostate; u, urethra. F/F, homozygous *Fgfr2*^{flox} mice; CN, *Fgfr2*^{cn} mice; b, bladder; s, seminal vesicle; E17.5, and E18.5, embryonic day 17.5 and 18.5, respectively; P0 and P5, postnatal day 0 and 5, respectively. Scar bars in B equal to 2 millimeters.

Fig. 3. *Fgfr2*^{cn} prostates exhibited basic prostate characteristics. A. Prostate tissues from 6-week-old mice were sectioned and stained with H&E for histological analyses. Inserts, high magnification views from the same tissues. **B.** Total RNAs were extracted from dorsolateral prostates of 3-week-old *Fgfr2*^{cn} and control mice and reverse translated with random hexanucleotide primers. RT-PCR was performed as

indicated, with β-actin and Gapdh as internal standards. Cycle numbers of amplification are indicated on the top. **C**. Real-time RT-PCR analyses of the same panel of molecules as in **B**. Data were normalized with β-actin loading control and were expressed as folds of difference from the control prostates. Only the results with significant differences were shown. Data were means of triplicate samples. *, $p<0.001$; F/F, homozygous *Fgfr2*^{flox} mice; CN, *Fgfr2*^{cn} mice; ap, anterior prostate; dp, dorsal prostate; lp, lateral prostate; vp, ventral prostate.

Fig. 4. Immunohistochemical characterization of the *Fgfr2*^{cn} prostate. **A**. The tissue sections of *Fgfr2*^{cn} and control prostates from 4-week-old mice were prepared and immunohistochemically stained with anti-α-actin or anti-cytokeratin 8 as indicated. **B**. Reduced population of p63 positive basal cells in *Fgfr2*^{cn} prostates. Prostate sections from *Fgfr2*^{cn} and control mice at the indicated ages were immunohistochemically stained with anti-p63 antibodies. Inserts, high magnification views from the same section. **C**. Ratios of p63 positive cells in the epithelial compartment were calculated from three samples. Data representing means and standard errors of triplicate sample. F/F, homozygous *Fgfr2*^{flox} mice; CN, *Fgfr2*^{cn} mice.

Fig. 5. Diminished androgen dependency in *Fgfr2*^{cn} prostates with respect to tissue homeostasis. A. Androgen deprivation only weakly induced epithelial cell apoptosis in *Fgfr2*^{cn} prostates. *Fgfr2*^{cn} and control mice were orchiectomized to eliminate testis-derived androgens. At the indicated day after the operation, the prostate tissues were harvested and apoptotic cells were detected with TUNEL assay.

B. H&E staining of the same tissues showing that castration failed to induce tissue atrophy in *Fgfr2*^{cn} prostates. F/F, homozygous *Fgfr2*^{flox} mice; CN, *Fgfr2*^{cn} mice.

Fig. 6. Expression of the AR in *Fgfr2*^{cn} prostates. Expression of the AR in *Fgfr2*^{cn} and control prostates from 6-week-old mice was assessed with anti-AR antibodies on tissue sections before (0 day) and at the indicated days after castration as described in Materials and Methods. Note that a considerate amount of AR in *Fgfr2*^{cn} prostates remained in the nuclei at day 14 after the castration. ap, anterior prostate; dp, dorsal prostate; lp, lateral prostate; vp, ventral prostate. F/F, homozygous *Fgfr2*^{flox} mice; CN, *Fgfr2*^{cn} mice.

Fig. 7. *Fgfr2*^{cn} prostate only weakly responded to androgen replenishment. A. Gross tissue appearance of dorsolateral prostates from *Fgfr2*^{cn} and control mice two weeks after castration or uncastrated mice at the same age. **B**. Dorsolateral prostates were dissected from *Fgfr2*^{cn} and control mice two weeks after castration (0 day), and at the indicated days after the androgen replenishment. **C**. The sections were immunostained with anti-PCAN antibodies to reveal the cells active in proliferation. **D**. The mean percentage of PCNA positive cells in regenerating prostates was calculated from 3 samples. Inserts, higher magnification views of the same tissue. Data representing means of triplicate samples. CN, *Fgfr2*^{cn} mice; F/F, *Fgfr2*^{flox} homozygous mice.

Fig. 8. Prostate development in *Fgfr2^{cn}* and control mice was partially inhibited by neonatal castration. Left panels, gross tissue appearance of prostates from *Fgfr2^{cn}* and control mice with or without neonatal castration at the indicated ages. Right panels, the same tissues as in left panels were microdissected to reveal the detailed ductal structures. CN, *Fgfr2^{cn}* mice; F/F, *Fgfr2^{flox}* homozygous mice; scale bar, 1 mm.

Fig. 9. Production of secretory proteins in *Fgfr2^{cn}* prostates remained to be androgen-dependent. **A**. Profiles of PBS-extractable secretory proteins in dorsolateral prostates. The secretory proteins collected from dorsolateral prostates of 2-month-old mice with the indicated genotypes were separated on 5-20% gradient SDS-PAGE and stained with Coomassie Brilliant Blue G250. **B.** Protein level of probasin and PSP94 in *Fgfr2^{cn}* prostates. The PBS-extracted prostatic secretory proteins from castrated or uncastrated mice were separated on SDS-PAGE and Western blotted with anti-probasin and PSP94 antibodies as indicated. **C.** Total RNA was extracted from uncastrated adult in *Fgfr2^{cn}* and control prostates and expression of probasin and PSP94 was determined by quantitative real-time PCR. Expression levels were normalized to that of β-actin that served as an internal loading control. The expression of each gene in control prostates was set to 1. Data are mean±SD of three independent experiments. F/F, homozygous *Fgfr2^{flox}* mice; CN, *Fgfr2^{cn}* mice.

Supplemental table 1: Nucleotide sequence of primers:

β-actin: GCA CCA AGG TGT GAT GGT G and GGA TGC CAC AGG ATT CCA TA;

BMP4: AGG AGG AGG AGG AAG AGC AG and TGT GAT GAG GTG TCC AGG AA;

BMP7: ACC TGG GCT TAC AGC TCT CTG T and CGG AAG CTG ACG TAC AGC TCA TG;

β-catenin: GGT GGA CTG CAG AAA ATG GT and TCG CTG ACT TGG GTC TGT CA;

FGF7: GGT GAG AAG ACT GTT CTG TC and GTG TGT CCA TTT AGC TGA TG;

FGF10: TGT GCG GAG CTA CAA TCA CC and GAT GCA TAG GTG TTG TAT CC;

FGFR2: GGG AAG GAG TTT AAG CAG GAG CAT and CTT CAG GAC CTT GAG GTA GGG CAG;

FGFR2IIIB: GCA CTC GGG GAT AAA TAG CTC and TGT TAC CTG TCT CCG CAG;

FGFR2IIIC: AGC TGC CGG TGT TAA CAC CAC and TGT TAC CTG TCT CCG CAG;

Foxa1: CCA TGA ACA GCA TGA CTG CG and TCG TGA TGA GCG AGA TGT AGG A;

Foxa2: GTG AAG ATG GAA GGG CTC GA and AGA CTC GGA CTC AGG TGA GG;

Gapdh: GGT GGA GCC AAA AGG GTC AT and GGC CAT CAC GCC ACA GCT TT,

Gli1: GAA GGA ATC CGT GTG CCA TT and GGA TCT GTG TAG CGC TTG GT;

Gli2: GGC ACC AAC CCT TCA GAC TA and CTG AGC TGC TCC TGG AGT TG;

Gli3: GTC AGC CCT GCG GAA TAC TA and GGA ACC ACT TGC TGA AGA GC;

HoxB13: GAT GTG TTG CCA AGG TGA ACA and TGA AAC CAG ATG GTA ATC TGG CG;

HoxD13: GCA AGA GCC AAG GAA GTG TC and TCG GTA GAC GCA CAT GTC CG;

Nkx3.1: ATT GTT CCG TGT CCC TTG TT and GTT TCT ACC AGT TCA GGT GT;

Notch1: CCC ACT GTG AAC TGC CCT AT and CAC CCA TTG ACA CAC ACA CA;

Ptch1: TCA ACC CAG CCG ACC CAG ATT and CCC TGA AGT GTT CAT ACA TTT GCT TGG;

Shh: ACA TCC ACT GTT CTG TGA AAG CA and TCT CGA TCA CGT AGA AGA CCT TCT TGG;

TGF-β1: CTA ATG GTG GAC CGC AAC AA and GTA CAA CTC CAG TGA CGT CA;

Wnt1: AAG ATC GTC AAC CGA GGC TG and CAT TTG CAC TCT TGG CGC AT;

Fig. 1

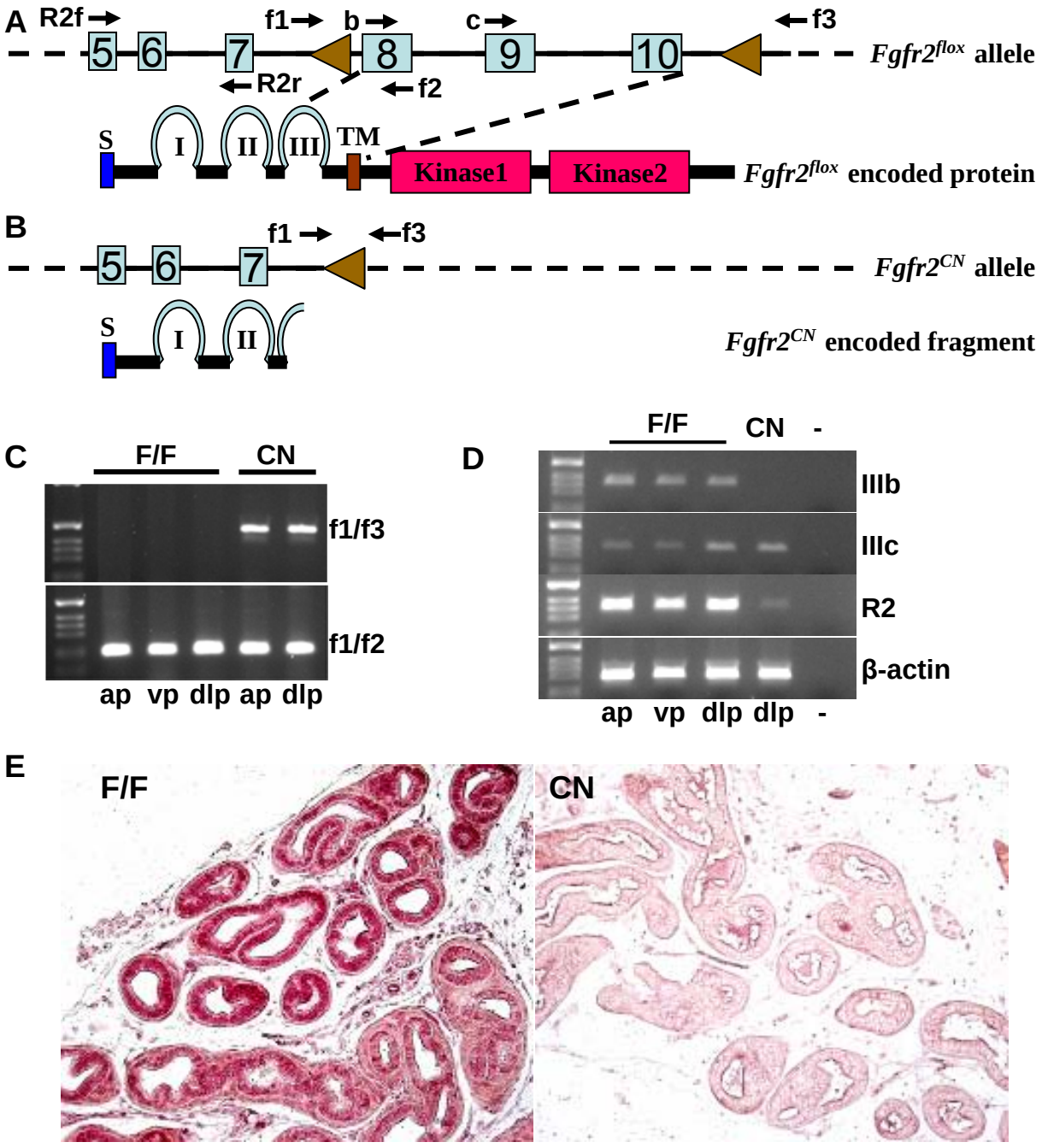
A
R2f
f1
b
c
f3
5
6
7
8
9
10
R2r
f2
Fgfr2flox allele
S
I
II
III
TM
Kinase1
Kinase2
Fgfr2flox encoded protein
B
f1
f3
Fgfr2CN allele
S
I
II
Fgfr2CN encoded fragment
C
F/F
CN
f1/f3
f1/f2
ap
vp
dlp
ap
dlp
D
F/F
CN
-
IIIb
IIIc
R2
β-actin
ap
vp
dlp
dlp
-
E
F/F
CN

Fig. 2

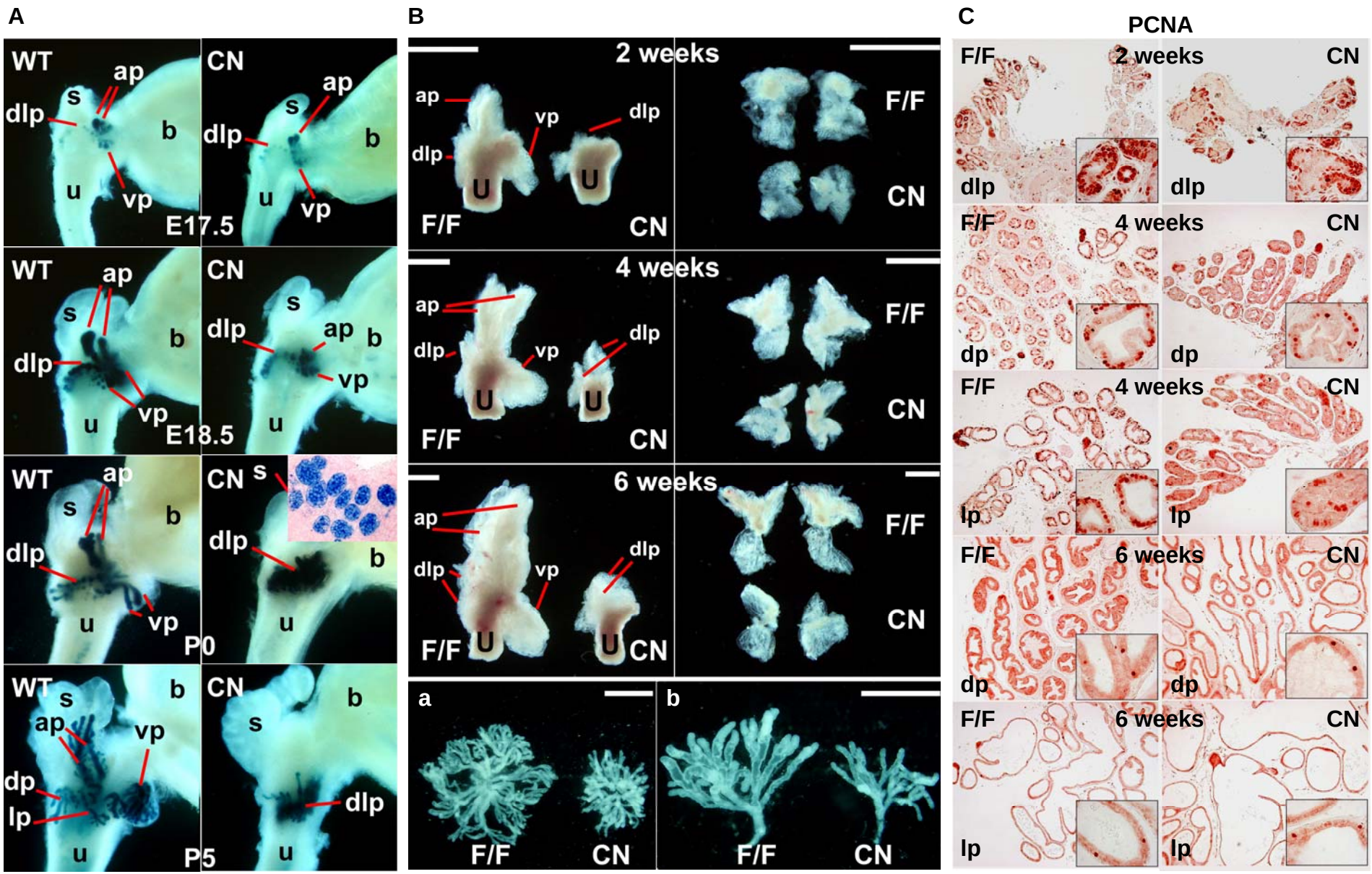
A
WT
CN
ap
s
dlp
b
u
vp
E17.5
E18.5
P0
P5
dp
lp
B
2 weeks
4 weeks
6 weeks
F/F
CN
U
a
b
C
PCNA
dlp
dp
lp

Fig. 3

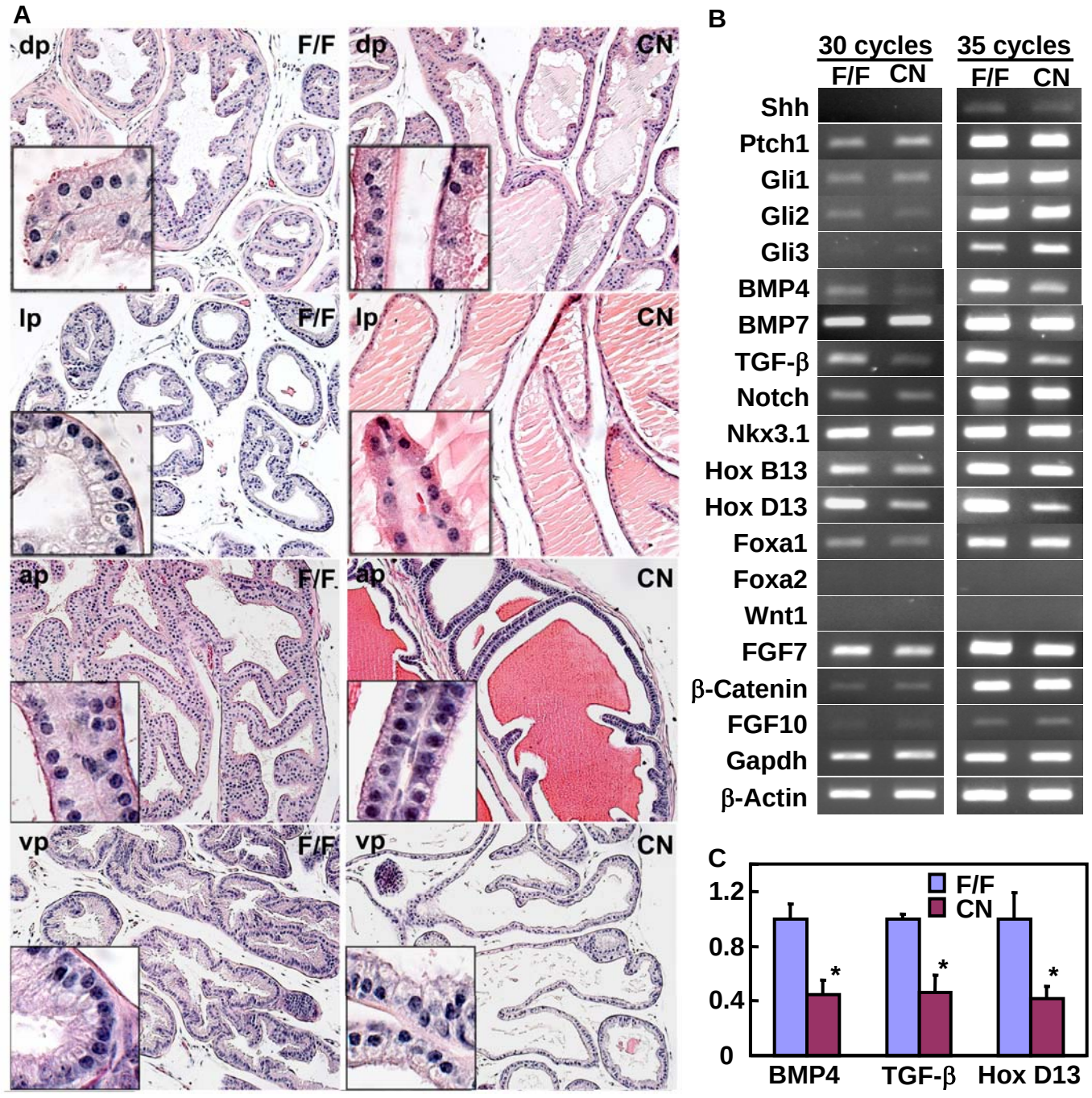
A
dp
F/F
dp
CN
lp
F/F
lp
CN
ap
F/F
ap
CN
vp
F/F
vp
CN
B
30 cycles
35 cycles
F/F
CN
F/F
CN
Shh
Ptch1
Gli1
Gli2
Gli3
BMP4
BMP7
TGF-β
Notch
Nkx3.1
Hox B13
Hox D13
Foxa1
Foxa2
Wnt1
FGF7
β-Catenin
FGF10
Gapdh
β-Actin
C
1.2
0.8
0.4
0
F/F
CN
*
*
*
BMP4
TGF-β
Hox D13

Fig. 4

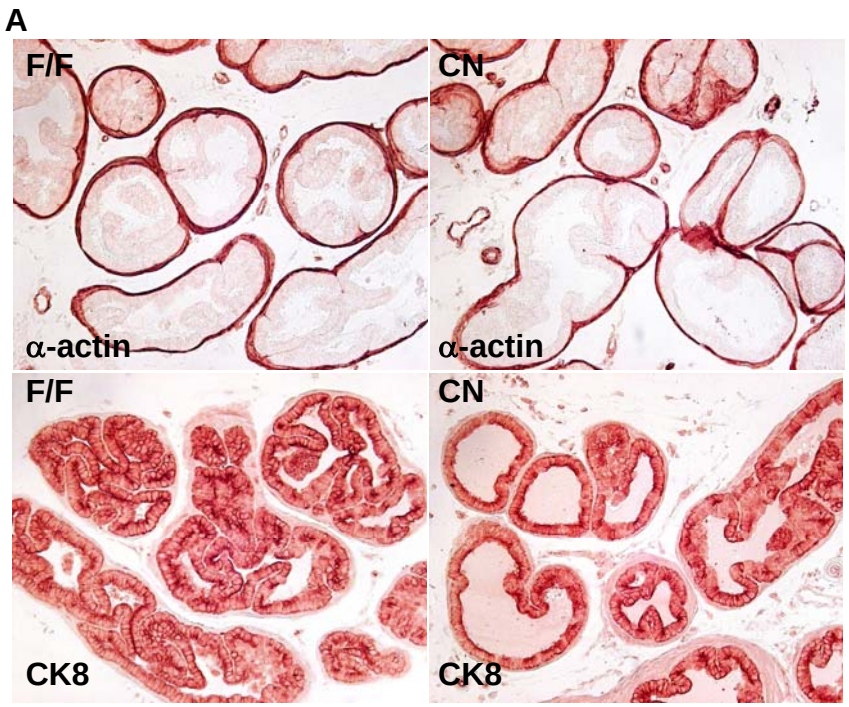
A
F/F
CN
α-actin
α-actin
F/F
CN
CK8
CK8

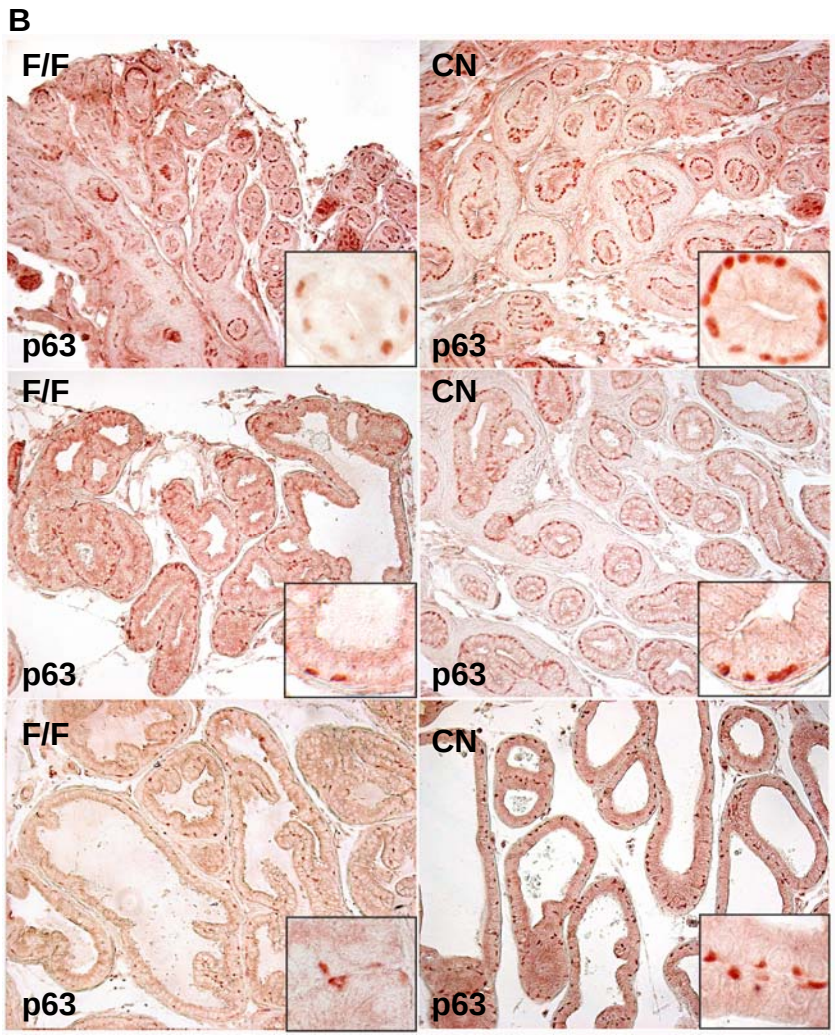
B
F/F
CN
p63
p63
F/F
CN
p63
p63
F/F
CN
p63
p63

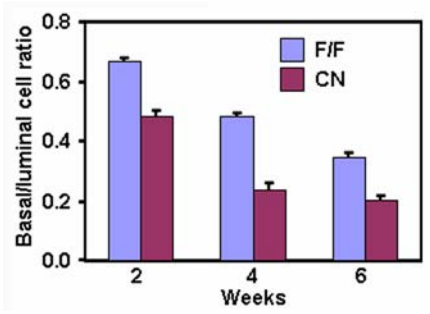
C
Basal/luminal cell ratio
0.0
0.2
0.4
0.6
0.8
F/F
CN
2
4
6
Weeks

Fig. 5

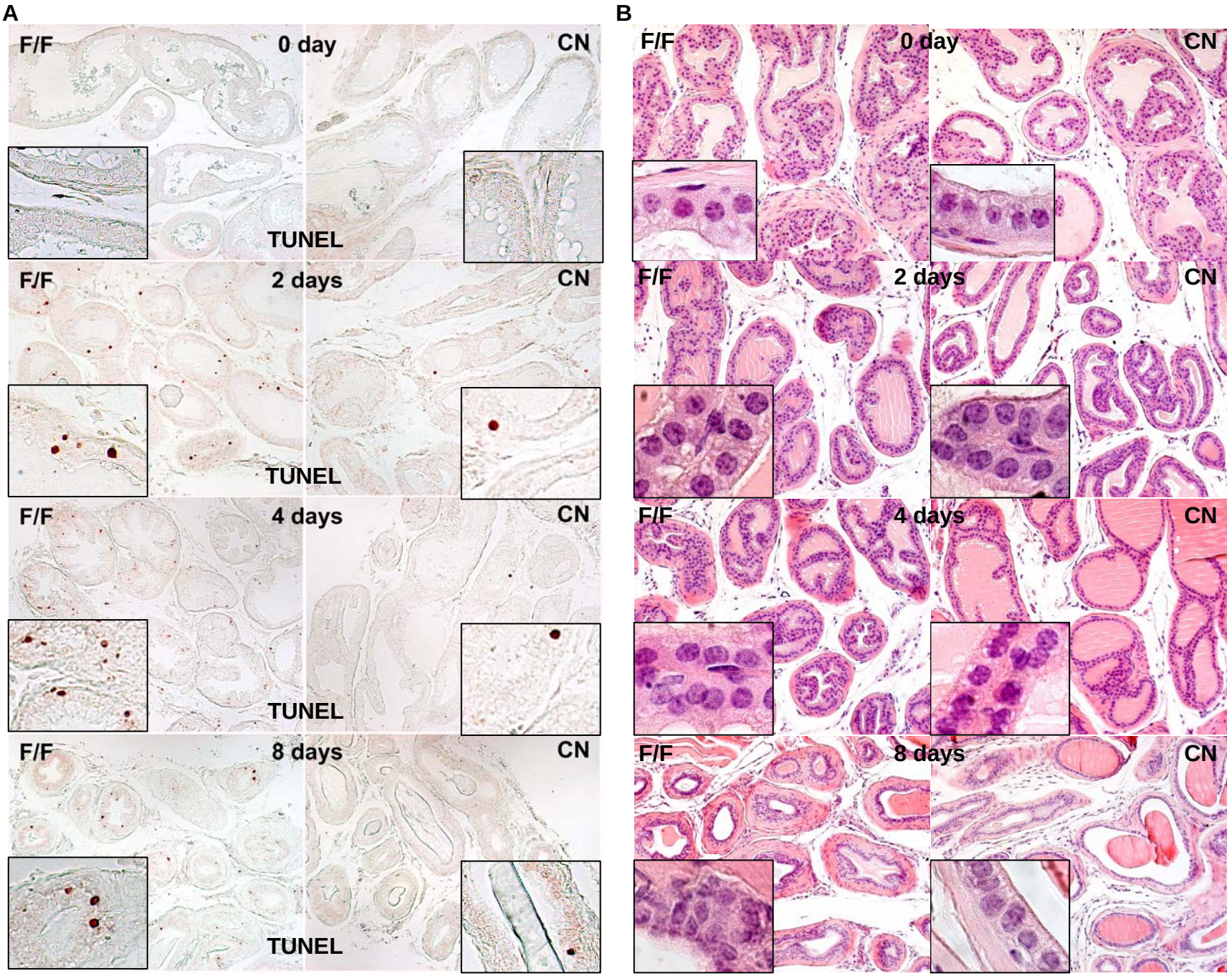
A
F/F
0 day
CN
TUNEL
F/F
2 days
CN
TUNEL
F/F
4 days
CN
TUNEL
F/F
8 days
CN
TUNEL
B
F/F
0 day
CN
F/F
2 days
CN
F/F
4 days
CN
F/F
8 days
CN

Fig. 6

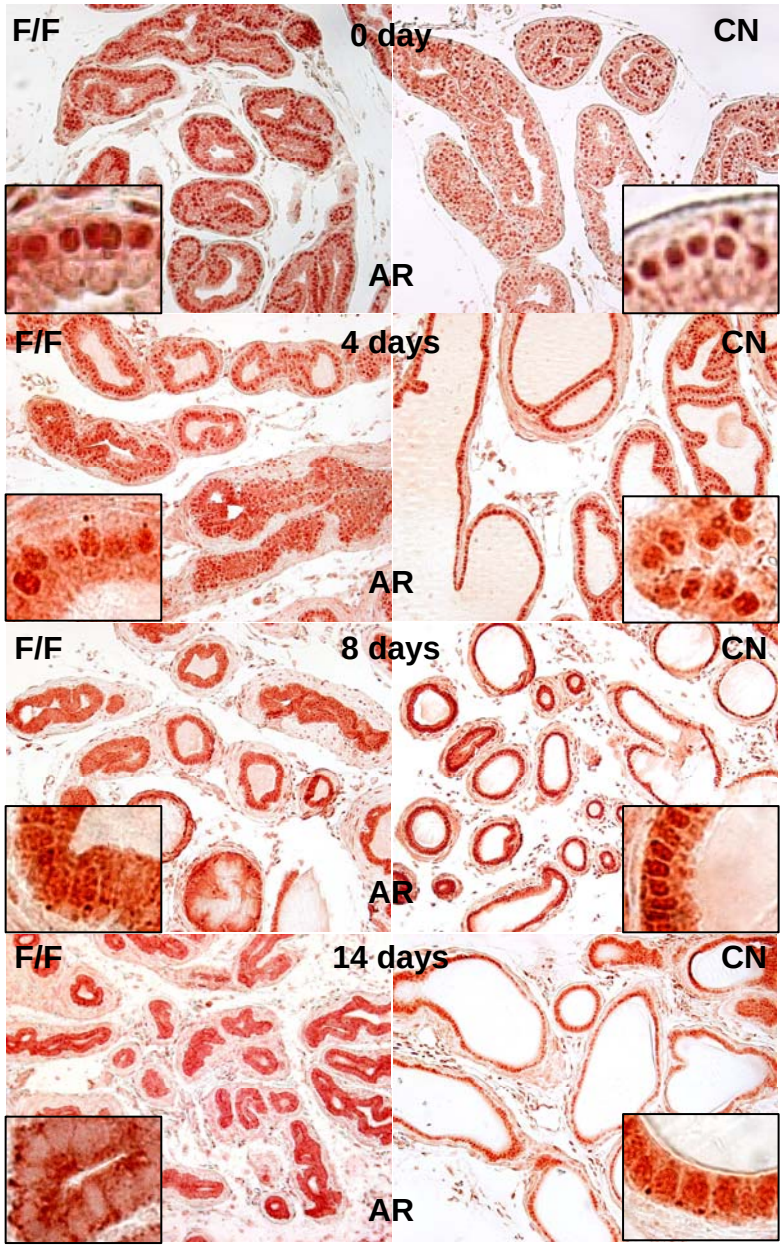

Fig. 7

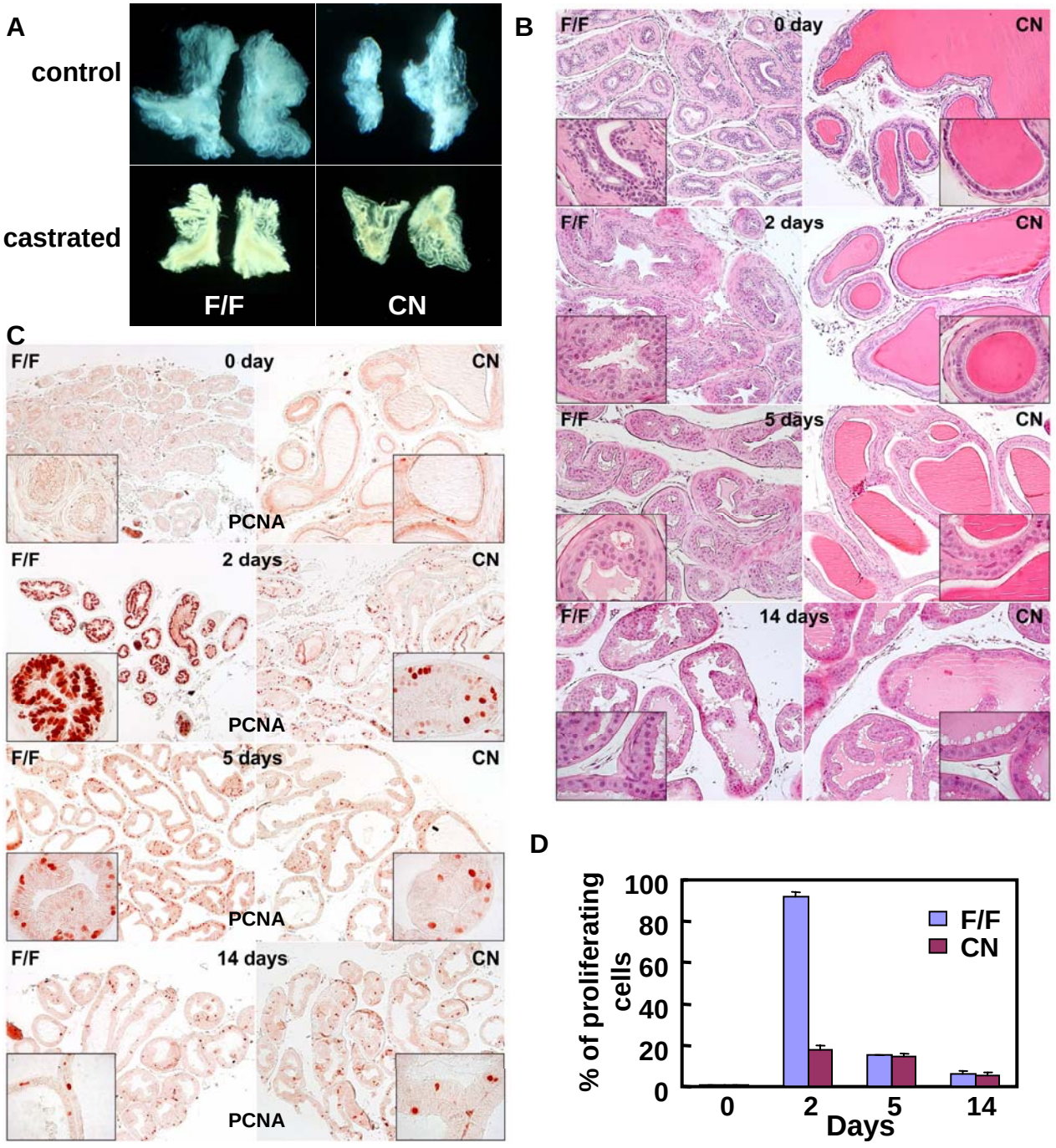
A
control
castrated
F/F
CN
B
F/F
0 day
CN
2 days
5 days
14 days
C
PCNA
D
% of proliferating cells
100
80
60
40
20
0
0
2
5
14
Days
F/F
CN

Fig. 8

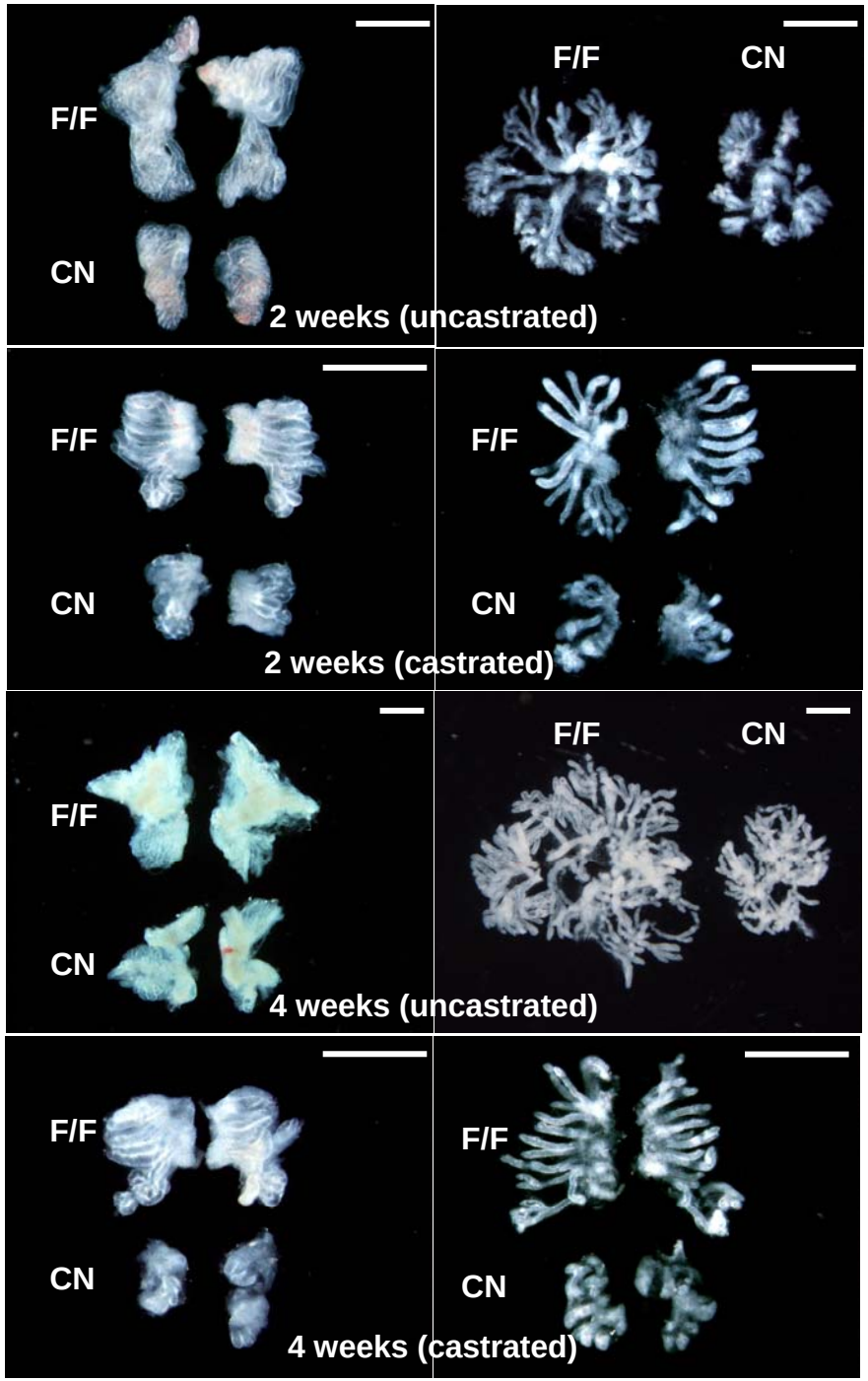
F/F
CN
2 weeks (uncastrated)
F/F
CN
F/F
CN
2 weeks (castrated)
F/F
CN
F/F
CN
4 weeks (uncastrated)
F/F
CN
F/F
CN
4 weeks (castrated)

Fig. 9

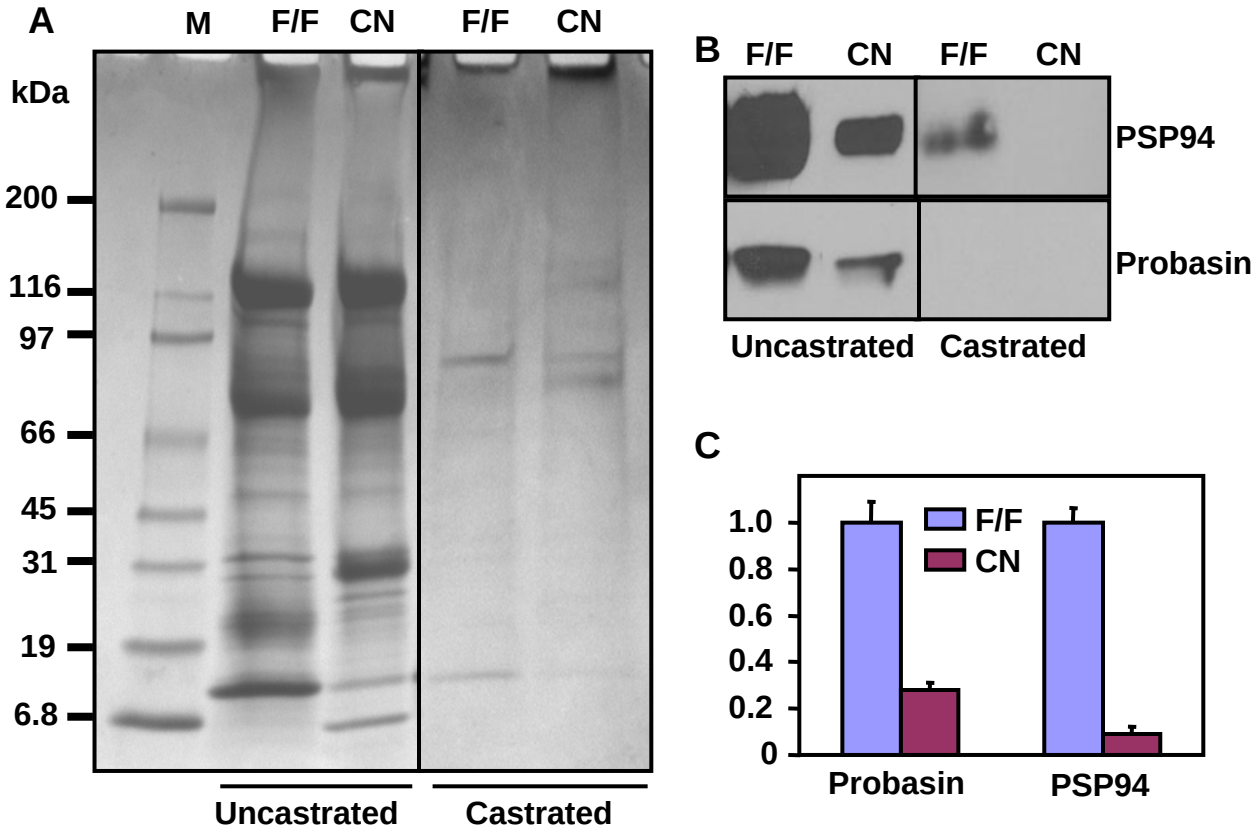
A
M
F/F
CN
F/F
CN
kDa
200
116
97
66
45
31
19
6.8
Uncastrated
Castrated
B
F/F
CN
F/F
CN
PSP94
Probasin
Uncastrated
Castrated
C
1.0
0.8
0.6
0.4
0.2
0
F/F
CN
Probasin
PSP94

Supplemental Fig. S1

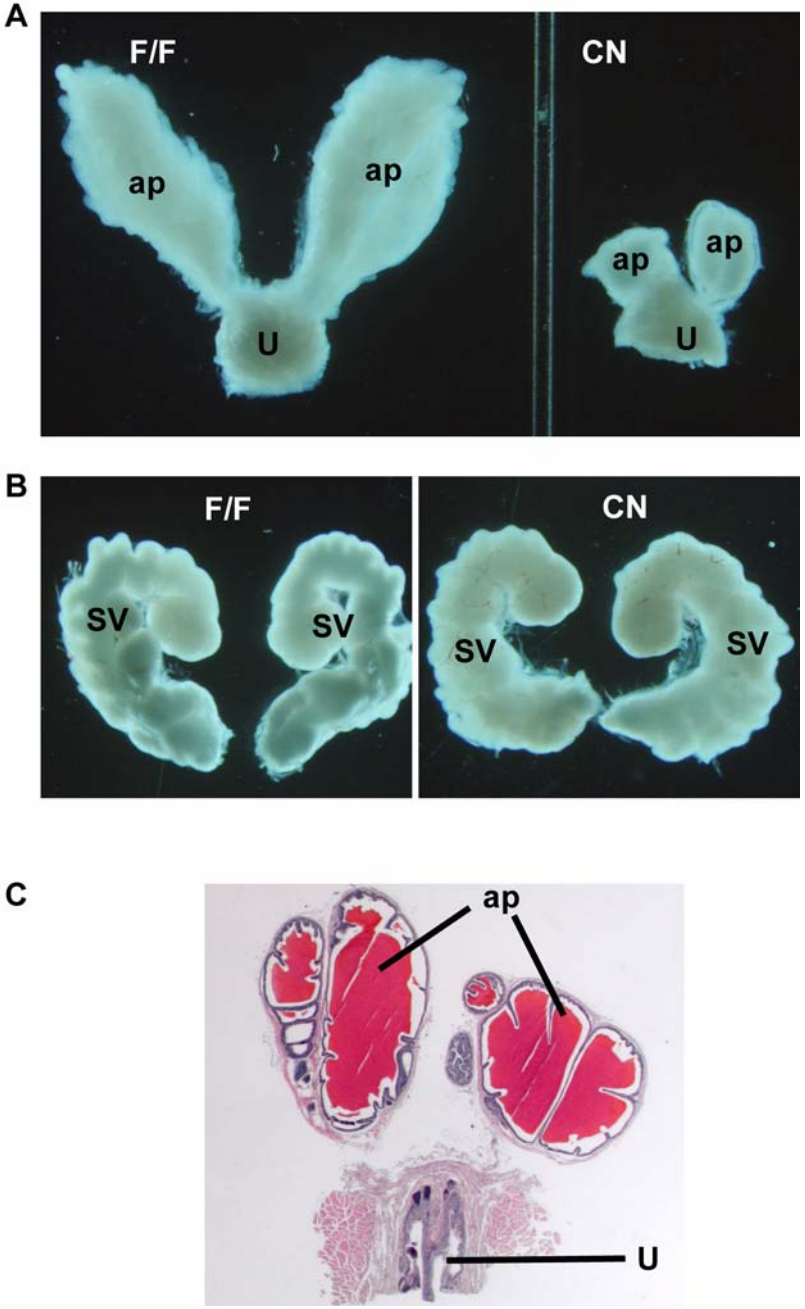

Fig. S1. Only a few *Fgfr2^{cn}* mice developed small ap lobes. **A.** Gross tissue appearance of ap lobes together with a part of urethra dissected from *Fgfr2^{cn}* and control mice as indicated. **B**. Gross tissue appearance of seminal vesicles dissected out from the same mime as in **A**. **C**. Low magnification view of H&E staining of tissue sections prepared from the *Fgfr2^{cn}* prostate shown in **A**. ap, anterior prostate; SV, seminal vesicle; U, urethra; CN, *Fgfr2^{cn}* mice; F/F, *Fgfr2^{flox}* homozygous mice.

Tyrosine autophosphorylation regulated binding of fibroblast growth factor receptor 1 (FGFR1) to FGFR substrate 2 alpha but not to FGFR substrate 2 beta

Yongyou Zhang, Kerstin McKeehan, Yongshun Lin, Jue Zhang, and Fen Wang*

Center for Cancer Biology and Nutrition, Institute of Biosciences and Technology, Texas A&M Health Science Center, 2121 W. Holcombe Blvd., Houston, TX 77030-3303, USA

*Correspondence: Dr. F. Wang, Center for Cancer Biology and Nutrition, Institute of Biosciences and Technology, Texas A&M Health Science Center, 2121 W. Holcombe Blvd., Houston, TX 77030-3303. USA.

E-mail: fwang@ibt.tmc.edu

Running Title: Interaction of FRS2 with FGFR1 tyrosine kinase

KEYWORDS: FGF; kinase; adaptor protein; signaling transduction; phosphorylation

Words: 7,018

Characters (no spaces): 40,611

Characters (with spaces): 47,847

9 Figures

Founded by:

- NIH/NCI; Grant Number: CA96824
- DOD; Grant Number: DAMD17-03-0014
- AHA; Grant Number: AHA0655077Y

ABSTRACT

The fibroblast growth factor (FGF) elicits regulatory signals by activating the FGF receptor (FGFR) tyrosine kinase, which then phosphorylates itself and multiple downstream signaling molecules. FGF receptor substrate 2 (FRS2) is an adaptor protein in the FGF signaling axis. Upon phosphorylation by activated FGFR kinases, it recruits multiple signaling molecules for the FGFR kinase. The two FRS2 homologues, FRS2α and FRS2β, share similarities in protein sequences and structural domains. It remained unclear whether the two FRS2 members bind to FGFR similarly and whether the binding is regulated. Here, we report that binding of full-length FRS2α, but not FRS2β, to FGFR1 was receptor autophosphorylation regulated. Although tyrosine phosphorylation on FRS2α only had minor impact on the binding; deletion of the FRS2 C-terminal sequence abolished the requirement of receptor phosphorylation for FRS2α/FGFR1 binding. In addition, the Grb2-binding sites on FRS2α were more important than the Shp2-binding sites for mediating FGF signals to activate the FiRE enhancer from the mouse syndecan 1 gene although the Grb2-binding sites are less important than the Shp2 binding sites for mediating mitogenic signals, suggesting that FRS2α mediated mitogenic and FiRE activating signals through different pathways. The results suggested a novel mechanism for the determination of FGF signaling intensity and specificity at the adaptor level.

Binding of the FGF to the FGFR tyrosine kinase-heparin sulfate complex induces receptor autophosphorylation as well as phosphorylation of downstream signaling molecules, which transmit regulatory signals to downstream cascades and regulate a broad spectrum of cellular activities. FRS2α, also called SNT1 for suc13-associating nuclear target 1, is a major FGFR substrate. It is extensively phosphorylated in response to FGF treatment, and functions as an adaptor protein in the FGFR signaling axis [Kouhara et al., 1997; Ong et al., 1996; Rabin et al., 1993]. Tyrosine phosphorylation on FRS2α by the FGFR kinase constitutes multiple binding sites for FGFR substrates, which recruit several downstream signaling molecules to the FGFR signaling axis, including Shp2 and Grb2 [Kouhara et al., 1997; Ong et al., 1996; Ong et al., 1997]. Two FRS2 members have been identified, FRS2α and FRS2β, which share an overall homology of 49% in the amino acid sequence and have similar structure domains. FRS2α is broadly expressed in adult and fetal tissues; disruption of *Frs2α* alleles results in embryonic lethality at E7-E7.5. The expression of FRS2β is more restricted than that of FRS2α [Hadari et al., 2001; McDougall et al., 2001; Zhou et al., 2003]. Although FRS2β can compensate for the loss of FRS2α in the activation of the MAP kinase mouse embryonic fibroblast (MEF) cells [Gotoh et al., 2004b], recent reports demonstrate that FRS2α and FRS2β may also mediate different signals in cells [Avery et al., 2006; Harada et al., 2005; Huang et al., 2004; Huang et al., 2006].

FRS2s are membrane-anchored proteins by virtue of myristylation on the conserved N-terminal myristylation sequence. Immediately downstream of the myristylation site is a phosphotyrosine binding (PTB) domain that binds to the juxtamembrane domain of the FGFR kinase [Xu et al., 1998], nerve growth factor receptor (TRK) [Dhalluin et al., 2000], and possible other receptor tyrosine kinases

[Dixon et al., 2006]. The PTB domain is also responsible for the binding of FRS2α with Cks1, a molecule that triggers degradation of cell cycle regulatory protein, $p27^{kip1}$, during the G1/S transition [Zhang et al., 2004]. The C-terminal sequence downstream of the PTB domain includes multiple candidate tyrosine and serine/threonine phosphorylation sites. The context sequences of Tyr196, Tyr306, Tyr349, and Tyr392 loosely fit the consensus Grb2 binding sequence, and those of Tyr436 and Tyr471 fit the Shp2 binding sites. Substitution of these tyrosine residues in the Grb2 and Shp2 binding sites with phenylalanine residues abrogates the activity to recruit Grb2 and Shp2, respectively [Gotoh et al., 2004a; Ong et al., 2000; Xu and Goldfarb, 2001]. Mice carrying mutations in the two Shp2 binding sites (Y436F and Y471F) exhibit a variety of developmental defects in many organs, including eye, branchial arch, limb, heart and corticogenesis. In contrast, mice carrying mutations in the four Grb2 binding sites (Y196F, Y306F, Y349F, and Y392F) have a less severe phenotype [Gotoh et al., 2004a; Yamamoto et al., 2005]. Furthermore, FGF stimulation causes FRS2α to be phosphorylated on multiple threonine residues by MAP kinases, which is likely to be involved in the negative feedback regulation of the FGF signaling. Prevention of FRS2α threonine phosphorylation by mutation of the candidate threonine phosphorylation sites results in enhancing the intensity and prolonging the duration of FGF signaling [Lax et al., 2002].

The FGFR kinase is a tyrosine kinase that phosphorylates its substrates as well as the receptor itself. Seven phosphorylated tyrosine residues in the FGFR intracellular domain have been reported [Hou et al., 1993; Mohammadi et al., 1996]. Among the autophosphorylation sites, Tyr653, and possibly 654 in concert, are important for derepression of the FGFR1 kinase. Autophosphorylated Tyr766 in the C-terminus interacts directly with PLCγ and is required for PLCγ phosphorylation and its

activation by the FGFR. Phosphotyrosine 766 and sequential activation of PLCγ are required for the time-dependent acquisition of the proliferative response to FGFR1, although they do not appear necessary for FGFR1-mediated mitogenesis once it is acquired [Wang et al., 2002]. It remains to be elucidated whether these tyrosine autophosphorylation sites are essential for association with FRS2, whether the FGFR kinase regulates binding of FRS2, and whether the two FRS2 members, FRS2α and FRS2β, bind to FGFR kinase equally.

Here we report that (1) the PTB domains of both FRS2α and FRS2β associated with FGFR1 kinase independent of tyrosine phosphorylation; (2) interaction of full-length FRS2α, but not FRS2β, with FGFR1 was regulated by receptor tyrosine autophosphorylation on Tyr653/654, Tyr730, and Tyr766 residues, but not on Tyr463 of FGFR1; (3) tyrosine phosphorylation on FRS2α only had minimal impact on FGFR1/FRS2α binding; (4) association of both FRS2α and FRS2β with FGFR1 was not dependent on the alternative spliced VT motif; and (5) the four Grb2-binding sites on FRS2α were more important than the two Shp2-binding sites for mediating FGF signals for inducing transcription activity of the FiRE from the mouse syndecan 1 gene, although the Grb2-binding sites are less important than Shp2-binding site for mediating FGF-induced mitogenic signals in cultured cells and generally less important for embryonic development in mice. The results here augment the comprehension of how FRS2α mediates FGFR1 signals to downstream pathways and further our understanding of the mechanisms behind the regulation of the signaling intensity and specificity of the FGFR1 signaling axis.

MATERIALS AND METHODS

Construction of FRS2 mutants. The cDNA encoding the Y196F mutant fragment was PCR amplified from FRS2α cDNA templates with primers pSNT1-1 [Wang, 2002] and a p196 (TGTAGTGTTGACAAAGGTATGTAC); the cDNA for the Y306F fragment with primers p306 (TCTGTTAACAAACTGCTGTTTGAAAATATA) and p436 (CAAGTCAACCTGTATGAAATTAAG); the cDNA for the Y349F fragment with primers pSNT1-2 [Wang, 2002] and p349-1 (TTATTAAACTTCGAAAATCTACCA); the cDNA for the Y392F with primers p392 (TAATCTAGATCCAATGCATAACTTTGTAAA) and p471-2 (CTCTCGATGTCTATCACGGCAAAGAGCTCT); the cDNA for the Y436F fragment with primers p392 and p436; the cDNA for the Y471F with primers pSNT1-2 and p471-1 (ACAGAGCTCTTTGCCGTGATAGACATCGAG). The mutant cDNA fragments were ligated with context sequences for full length FRS2α mutants bearing a single point mutation or all six substitutions. Other FRS2α and FGFR mutants were prepared as described [Zhang et al., 2004]. The resulted full-length FRS2α cDNAs were sequence verified and subcloned to pVL1393 for preparation of recombinant baculoviruses, or pcDNA-zeo-3.1(+) for expression in mammalian cells [Zhang et al., 2004].

Construction and expression of wildtype and mutant FRS2β. cDNAs encoding for full-length mouse FRS2β were generated by ligation of 2 RT-PCR fragments cloned from kidney RNA pools with primers: ms2-1 (CCGATAGGATCCTCTGACACCATGGGGAGC), and ms2-2 (GTGATGGGGAGGGTCCTGCATGCC); ms2-3 (CAGGTGATGAAGTGCCAGAGCCTC) and ms2-4

(GCAGGCGAATTCCCAGGTCTACAGAGGCAG), respectively. The cDNA for PTBβ-His was generated with PCR-mediated mutagenesis with primers ms2-1 and ms2-6 (GCCCTCGAGAGTACTAGGGCAGCCAGGGAAGCCATT) with the full-length FRS2β template as described [Zhang et al., 2004]. The resulted cDNAs were subcloned in pVL1392 vector for preparation of recombinant baculoviruses for expression in Sf9 insect cells, or pcDNA-zeo-3.1(+) vector for expression in mammalian cells.

Pull-down with Ni-beads. Sf9 cells ($3X10^6$) infected with indicated recombinant viruses were lysed with 1 % Triton X-100 in PBS. The cell lysates were diluted with an equal volume of the washing buffer (0.5 M NaCl, 50 mM imidazole, and 10 mM Tris-HCl pH 7.5). The mixtures were gently rocked with 30 μl of Ni-agarose beads (Amersham Pharmacia Biotech Lab, Uppsala, Sweden) at 4 °C for 45 minutes. The FRS2-His-Ni-agarose complexes were then washed 3 times with the washing buffer, and specifically bound fractions were recovered from beads with the SDS-sample buffer.

Pull-down with heparin-beads. The cell lysates were mixed with heparin-beads (Amersham Pharmacia Biotech Lab, Uppsala, Sweden) as indicated and incubated at 4 °C for 1.5 hour. The beads were washed with 0.2 N NaCl-PBS for 3 times, and specifically bound fractions were recovered from the beads with the SDS-sample buffer.

Phosphorylation of FRS2 by FGFR1 kinase. Sf9 insect cells ($3X10^6$) co-infected with the indicated FRS2 and FGFR1 bearing baculoviruses were lysed, and the cell lysates were incubated with glutathione beads or Ni-beads as indicated. Specifically bound fractions were subjected to Western analyses with anti-phosphotyrosine 4G10 (Upstate Biotechnology, Lake Placid, NY), anti-His (Santa Cruz Biotechnology, Inc.,

Santa Cruz, CA), and anti-FGFR1 antibodies (17A3) as indicated. Immunoreactivity was visualized with the Enhanced Chemiluminescence (ECL)-Plus reagents (Amersham Pharmacia Biotech Lab, Uppsala, Sweden) according to the manufacturer's instruction. For re-probing, the membranes were stripped off the antibodies by incubation with the stripping buffer (62.5 mM Tris–HCl, pH 6.8, 2% SDS, 100 mM β-mercaptoethanol) at 50 °C for 30 minutes before incubation with new antibodies.

Dephosphorylation. To release the phosphate groups on the FGFR1-FRS2α complex, the Sf9 insect cell-expressed proteins coupled to Ni-agarose beads were washed with the washing buffer (2 mM Tris-HCl, pH 7.5) for three times and incubated with 10 units of the YOP phosphatase (New England Biolabs, Ipswich, MA) in 50 μl reaction buffer at 37 °C for 30 minutes. After being washed with the washing buffer for two times, and specifically bound fractions were recovered with the SDS-sample buffer for Western blot analyses.

Establishing mouse embryonic fibroblast (MEF) cultures and FiRE assay. Mouse embryonic fibroblast (MEF) cells were prepared from E14.5 embryos carrying homozygous LoxP-flanked *Frs2α* (*Frs2α*^{flox}) alleles [Lin et al., 2006]. The cells were transfected with the pCMV-Cre plasmid to excise the LoxP flanked FRS2α sequences, the FiRE reporter, and indicated FRS2α mutants with Lipofectamine-Plus reagents (Invitrogen, Carlsbad, CA) according to manufacturer's suggestions. Disruption of the *Frs2α*^{flox} alleles was confirmed by PCR analyses (Supplemental Fig. 2B), and loss of FRS2α activity was evaluated with the FiRE-luciferase reporter analyses [Wang et al., 2002].

(GCAGGCGAATTCCCAGGTCTACAGAGGCAG), respectively. The cDNA for PTBβ-His was generated with PCR-mediated mutagenesis with primers ms2-1 and ms2-6 (GCCCTCGAGAGTACTAGGGCAGCCAGGGAAGCCATT) with the full-length FRS2β template as described [Zhang et al., 2004]. The resulted cDNAs were subcloned in pVL1392 vector for preparation of recombinant baculoviruses for expression in Sf9 insect cells, or pcDNA-zeo-3.1(+) vector for expression in mammalian cells.

Pull-down with Ni-beads. Sf9 cells ($3X10^6$) infected with indicated recombinant viruses were lysed with 1 % Triton X-100 in PBS. The cell lysates were diluted with an equal volume of the washing buffer (0.5 M NaCl, 50 mM imidazole, and 10 mM Tris-HCl pH 7.5). The mixtures were gently rocked with 30 μl of Ni-agarose beads (Amersham Pharmacia Biotech Lab, Uppsala, Sweden) at 4 °C for 45 minutes. The FRS2-His-Ni-agarose complexes were then washed 3 times with the washing buffer, and specifically bound fractions were recovered from beads with the SDS-sample buffer.

Pull-down with heparin-beads. The cell lysates were mixed with heparin-beads (Amersham Pharmacia Biotech Lab, Uppsala, Sweden) as indicated and incubated at 4 °C for 1.5 hour. The beads were washed with 0.2 N NaCl-PBS for 3 times, and specifically bound fractions were recovered from the beads with the SDS-sample buffer.

Phosphorylation of FRS2 by FGFR1 kinase. Sf9 insect cells ($3X10^6$) co-infected with the indicated FRS2 and FGFR1 bearing baculoviruses were lysed, and the cell lysates were incubated with glutathione beads or Ni-beads as indicated. Specifically bound fractions were subjected to Western analyses with anti-phosphotyrosine 4G10 (Upstate Biotechnology, Lake Placid, NY), anti-His (Santa Cruz Biotechnology, Inc.,

Results

Tyrosine phosphorylation promoted interaction of FGFR1 with full-length FRS2α, but not the PTB domain. To determine whether the interaction of FRS2α with FGFR1 was receptor tyrosine kinase dependent, full-length FRS2α with a hexahistidine tag at the C-terminal was coexpressed in Sf9 insect cells with wide-type FGFR1 (R1βa1) or the kinase-inactive mutant of FGFR1 (R1KN) [Zhang et al., 2004]. Affinity pull-down with Ni-agarose beads showed that disruption of the FGFR1 kinase activity significantly reduced the interaction between FGFR1 and FRS2α (Fig. 1A). To further confirm this, the Sf9 cell-expressed FGFR1-FRS2α complexes immobilized on Ni-beads were treated with the YOP phosphatase that specifically released phosphate groups from phospho-tyrosine residues in proteins. The results showed that dephosphorylation on tyrosine residues significantly reduced the interaction of FGFR1 with full-length FRS2α (Fig. 1A). The PTB domain has been shown to be the binding site for the juxtamembrane domain of FGFR1 [Ong et al., 2000; Xu et al., 1998]. To determine whether binding of PTB with FGFR1 is also tyrosine phosphorylation regulated, similar experiments were carried out with hexahistidine tagged PTB domain. The results showed that interaction of FGFR1 with the PTB domain was not reduced by disruption of the tyrosine kinase activity of FGFR1 or dephosphorylation with the YOP phosphatase. Furthermore, under the same condition, the interaction of FGFR1 with the PTB domain was significantly stronger than with full-length FRS2α. Deletion of the PTB domain eliminated the activity of FRS2α to interact with FGFR1 under the same condition (Supplemental Fig.1). To confirm the results in mammalian cells, the same FRS2α and FGFR pcDNA-zeo-3.1(+) constructs were expressed in 293T cells, and pulled down with Ni-

beads with or without preincubation with FGF2 for 10 minutes (Fig.1B). The results showed that preincubation with FGF2 increased pull-down of FGFR1 by FRS2α. This indicates that activation of the FGFR1 kinase enhances the interaction of FGFR1 with FRS2α, which supports the conclusion derived from the insect cell experiments. Together, the result showed that (1) the PTB domain bound to FGFR1 was independent of tyrosine phosphorylation, and was the only structure domain in FRS2α that bound to FGFR1; (2) the C-terminal sequence downstream of the PTB domain negatively regulated the binding; and (3) the negative regulation was abrogated by tyrosine phosphorylations.

Tyrosine phosphorylation of FRS2a was not essential for interaction with the FGFR1 kinase. To investigate whether the phosphorylation on tyrosine residues of FRS2α was essential for abrogating the negative impact on interaction with FGFR1, the candidate tyrosine phosphorylation sites on FRS2α were substituted with phenylalanine residues and the mutants were coexpressed with FGFR1 in Sf9 cells. Pull-down assays showed that the FRS2α mutants with a mutation on a single tyrosine phosphorylation site (FRS2αY196F, FRS2αY306F, FRS2αY349F, FRS2αY392F, FRS2αY436F, and FRS2αY471F), and on all six tyrosine phosphorylation sites (FRS2α6F) remained active in interacting with the FGFR1 kinase, although the interaction was somewhat attenuated by the mutations (Fig.2). In addition, all mutants, except FRS2α6F were tyrosine-phosphorylated by the FGFR1 kinase. The results indicated that tyrosine phosphorylation on the C-terminal sequence downstream of the PTB domain only had limited impact on lifting the C-terminal inhibition on binding with FGFR1.

Receptor autophosphorylation promoted FGFR1/FRS2α interaction by abrogating the inhibition imposed by the C-terminus of FRS2α. Binding of the FGF to the FGFR activates receptor tyrosine kinase activity and leads to receptor autophosphorylation on mainly five tyrosine residues, Tyr463, Tyr653, Tyr654, Tyr730, and Tyr766, in the intracellular domain [Hou et al., 1993; Mohammadi et al., 1996]. To determine the impact of receptor tyrosine autophosphorylation on interaction with FRS2α, a series of FGFR1 mutants bearing point mutations on the tyrosine autophosphorylation sites were coexpressed with FRS2α in Sf9 cells. Pull-down assays showed that substitution of tyrosine autophosphorylation sites Tyr653/654, Tyr730, and Tyr766 with phenylalanine significantly reduced interaction with FRS2α (Fig. 3A), but not with the PTB domain (Fig. 3B), suggesting that autophosphorylation on these tyrosine residues attenuated the FRS2α C-terminal inhibition on FGFR1-FRS2α interaction. In contrast, substitution of Tyr463 on FGFR1 did not have detectable impact on the interaction.

Both FGFR1 and FGFR2 encode an alternatively spliced VT (valine-threonine) motif at the intracellular juxtamembrane domain [Brackenridge et al., 2003; Kan et al., 1993; Paterno et al., 2000], which has been reported import for association with FRS2α [Burgar et al., 2002; Dhalluin et al., 2000; Xu et al., 1998]. Interestingly, pull-down experiments also showed that the FGFR1βb1 isoform that lacked VT motif not only bound to, but also phosphorylated FRS2α; no significant difference was observed between the VT positive isoform of FGFR1 (FGFR1βa1) and the VT negative FGFR1βb1 isoform (Fig. 3A). Similar experiments were carried out in 293T cells to confirm the FGFR1βb1 isoform bound and phosphorylated FRS2α and FRS2β in mammalian cells (Supplemental Fig. 3). The results suggested that the VT

motif was not essential for FGFR1 (β isoform) to interact with and phosphorylate FRS2, which was different from literature data that the alternative spliced VT motif is important both for FRS2α and FGFR1 interaction, and for FGFR-mediated FRS2α phosphorylation [Burgar et al., 2002; Dhalluin et al., 2000; Xu et al., 1998].

The *FRS2β/FGFR1 interaction was tyrosine phosphorylation-independent*. The two FRS2 homologues, FRS2α and FRS2β, have been shown to share redundant signaling activities in several experimental systems, although no direct evidence is available to date showing that FGFR1 binds and phosphorylates FRS2β. To determine whether FRS2β bound to FGFR1 kinase, FRS2β was coexpressed with FGFR1 as described above. The results show that FRS2β bound to FGFR1 and was phosphorylated by the FGFR1 kinase (Fig 4A). Unlike FRS2α, the interaction of FRS2β with FGFR1 was not tyrosine phosphorylation regulated. As expected, affinity pull-down analyses further confirmed that interaction of the PTB domain of FRS2β (PTBβ) with FGFR1 was also independent of the receptor kinase activity (Fig. 4B). Similar experiments carried out in 293T cells further confirmed the results in mammalian cells (Fig. 4C).

In comparison to full-length inactive mutants, the truncated PTB was a more efficient dominant negative inhibitor of the FGF2 signaling axis. Since the PTB domain exhibited a higher affinity for FGFR1 kinase than did full-length FRS2α, it was hypothesized that the PTB domain could compete with endogenous FRS2α for FGFR and functioned as a better dominant negative inhibitor for the FGF signaling pathway than the full-length inactive mutant. To test this hypothesis, the PTB and 6F mutants were coexpressed with the FiRE reporter in NIH 3T3 cells that strongly expressed endogenous FGFR1 and FRS2α. The results showed that FGF2 induced

phosphorylation of FRS2α and activated the FiRE reporter as described [Wang et al., 2002]. Expression of the truncated PTB domain in the cells by cotransfection almost completely abolished the FGF2-induced FRS2α phosphorylation (Fig. 5A). In addition, activation of the MAP kinase pathway (Fig. 5A) and the activation of the FiRE reporter (Fig. 5B) were also significantly reduced by expression of the PTB domain. In contrast, expression of the 6F mutant in the cells only partially inhibited the FGF2-induced FRS2α phosphorylation, the MAP kinase activation, and the FiRE activation. Thus, the results suggested that the PTB domain was a better dominant negative inhibitor for the FGF signaling axis than inactive full-length mutants due to its high affinity for the FGFR kinase.

The Grb2-recruiting sites on FRS2α were more critical for mediating FGF2 signals to activate the FiRE transcription enhancer from mouse syndecan 1 gene. The results in Supplemental Fig. 2A showed that expression of the FiRE reporter was diminished 48 hours after the transfection of Cre plasmid to *Frs2α*^{flox}-MEF cells, which indicated that FRS2α is required for FGF2-induced FiRE response. To further characterize which substrate-recruiting site(s) was/were essential for the FRS2α to mediate FiRE-activating signals, the indicated FRS2α mutants were coexpressed with Cre and the FiRE-luciferase reporter in *Frs2α*^{flox}-MEF cells (Fig. 6). Results showed that expression of full-length FRS2α recovered the activity of FGF2 in activating the FiRE element, suggesting that the FiRE-activating signal of FGF2 in the MEF cells was mediated by FRS2α. Elimination of a single substrate-recruiting phosphorylation site only weakly reduced the activity of FRS2α to mediate FiRE activation; elimination of all six phosphorylation sites (6F) fully inactivated FRS2α. Among the six tyrosine phosphorylation sites, Tyr196, Tyr306, Tyr349, and Tyr392 are

categorized as Grb2 recruiting sites, and Tyr436 and Tyr471 are Shp2 recruiting sites. To determine which signaling pathway mediated the FiRE activating signals, mutant 4F bearing substitutions on all 4 Grb2 binding sites and 2F bearing substitutions on the 2 Shp2 binding sites were constructed and their capacity to mediate FiRE activation signals were tested (Fig. 6). The results showed that disruption of the four Grb2-binding sites significantly impaired the capacity of FRS2α to mediate FiRE activation, while disruption of the two Shp2-binding sites only had limited impact on the capacity. The results prompted us to test the hypothesis that the 4F mutant, but not the 2F mutant, can function as a dominant negative inhibitor for FiRE activation signals mediated by endogenous FRS2α in 3T3 cells. Indeed, data in Fig. 5B showed that the 4F mutant, exhibited better inhibitory activity towards FiRE activation by FGF2 than the 2F mutant, which further confirmed the finding that activation of the FiRE reporter was a composite outcome of signals mainly mediated by molecules recruited to the four Grb2-recruiting sites, although the Grb2-binding site are generally less important for mediating mitogenic signals than did the Shp2 binding sites.

Discussion

Binding of full-length FRS2α, but not FRS2β, to FGFR1 was receptor autophosphorylation regulated. Although it has been shown that FRS2α, an adaptor protein in the FGF signaling axis that links the FGFR kinase to downstream signaling cascades, binds to the intracellular juxtamembrane domain of FGFR1 via the PTB domain, whether the receptor tyrosine kinase regulates the interaction of FRS2α and FGFR1 is not well documented. Here we report that the binding of full-length FRS2α with the FGFR1 kinase was regulated by receptor autophosphorylation although that of the PTB domain was phosphorylation independent, which implies that the C-terminal effector domain of FRS2α inhibits interaction of the PTB domain with FGFR1, and the inhibition is lifted when the receptor is autophosphorylated upon binding with FGF ligands. It remains to be elucidated how receptor tyrosine autophosphorylation changes the three-dimensional conformation of the FGFR1 kinase domain and eliminates the negative impact of the effector domain on the binding. The result that substitution of the autophosphorylation site Tyr766 significantly reduced binding of FGFR1 to full-length FRS2α is consistent with the recent report that Tyr769, the counterpart autophosphorylation site of Tyr766 in FGFR1, is required for FGFR2IIIB to activate FRS2α, PLCγ, mitogen activated protein kinases (MAPKs), and cell proliferation [Ceridono et al., 2005]. Interestingly, FRS2α also associate with Cks1 via the PTB domain, and the association with Cks1 is regulated FGFR1 kinase releases as well [Zhang et al., 2004]. Phosphorylation of FRS2α by FGFR1 releases Cks1, which, in turn, relays the signal to downstream cascades and controls the cell cycle progression. Together, it is suggested that (1) the C-terminal effector sequence of FRS2α functions as a regulator for interaction of the PTB domain with other signaling molecules, in addition to being binding sites for

downstream molecules; (2) the function of the C-terminal effector domain on PTB binding can be regulated by tyrosine phosphorylation, either on the effector itself or on its interacting partners.

FRS2α is a membrane-anchored protein by virtue of the N-terminal myristylation motif consisting of 6 amino acid residues (MGSCCS). Deletion of the sequence significantly reduced binding of the PTB domain to FGFR1 (supplemental Fig. 1) and Cks1 [Zhang et al., 2004]. The interaction was cell context-dependent; the PTB domain only weakly pulled down FGFR1 when separately expressed, suggesting that membrane anchorage was important for maintaining the right conformation of the PTB domain to interact with FGFR1 and Cks1 as reported [Ong et al., 2000; Zhang et al., 2004]. Furthermore, to rule out the possibility that the myristylation domain directly interacted with FGFR1, a mutant (ΔmFRS2α) was generated that had deletion of the PTB and part of the C-terminal sequence, while retaining the intact myristylation domain. Pull-down experiments showed that the mutant failed to pull-down FGFR1, further confirming that the myristylation domain did not directly bind to FGFR1 (Supplemental Fig. 1).

The alternatively spliced VT motif in the juxtamembrane domain of FGFR1 was dispensable for interaction with FRS2. Affinity pull-down experiments with Sf9 insect cell or 293T mammalian cell-expressed recombinant proteins showed that the alternatively spliced VT motif in the juxtamembrane domain was not obligatory for FGFR1 to interact with FRS2α and FRS2β. This is different from previous reports that the VT domain is essential for the interaction of FGFR1 and FRS2α, concluded from the data that mammalian cell-expressed FcFGFR1 fusion proteins and bacterial expressed or synthetic PTB does not bind to the FGFR1 juxtamembrane domain devoid of the VT motif [Burgar et al., 2002; Ong et al., 2000; Xu et al., 1998]. The

FcFGFR1 fusion protein is composed of an Fc region of human antibody molecules in the ectodomain and the transmembrane and intracellular regions of murine FGFR1 kinase. The function of FRS2α is membrane anchorage-dependent [Kouhara et al., 1997]. Results in supplemental Fig. 1 also indicated that the intact myristylation site was indispensable for full-length FRS2α or the PTB domain to interact with FGFR1. Furthermore, unpublished data showed that separately expressed FRS2α only weakly interacted with FGFR1 when being mixed in test tubes. Therefore, it is possible that interaction of FRS2α with FGFR is also dependent on the conformation of the FGFR signaling complex. Thus, substitution of the ectodomain with the Fc fragment may alter conformation of the intracellular domain [Uematsu et al., 2001], and may amend the substrate binding profile of the kinase domain.

The Grb2 recruiting sites were essential for FRS2α to mediate FiRE activation signals. How the FGF activates the FiRE element is still not well characterized to date, although it requires cooperation between protein kinase A and the Ras/ERK signaling pathway [Pursiheimo et al., 2002]. Inhibition of both ERK and p38 MAP kinase pathways diminishes FiRE activation by FGF2 [Jaakkola et al., 1997]. Among the six tyrosine phosphorylation sites on FRS2, the two Shp2-binding sites are primarily responsible for mediating Ras/ERK activation by the FGF, whereas the Grb2-binding sites are for recruitment of Gab1, phosphatidylinositol (PI-3) kinase, and ubiquitin ligase Cb1 [Gotoh et al., 2004a]. The data here show that the Grb2 associating pathways were more important for FRS2α to mediate FGF2 signals for activating FiRE than the Shp2-associated pathways, suggesting that the FiRE activating pathway was different from mitogenic pathways where the Shp2-binding sites are essential [Yamamoto et al., 2005].

The PTB domain was an effective dominant negative inhibitor for the FGF signaling axis. It has been shown that expression of the PTB domain of FRS2α in mammalian cells prevent FGF from activating MAP kinase and PI3-kinase pathways in the cells and attenuates FGF1 activity to promote antiestrogen-resistant growth in human breast carcinoma cells [Manuvakhova et al., 2006]. The data here further demonstrate that the FRS2α-PTB domain exhibited a higher dominant negative activity for FGF2 activity in 3T3 cells than the full-length inactive mutant. This is consistent with the data that binding of the PTB domain to FGFR1 was stronger than binding of full-length FRS2α to FGFR1, and that the binding of FGFR1 with the PTB domain was constitutive and phosphorylation independent. Therefore, the FRS2α-PTB domain may be used as a molecule to shut down FGF signaling pathways in malignant cells, which have been shown to be aberrantly activated in tumors of variable tissue origins.

In summary, the data here suggest that FRS2α binding to the FGFR1 kinase is regulated through tyrosine autophosphorylation of the receptor, and demonstrate that substrate-recruiting sites on FRS2α contribute to specificity of the FGF signaling axis. Furthermore, the results here suggest new venues for manipulating the FGF signaling axis based on selective or entire inhibition of FRS2α activation, which can be of great therapeutic potential.

Acknowledgements

This work was supported by Public Health Service Grants DAMD17-03-0014 from the U.S. Department of Defense, CA96824 from the National Cancer Institute, and AHA0655077Y from The America Heart Association. We thank Mary Cole and Xinchen Wang for critical reading of this manuscript.

References

Avery A. W., Figueroa C., Vojtek A. B. 2006. UNC-51-like kinase regulation of fibroblast growth factor receptor substrate 2/3. Cell Signal.

Brackenridge S., Wilkie A. O., Screaton G. R. 2003. Efficient use of a 'dead-end' GA 5' splice site in the human fibroblast growth factor receptor genes. Embo J 22:1620-31.

Burgar H. R., Burns H. D., Elsden J. L., Lalioti M. D., Heath J. K. 2002. Association of the signaling adaptor FRS2 with fibroblast growth factor receptor 1 (Fgfr1) is mediated by alternative splicing of the juxtamembrane domain. J Biol Chem 277:4018-23.

Ceridono M., Belleudi F., Ceccarelli S., Torrisi M. R. 2005. Tyrosine 769 of the keratinocyte growth factor receptor is required for receptor signaling but not endocytosis. Biochem Biophys Res Commun 327:523-32.

Dhalluin C., Yan K. S., Plotnikova O., Lee K. W., Zeng L., Kuti M., Mujtaba S., Goldfarb M. P., Zhou M. M. 2000. Structural basis of SNT PTB domain interactions with distinct neurotrophic receptors. Mol Cell 6:921-9.

Dixon S. J., MacDonald J. I., Robinson K. N., Kubu C. J., Meakin S. O. 2006. Trk receptor binding and neurotrophin/fibroblast growth factor (FGF)-dependent activation of the FGF receptor substrate (FRS)-3. Biochim Biophys Acta 1763:366-80.

Gotoh N., Ito M., Yamamoto S., Yoshino I., Song N., Wang Y., Lax I., Schlessinger J., Shibuya M., Lang R. A. 2004a. Tyrosine phosphorylation sites on FRS2{alpha} responsible for Shp2 recruitment are critical for induction of lens and retina. PNAS 101:17144-17149.

Gotoh N., Laks S., Nakashima M., Lax I., Schlessinger J. 2004b. FRS2 family docking proteins with overlapping roles in activation of MAP kinase have distinct spatial-temporal patterns of expression of their transcripts. FEBS Lett 564:14-8.

Hadari Y. R., Gotoh N., Kouhara H., Lax I., Schlessinger J. 2001. Critical role for the docking-protein FRS2 alpha in FGF receptor-mediated signal transduction pathways. Proc Natl Acad Sci U S A 98:8578-83.

Harada A., Katoh H., Negishi M. 2005. Direct interaction of Rnd1 with FRS2 beta regulates Rnd1-induced down-regulation of RhoA activity and is involved in fibroblast growth factor-induced neurite outgrowth in PC12 cells. J Biol Chem 280:18418-24.

Hou J., McKeehan K., Kan M., Carr S. A., Huddleston M. J., Crabb J. W., McKeehan W. L. 1993. Identification of tyrosines 154 and 307 in the extracellular domain and 653 and 766 in the intracellular domain as phosphorylation sites in the heparin-binding fibroblast growth factor receptor tyrosine kinase (flg). Protein Sci 2:86-92.

Huang L., Gotoh N., Zhang S., Shibuya M., Yamamoto T., Tsuchida N. 2004. SNT-2 interacts with ERK2 and negatively regulates ERK2 signaling in response to EGF stimulation. Biochem Biophys Res Commun 324:1011-7.

Huang L., Watanabe M., Chikamori M., Kido Y., Yamamoto T., Shibuya M., Gotoh N., Tsuchida N. 2006. Unique role of SNT-2/FRS2beta/FRS3 docking/adaptor protein for negative regulation in EGF receptor tyrosine kinase signaling pathways. Oncogene.

Jaakkola P, Vihinen T, Maatta A, Jalkanen M. 1997. Activation of an enhancer on the syndecan-1 gene is restricted to fibroblast growth factor family members in mesenchymal cells. Mol. Cell. Biol. 17:3210-3219.

Kan M., Wang F., Xu J., Crabb J. W., Hou J., McKeehan W. L. 1993. An essential heparin-binding domain in the fibroblast growth factor receptor kinase. Science 259:1918-21.

Kouhara H., Hadari Y. R., Spivak-Kroizman T., Schilling J., Bar-Sagi D., Lax I., Schlessinger J. 1997. A lipid-anchored Grb2-binding protein that links FGF-receptor activation to the Ras/MAPK signaling pathway. Cell 89:693-702.

Lax I., Wong A., Lamothe B., Lee A., Frost A., Hawes J., Schlessinger J. 2002. The docking protein FRS2alpha controls a MAP kinase-mediated negative feedback mechanism for signaling by FGF receptors. Mol Cell 10:709-19.

Lin Y., Zhang J., Liu G., McKeehan K., Wang F. 2006. Generation of an FRS2a conditional null allele. (in preparation).

Manuvakhova M., Thottassery J. V., Hays S., Qu Z., Rentz S. S., Westbrook L., Kern F. G. 2006. Expression of the SNT-1/FRS2 phosphotyrosine binding domain inhibits activation of MAP kinase and PI3-kinase pathways and antiestrogen resistant growth induced by FGF-1 in human breast carcinoma cells. Oncogene.

McDougall K., Kubu C., Verdi J. M., Meakin S. O. 2001. Developmental expression patterns of the signaling adapters FRS-2 and FRS-3 during early embryogenesis. Mech Dev 103:145-8.

Mohammadi M., Dikic I., Sorokin A., Burgess W. H., Jaye M., Schlessinger J. 1996. Identification of six novel autophosphorylation sites on fibroblast growth factor receptor 1 and elucidation of their importance in receptor activation and signal transduction. Mol Cell Biol 16:977-89.

Ong S. H., Goh K. C., Lim Y. P., Low B. C., Klint P., Claesson-Welsh L., Cao X., Tan Y. H., Guy G. R. 1996. Suc1-associated neurotrophic factor target (SNT)

protein is a major FGF-stimulated tyrosine phosphorylated 90-kDa protein which binds to the SH2 domain of GRB2. Biochem Biophys Res Commun 225:1021-6.

Ong S. H., Guy G. R., Hadari Y. R., Laks S., Gotoh N., Schlessinger J., Lax I. 2000. FRS2 proteins recruit intracellular signaling pathways by binding to diverse targets on fibroblast growth factor and nerve growth factor receptors. Mol Cell Biol 20:979-89.

Ong S. H., Lim Y. P., Low B. C., Guy G. R. 1997. SHP2 associates directly with tyrosine phosphorylated p90 (SNT) protein in FGF-stimulated cells. Biochem Biophys Res Commun 238:261-6.

Paterno G. D., Ryan P. J., Kao K. R., Gillespie L. L. 2000. The VT+ and VT- isoforms of the fibroblast growth factor receptor type 1 are differentially expressed in the presumptive mesoderm of Xenopus embryos and differ in their ability to mediate mesoderm formation. J Biol Chem 275:9581-6.

Pursiheimo J. P., Saari J., Jalkanen M., Salmivirta M. 2002. Cooperation of protein kinase A and Ras/ERK signaling pathways is required for AP-1-mediated activation of fibroblast growth factor-inducible response element (FiRE). J Biol Chem 277:25344-55.

Rabin SJ, Cleghon V, Kaplan DR. 1993. SNT, a differentiation-specific target of neurotrophic factor-induced tyrosine kinase activity in neurons and PC12 cells. Mol. Cell. Biol. 13:2203-2213.

Uematsu F., Jang J. H., Kan M., Wang F., Luo Y., McKeehan W. L. 2001. Evidence that the intracellular domain of FGF receptor 2IIIb affects contact of the ectodomain with two FGF7 ligands. Biochem Biophys Res Commun 283:791-7.

Wang F. 2002. Cell- and receptor isotype-specific phosphorylation of SNT1 by fibroblast growth factor receptor tyrosine kinases. In Vitro Cell Dev Biol Anim 38:178-83.

Wang F., McKeehan K., Yu C., McKeehan W. L. 2002. Fibroblast growth factor receptor 1 phosphotyrosine 766: molecular target for prevention of progression of prostate tumors to malignancy. Cancer Res 62:1898-903.

Xu H., Lee K. W., Goldfarb M. 1998. Novel recognition motif on fibroblast growth factor receptor mediates direct association and activation of SNT adapter proteins. J Biol Chem 273:17987-90.

Xu Hong, Goldfarb Mitchell. 2001. Multiple Effector Domains within SNT1 Coordinate ERK Activation and Neuronal Differentiation of PC12 Cells. J. Biol. Chem. 276:13049-13056.

Yamamoto S., Yoshino I., Shimazaki T., Murohashi M., Hevner R. F., Lax I., Okano H., Shibuya M., Schlessinger J., Gotoh N. 2005. Essential role of Shp2-binding sites on FRS2{alpha} for corticogenesis and for FGF2-dependent proliferation of neural progenitor cells. Proc Natl Acad Sci U S A.

Zhang Y., Lin Y., Bowles C., Wang F. 2004. Direct cell cycle regulation by the fibroblast growth factor receptor (FGFR) kinase through phosphorylation-dependent release of Cks1 from FGFR substrate 2. J Biol Chem 279:55348-54.

Zhou L., McDougall K., Kubu C. J., Verdi J. M., Meakin S. O. 2003. Genomic organization and comparative sequence analysis of the mouse and human FRS2, FRS3 genes. Mol Biol Rep 30:15-25.

Legends

Fig. 1. Tyrosine phosphorylation regulated the interaction of FGFR1 with full-length FRS2α, but not the PTB domain. **A**. Sf9 cell expressed FRS2α and FGFR1 were pulled down with Nickel- or heparin-agarose beads as specified and incubated with dephosphorylation buffer with or without YOP phosphatase as indicated. The specifically bound fractions were Western analyzed with indicated antibodies. **B**. 293T cells transiently expressed the indicated FRS2α and FGFR1 constructs were lysed with or without FGF-2 stimulation. The cell lysates were then incubated with Ni- or heparin-beads as indicated. Specifically bound fractions were Western analyzed with the antibodies as indicated. R1βa1, FGFR1βa1 isoform; R1KN, kinase-inactive mutant of FGFR1βa1; PTBα, PTB domain of FRS2α; pFGFR, phosphorylated FGFR1; pFRS2α, phosphorylated FRS2α; R1, anti-FGFR1 antibody; His, anti-His-tag antibody; pTyr, anti-phosphotyrosine antibody; PD, pull-down; WB, Western blot.

Fig. 2. The candidate tyrosine phosphorylation sites were not essential for FRS2α to interact with FGFR1. Sf9 cells expressed FRS2α mutants and FGFR1 were pulled down with Ni-beads, or heparin-beads as indicated. The specifically bound fractions were Western analyzed with the indicated antibodies. R1βa1, FGFR1βa1 isoform; pFGFR, phosphorylated FGFR1; pFRS2α, phosphorylated FRS2α; R1, anti-FGFR1 antibody; His, anti-His-tag antibody; pTyr, anti-phosphotyrosine antibody; 196F, FRS2αY196F; 306F, FRS2αY306F; 349F, FRS2αY349F; 392F, FRS2αY392F; 436F, FRS2αY436F; 471F, FRS2αY471F; 6F, FRS2α mutant with substitutions of all 6 tyrosine phosphorylation sites with phenylalanine; None, FGFR1 only; PD, pull-down; WB, Western blot.

Fig. 3. Receptor tyrosine autophosphorylation enhanced the interaction of FGFR1 with full-length FRS2α but not the PTB domain. Sf9 cells expressed full-length FRS2α (**A**) or PTB (**B**) and indicated FGFR1 mutants were pulled down with Nickel- or heparin-beads as specified, and Western analyzed with the indicated antibodies. R1βa1, FGFR1βa1 isoform; R1βb1, FGFR1βb1 isoform; R1KN, kinase-inactive mutant of FGFR1βa1; R1Y463F, FGFR1463F; R1Y653/4F, FGFR1Y653/654F; R1Y730, FGFR1Y730F; R1Y766F, FGFR1Y766F; None, FRS2α/PTBα only; pFGFR, phosphorylated FGFR1; pFRS2α, phosphorylated FRS2α; R1, anti-FGFR1 antibody; His, anti-His-tag antibody; pTyr, anti-phosphotyrosine antibody; PD, pull-down; WB, Western blot.

Fig. 4. Interaction of FRS2β with FGFR1 was independent of FGFR1 kinase activity. Sf9 cells expressed full-length FRS2β (**A**) or PTB (**B**) and indicated FGFR1 were pulled-down with Nickel- or heparin-beads as specified, and Western analyzed with the indicated antibodies. **C.** 293T cells coexpressed full-length or the PTB domain of FRS2β and indicated FGFR1 constructs were pulled-down with Nickel- or heparin-beads with or without FGF-2 stimulation as specified, and Western analyzed with the indicated antibodies. R1βa1, FGFR1βa1 isoform; R1N, kinase-inactive mutant of FGFR1βa1; PTBβ, PTB domain of FRS2β; pFGFR, phosphorylated FGFR1; pFRS2β, phosphorylated FRS2β; R1, anti-FGFR1 antibody; His, anti-His-tag antibody; pTyr, anti-phosphotyrosine antibody; His, His-tag; PD, pull-down; WB, Western blot.

Fig. 5. Dominant negative activity of the PTB domain. A. NIH 3T3 cells transfected with the indicated FRS2α mutants were treated with FGF2 for 10 minutes whereas indicated before lysed with the RIPA buffer. The cell lysates were Western analyzed with the indicated antibodies. Bottom panel, the same cell lysates were incubated with Suc13-beads, and the specifically bound fractions were Western analyzed with the anti-phosphotyrosine antibody. **B**. NIH 3T3 cells cotransfected with the indicated FRS2α mutants and the FiRE-luciferase reporter plasmids were stimulated with FGF2 overnight where indicated. The cells were then lysed and the luciferase activity was measured. Data were means of triplicate experiments. **C**. Expression of FRS2α mutants. Cells from the same transfected experiment as in A were lysed. The expressed FRS2α mutants were enriched with Ni-beads and Western analyzed with the anti-His tag antibody. His, anti-His-tag antibody; Erk, anti-Erk antibody; pErk, anti-phosphorylated Erk; pFRS2α, anti-phosphoFRS2α antibody; pTyr, anti-phosphotyrosine antibody; PTB, PTB domain of FRS2α; 6F, FRS2α mutant with substitutions of all 6 phosphorylation sites with phenylalanine residues; None, vector only; PD, pull-down; WB, Western blot.

Fig. 6. The Grb2-recruiting sites on FRS2α were essential for mediating FGF2 signals to activate the FiRE transcription enhancer. A. *Frs2α*$^{flox/flox}$ MEF cells cotransfected with PCMV-Cre and FiRE-luciferase reporter plasmids were stimulated with FGF2 overnight, and the luciferase activity was analyzed. The data were means of triplicate samples. **B**. The same transfected MEF were lysed. The FRS2α recombinant proteins were immobilized on Ni-beads and Western analyzed with the anti-his tag antibody. **C**. Expression of the 4F, but not 2F, mutant significantly inhibited activation of FiRE by FGF2 in 3T3 cells. 3T3 cells were cotransfected with

the indicated FRS2 mutants and the FiRE reporter, and the FGF2 induced expression of the FiRE reporter was determined as described in Material and methods. **D**. Expression of 2F and 4F in 3T3 cells. The same cells as in **C** were lysed and the expression of the FRS2α mutants was checked by Western blot. 196F, FRS2αY196F; 306F, FRS2αY306F; 349F, FRS2αY349F; 392F, FRS2αY392F; 436F, FRS2αY436F; 471F, FRS2αY471F; 2F, FRS2α mutant with substitutions of the 2 Shp2-binding tyrosine with phenylalanine; 4F, FRS2α mutant with substitution of the 4 Grb2-binding tyrosine with phenylalanine; 6F, FRS2α mutant with substitutions of all 6 phosphorylation sites with phenylalanine; None, pCDNA-zeo-3.1(+) vector only.

Supplemental Fig. 1. The PTB domain was required for FRS2α to associate with the FGFR1 tyrosine kinase. A. Schematic of FRS2α mutants. Oval, the conserved myristylation sequence; open box, the PTB domain; hatched box, the C-terminal sequence; triangles, the hexahistidine tag; arrows, the candidate tyrosine phosphorylation sites of FRS2α, the position of the candidate sites are labeled. **B & C**. Association of FRS2α with FGFR1 required the PTB domain. The lysates of Sf9 cells (equivalent to $3X10^6$ cells) infected with baculoviruses bearing coding sequences for the indicated FRS2α mutants and FGFR1 kinase were incubated with Nickel- (**B**) or heparin-agarose (**C**) beads as described. After being washed with the washing buffer for four times, specifically bound fractions were analyzed by Western blot with the indicated antibodies. WB, Western blot; Anti-R1, anti-FGFR1 antibody; Anti-pTyr, anti-phosphotyrosine antibody; Anti-His, anti-His tag antibody; R1βa1, FGFR1βa1 isoform; PD, pull-down; pFGFR, phosphorylated FGFR1; pFRS2α, phosphorylated FRS2α.

Supplemental Fig. 2. Generation of *FRS2α*$^{-/-}$ MEF cells. A. *Frs2α*$^{flox/flox}$ MEF cells were cotransfected with PCMV-Cre and FiRE-luciferase reporter plasmids for the indicated time in the presence and absence of 2 ng/ml FGF2. The cells were then lysed and the luciferase activity was analyzed. The data were means of triplicate samples. **B**. PCR analyses of the conditional null alleles. MEF cells carrying the indicated *Frs2α* alleles were transfected with the pCMV-Cre for 48 hours as in **A.** Genomic DNA was extracted for PCR genotyping as described [Lin et al., 2006]. The bands representing the disrupted FRS2α alleles were shown. w/w, homozygous wildtype *Frs2α* alleles; w/f, heterozygous *Frs2α*^{flox} allele; f/f, homozygous *Frs2α*^{flox} alleles.

Supplemental Fig. 3. The FGFR1/FRS2 interaction was independent of the alternatively spliced VT motif. 293T cells transiently coexpressed the indicated FRS2 and FGFR1βα1 constructs were lysed with or without exposure to FGF2 for 10mins. The lysates were Western blotted with indicated antibody .βb1, FGFR1βb1 isoform; None, FGFR1βb1 only; pFGFR, phosphorylated FGFR1; pFRS2β, phosphorylated FRS2β; R1, anti-FGFR1 antibody; His, anti-His-tag antibody; pTyr, anti-phosphotyrosine antibody; His, anti-His tag antibody; PD, pull-down; WB, Western blot.

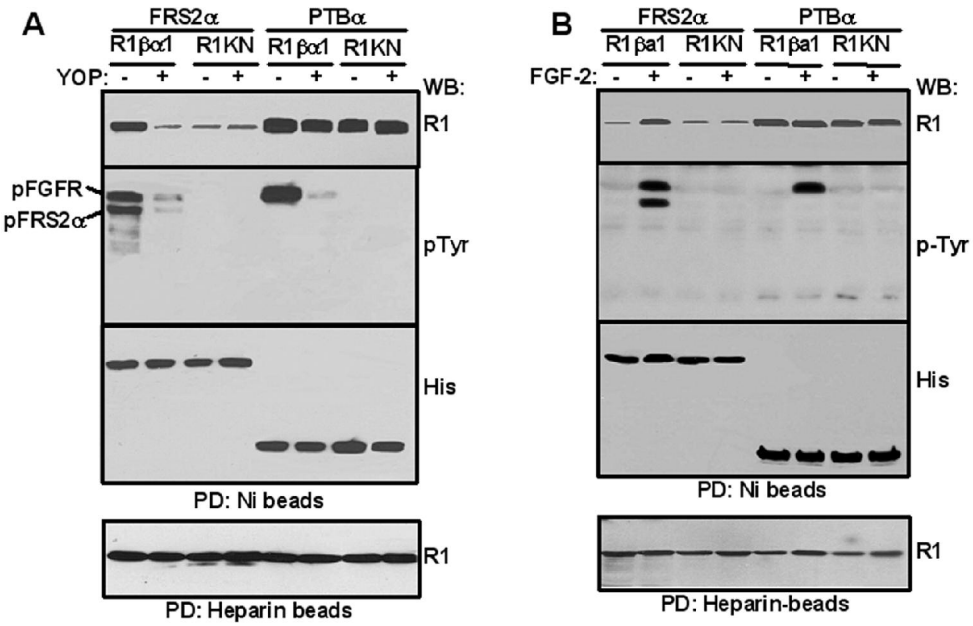
A
FRS2α
PTBα
R1βα1
R1KN
R1βα1
R1KN
YOP: - + - + - + - +
WB:
R1
pFGFR
pFRS2α
pTyr
His
PD: Ni beads
R1
PD: Heparin beads
B
FRS2α
PTBα
R1βa1
R1KN
R1βa1
R1KN
FGF-2: - + - + - + - +
WB:
R1
p-Tyr
His
PD: Ni beads
R1
PD: Heparin-beads

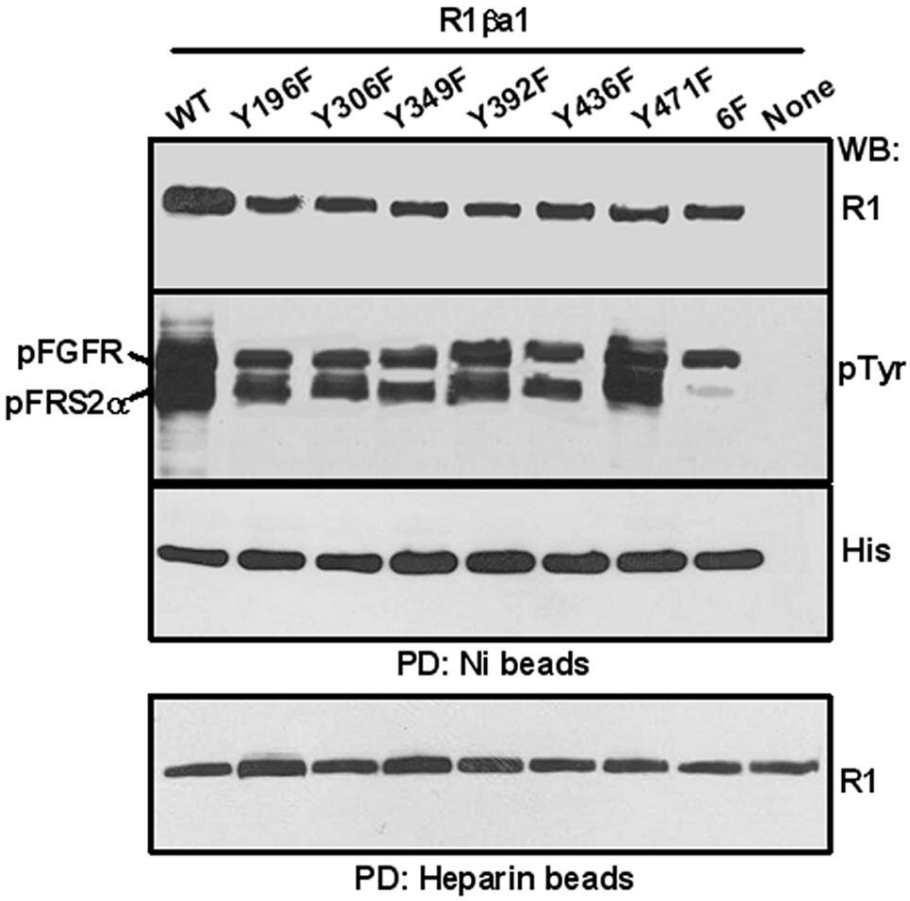
R1βa1
WT
Y196F
Y306F
Y349F
Y392F
Y436F
Y471F
6F
None
WB:
R1
pFGFR
pFRS2α
pTyr
His
PD: Ni beads
R1
PD: Heparin beads

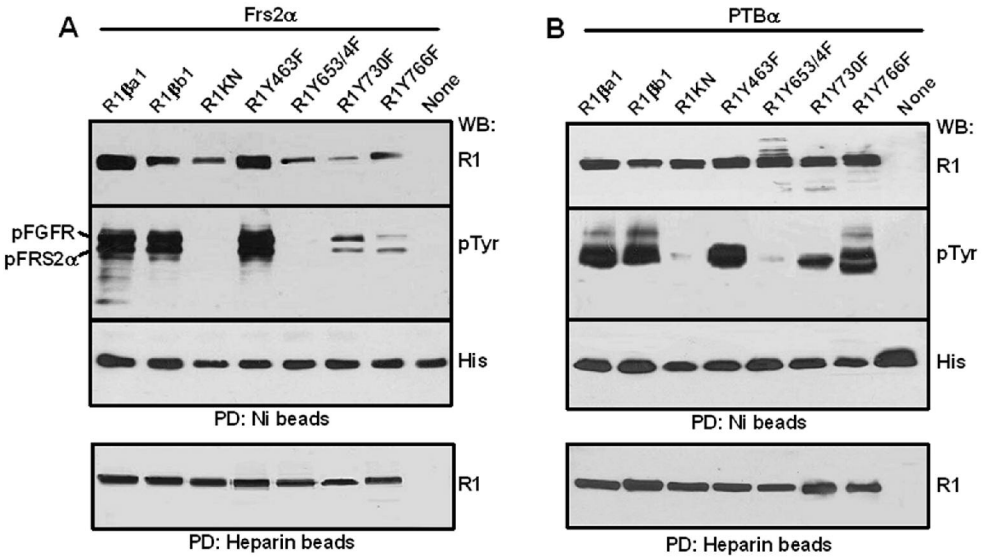
A
Frs2α
R1βa1
R1βb1
R1KN
R1Y463F
R1Y653/4F
R1Y730F
R1Y766F
None
WB:
R1
pFGFR
pFRS2α
pTyr
His
PD: Ni beads
R1
PD: Heparin beads
B
PTBα
R1βa1
R1βb1
R1KN
R1Y463F
R1Y653/4F
R1Y730F
R1Y766F
None
WB:
R1
pTyr
His
PD: Ni beads
R1
PD: Heparin beads

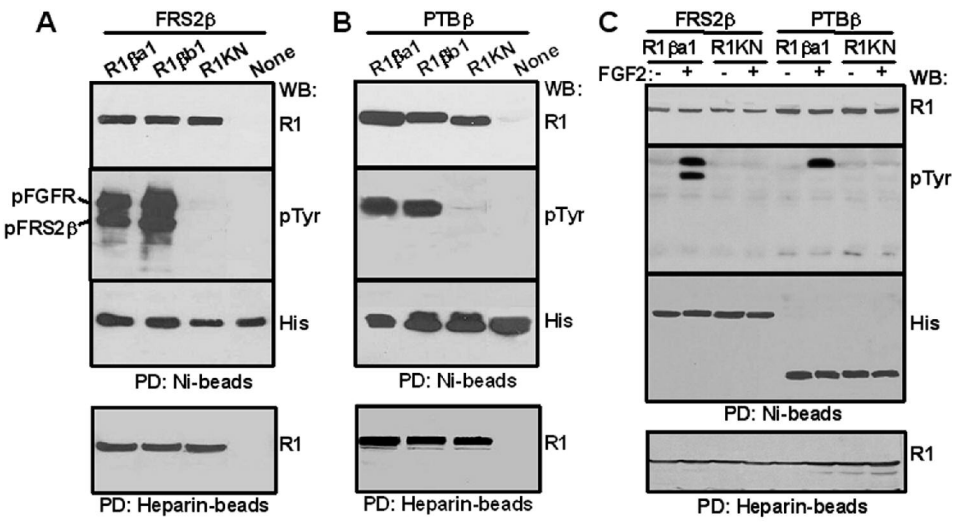
A
FRS2β
R1βa1
R1βb1
R1KN
None
WB:
R1
pFGFR
pFRS2β
pTyr
His
PD: Ni-beads
R1
PD: Heparin-beads
B
PTBβ
R1βa1
R1βb1
R1KN
None
WB:
R1
pTyr
His
PD: Ni-beads
R1
PD: Heparin-beads
C
FRS2β
PTBβ
R1βa1
R1KN
R1βa1
R1KN
FGF2: - + - + - + - +
WB:
R1
pTyr
His
PD: Ni-beads
R1
PD: Heparin-beads

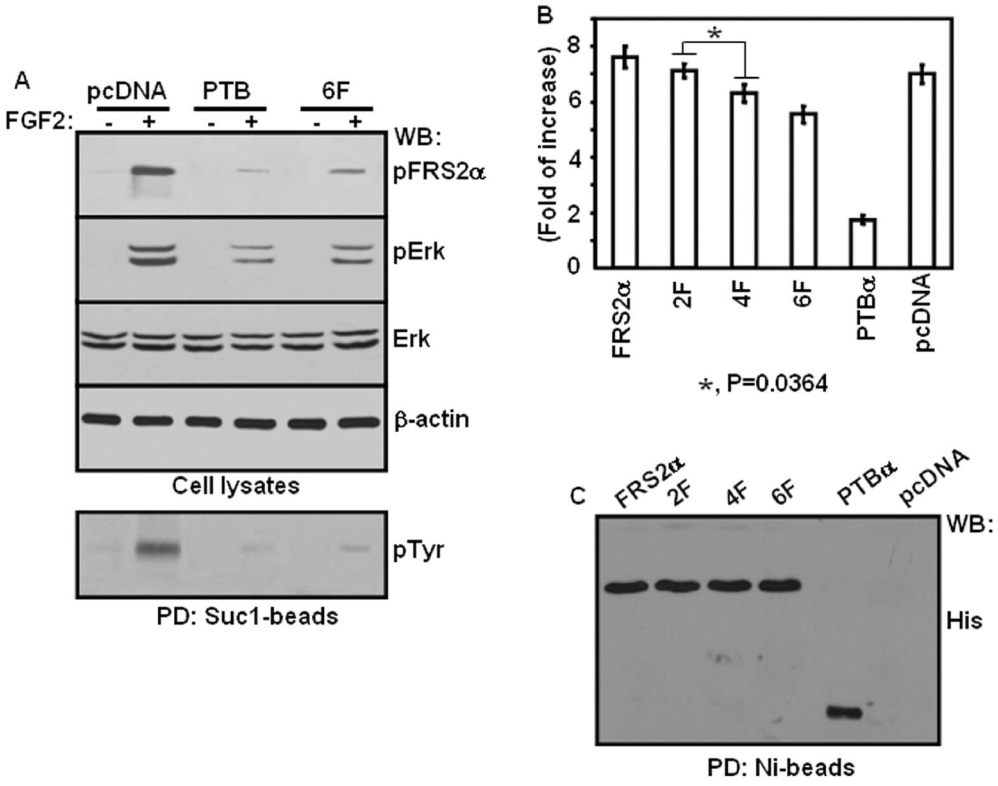
A
pcDNA
PTB
6F
FGF2:
- + - + - +
WB:
pFRS2α
pErk
Erk
β-actin
Cell lysates
pTyr
PD: Suc1-beads
B
(Fold of increase)
0
2
4
6
8
*
FRS2α
2F
4F
6F
PTBα
pcDNA
*, P=0.0364
C
FRS2α
2F
4F
6F
PTBα
pcDNA
WB:
His
PD: Ni-beads

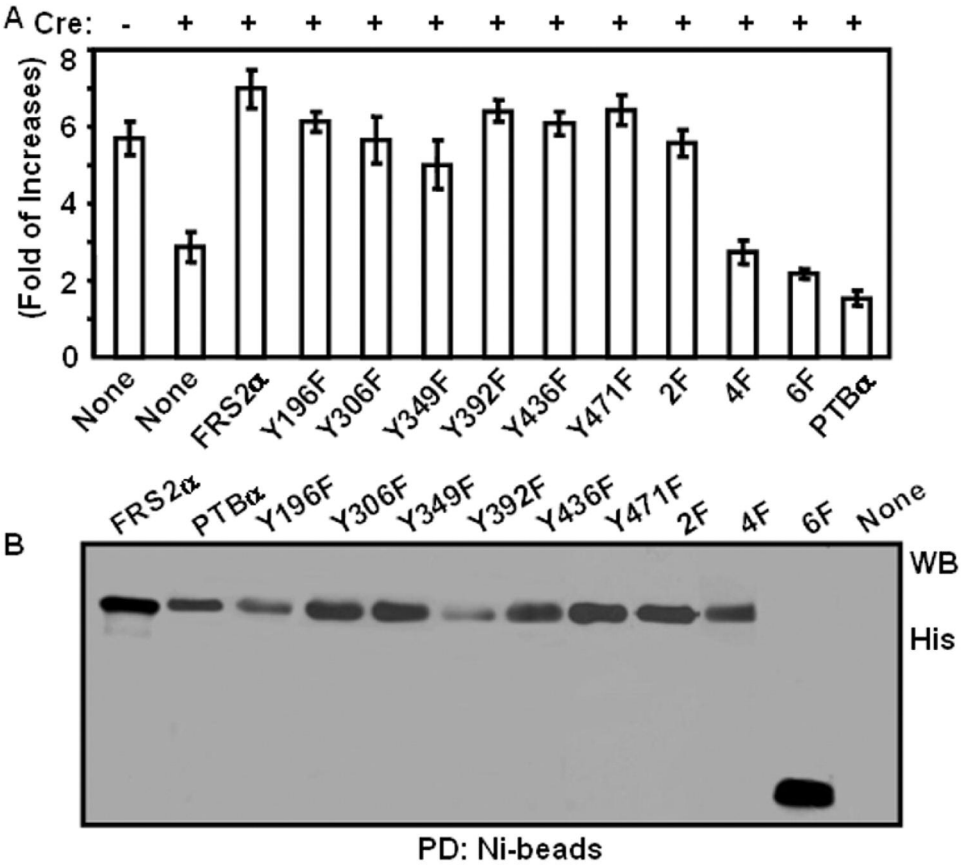
A
Cre: - + + + + + + + + + + + +
(Fold of Increases)
8
6
4
2
0
None
None
FRS2α
Y196F
Y306F
Y349F
Y392F
Y436F
Y471F
2F
4F
6F
PTBα
B
FRS2α
PTBα
Y196F
Y306F
Y349F
Y392F
Y436F
Y471F
2F
4F
6F
None
WB
His
PD: Ni-beads

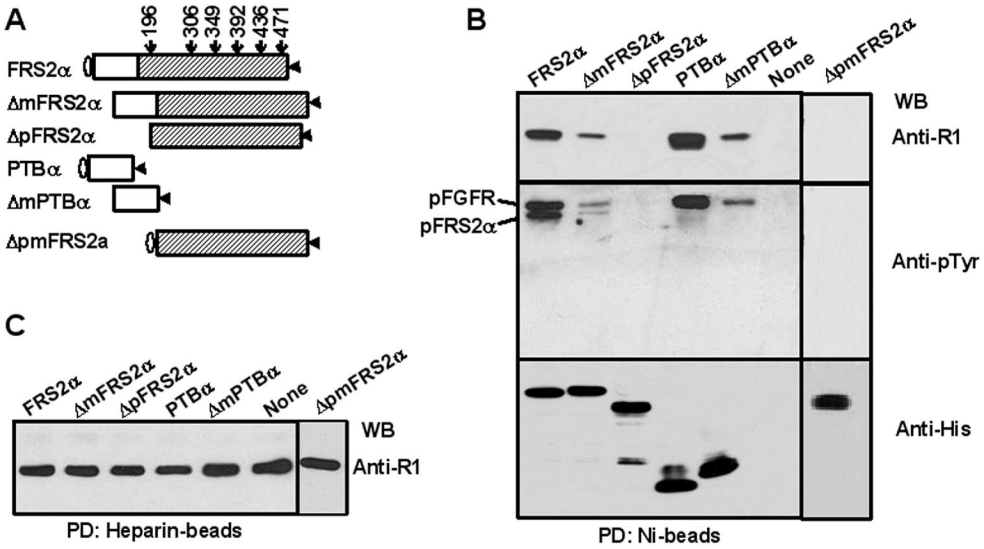
A
196
306
349
392
436
471
FRS2α
ΔmFRS2α
ΔpFRS2α
PTBα
ΔmPTBα
ΔpmFRS2a
B
FRS2α
ΔmFRS2α
ΔpFRS2α
PTBα
ΔmPTBα
None
ΔpmFRS2α
WB
Anti-R1
pFGFR
pFRS2α
Anti-pTyr
Anti-His
PD: Ni-beads
C
FRS2α
ΔmFRS2α
ΔpFRS2α
PTBα
ΔmPTBα
None
ΔpmFRS2α
WB
Anti-R1
PD: Heparin-beads

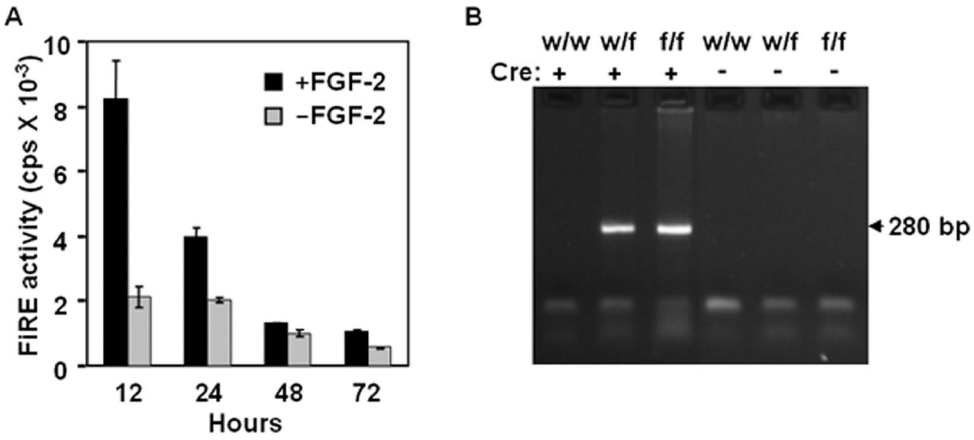

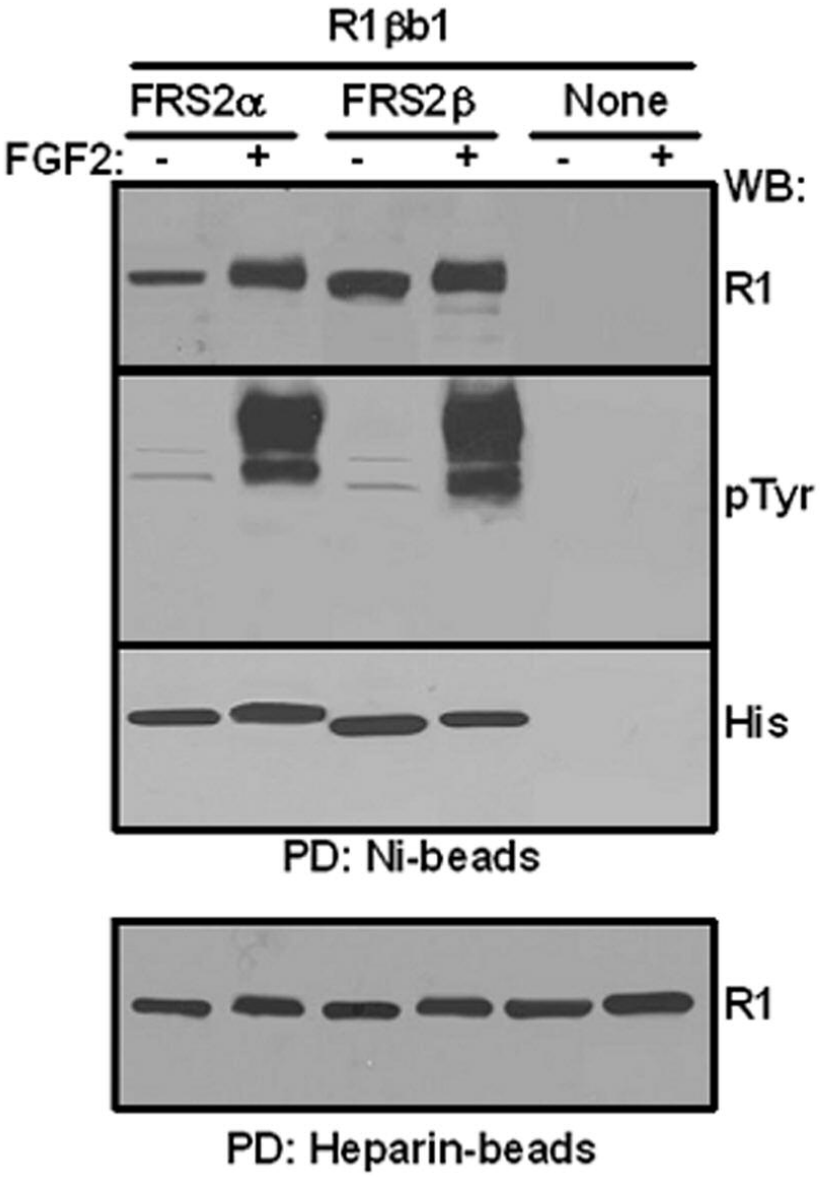
R1βb1
FRS2α
FRS2β
None
FGF2: - + - + - +
WB:
R1
pTyr
His
PD: Ni-beads
R1
PD: Heparin-beads

Generation of an *Frs2α* Conditional Null Allele

Yongshun Lin, Jue Zhang, Yongyou Zhang, and Fen Wang*

Center for Cancer Biology and Nutrition, Institute of Biosciences and Technology, Texas A&M Health Science Center, 2121 W. Holcombe Blvd., Houston, TX 77030-3303

* Corresponding author

Center for Cancer Biology and Nutrition, Institute of Biosciences and Technology, Texas A&M Health Science Center, 2121 W. Holcombe Blvd., Houston, TX 77030-3303

Phone: 713-677-7520

Fax: 713-677-7512

e-mail: fwang@ibt.tmc.edu

Key Words: Fibroblast growth factors, FRS2α, gene targeting, Cre-loxP, prostate

Running title: *Frs2α* conditional null allele

Summary

The fibroblast growth factor (FGF) signaling family controls a broad spectrum of cellular processes in development and adult tissue homeostasis and function, which is expressed in almost all tissues at all stages. FGF receptor substrate 2 alpha (FRS2α) is an adaptor protein that recruits downstream substrates to the FGF receptor (FGFR) tyrosine kinase. Disruption of *Frs2α* abrogates activation of the mitogen activated protein (MAP) kinase pathway by the FGFR and leads to early embryonic lethality (E7.5). To circumvent the embryonic lethality resulting from disruption of the *Frs2α* gene, which hinders further characterization of the role of FRS2α in adult tissue function and homeostasis, we generated an *Frs2α* conditional null allele for temporal and tissue specific disruption of the *Frs2α* allele. Using gene targeting in mouse embryonic stem (ES) cells, we introduced two loxP sites flanking the largest coding exon, exon 5, in *Frs2α* alleles. Our results indicated that the *Frs2α* conditional null allele was a true conditional null that encoded wildtype activity and reverted to a null allele after Cre recombinase mediated recombination.

The FGF family regulates many cellular functions, including cell growth, differentiation, and apoptosis by activating the FGFR transmembrane tyrosine kinases (McKeehan *et al.*, 1998; Wang and McKeehan, 2003), which tyrosine phosphorylate multiple downstream signaling molecules. These downstream molecules bind to the FGFR kinase directly or indirectly through adaptor proteins, including FRS2α, which is one of the major proteins that undergoes intensive phosphorylation in response to FGF treatments (Kouhara *et al.*, 1997). FRS2α is widely expressed in mouse embryos as early as E7, and almost ubiquitously in adult and fetal tissues, including bone marrow, brain, gallbladder, heart, intestine, kidney, liver, lung, skin, spleen, skeletal muscle, stomach, testis, and uterus (McDougall *et al.*, 2001). Disruption of the *Frs2α* gene abrogates the FGF-induced activation of the MAP kinase and phosphatidylinositol-3 (PI-3) kinase, chemotactic response, and cell proliferation, and causes severe impairment in mouse development resulting in embryonic lethality at E7-E7.5 (Hadari *et al.*, 2001). FRS2α has four Grb2 binding sites and two Shp2 binding sites. Mice carrying mutation sites in the Shp2 binding sites exhibit a variety of developmental defects in many organs, including eye, branchial arch, limb and heart (Gotoh *et al.*, 2004a). Although about 20% of mice carrying mutations in the Grab2 binding sites die postnatal day1, most of the mutant mice survive and do not show obvious morphological defects (Gotoh *et al.*, 2004b).

In adult prostate epithelial cells, phosphorylation of FRS2α by the FGFR1 kinase is closely associated with the mitogenic activity and tumorigenicity of the ectopic FGFR1 kinase (Wang, 2002; Wang *et al.*, 2002). Together with data that each FGFR isoform

elicits distinct regulatory function in many experimental systems as well as that the regulatory function of the FGFR kinase is cell context related, it is suggested that FRS2α may play an important role in receptor specific regulatory activity of FGFR kinases and may be important for adult tissue homeostasis and tumorigenesis. The *Frs2α* null mutant mice die at early embryonic stages, which prevents generation of a mouse model to study the role of FRS2α in prostate development and the cellular and molecular mechanisms how FRS2α mediates FGF signals in regulating tissue homoeostasis and function of the prostate as well as in other tissues. To address these questions, we generated an *Frs2α* condition null allele, the $Frs2\alpha^{flox/neo}$ allele.

The mouse *Frs2α* locus contains five coding exons and four introns as well as five non-coding exons preceding the 5' end of the *Frs2α* coding exons (Zhou *et al.*, 2003). The full length *Frs2α* transcript is 5.7 kb that encodes a deduced protein of 509 amino acid residues in length. The first coding exon encodes 22 amino acids at the N-terminus. The second exon encodes 62 amino acids; the third exon encodes 53 amino acids, and the fourth exon encodes 55 amino acids. The last exon (exon 5) is the largest exon that consists of a 951 base pair coding sequence for the 317 amino acids at the C-terminal and a 3801-base pair non-coding region at the 3'-end. To construct the $Frs2\alpha^{floxneo}$ allele, we built a targeting vector that contained two LoxP sites flanking the entire coding region of exon 5 and 600 base pairs of non-coding region immediately downstream of the translational termination codon. Deletion of this exon would be predicted to result in a null allele.

First, we PCR amplified the genomic DNA fragments as indicated in Fig. 1 with the High Fidelity PCR Plus System (Roche Allied Science, Indianapolis, IN). The entire sequence of these fragments was verified. Only the fragments without mutations were used for construction of the *Frs2*$\alpha^{flox/neo}$ targeting vector. We then introduced a 5' LoxP site to 305 base pairs upstream of exon 5, and a 3' LoxP site to 600 base pairs downstream of the translational termination codon in exon 5. To facilitate screening for recombinant ES clones, we also introduced a PacI site next to the downstream LoxP site (Fig.1A). Next, we introduced a *Phosphoglyceral Kinase Neomycin-resistance* (Pgk-Neo) cassette flanked by two Frt sites to 153 base pairs upstream the 5' LoxP site for positive selection. After electroporation, correctly targeted ES cell clones were identified by Southern hybridization of the EcoR1 digested genomic DNA with the 5' external probe as illustrated in Figure 1. Positive clones were then verified by Southern hybridization of EcoRV single digested (Fig. 1B) and PacI/BglII double digested (Fig. 1C) genomic DNA with the same 5' external probe as indicated. Four positive ES cell clones identified from a total of 768 clones were microinjected to blastocysts harvested from C57/BL6 mice according to standard protocols. The agouti F1 mice were analyzed by Southern blot with the 5' external probes to validate germline transmission of the *Frs2*$\alpha^{flox/neo}$ allele.

To test whether homozygous *Frs2*$\alpha^{flox/neo}$ mice were viable, the F1 mice bearing an *Frs2*$\alpha^{flox/neo}$ allele were intercrossed. All F2 newborn mice were viable, did not exhibit obvious defect, and were fertile in both genders. Genotype ration of WT, homozygous, and heterozygous *Frs2*$\alpha^{flox/neo}$ fitted the Mandel ratio of 1:2:1. The results suggested that the insertion of the 1.8 kb Pgk-Neo cassette in the intronic sequence

between exon 4 and 5, and the insertion of 95 base pairs of targeting vector sequence downstream of the non-coding sequence of exon 5 did not interfere with normal *Frs2α* function. Nevertheless, to minimize the interference of the insertion sequence in the *Frs2α*$^{flox/neo}$ allele, the mice bearing an *Frs2α*$^{flox/neo}$ allele were crossed with *ROSA 26*$^{flp\ recombinase}$ mice that express the Flp recombinase to remove the Frt flanked Pgk-neo cassette (Farley *et al.*, 2000), to remove the Frt flanked Pgk-neo cassette. Southern blot (Fig. 1D) and PCR analyses (Fig. 2B) of tail DNA samples extracted from *Frs2α*$^{flox/neo}$*-ROSA 26*^{flp} mice showed that the Pgk-neo cassette was removed. Intercrosses revealed that the *Frs2α*$^{flox/neo}$ homozygous mice had no discernible phenotype further indicating that insertions of the two LoxP fragments did not interfere with normal *Frs2α* function.

To determine whether the LoxP flanked exon in the *Frs2α*$^{flox/neo}$ could be excised by Cre mediated recombinase to give rise to an *Frs2α*^{null} allele, the male *Frs2α*$^{flox/neo}$ heterozygous mice were crossed with female *Nestin Cre* transgenic mice that express Cre recombinase (Trumpp *et al.*, 1999). Genomic DNAs extracted from kidney of *Frs2α*$^{flox/neo}$*-Nestin Cre* mice were Southern blot analyzed with the 5'-external probe (Fig. 1E). The data showed that the floxed fragment could be deleted. Since Nestin-Cre also mediates germline recombination occationally, PCR analyses were used to select germline transmitted *Frs2α*^{null} alleles. Detailed PCR strategies for genotyping for wildtype *Frs2α* and *Frs2α*^{flox}, *Frs2α*$^{flox/neo}$, and *Frs2α*^{null} mutant alleles were illustrated in Fig. 2. Furthermore, to confirm that deletion of exon 5 abrogated function of FRS2α, heterozygous *Frs2α*^{null} mice were intercrossed. Among 60 newborn pups, 41 carried

heterozygous *Frs2α*^{null} allele, and 19 carried homozygous *Frs2α*^{flox} alleles; no homozygous *Frs2α*^{null} mice were found, suggesting that homozygous *Frs2α*^{null} was embryonic lethal. Furthermore, no homozygous *Frs2α*^{null} embryos were found at E12.5, indicating that the embryos carrying homozygous allele of exon 5 deletion died earlier than E12.5, similar to the deletion of coding exon 1 as reported (Hadari *et al.*, 2001). To further confirm that excision of exon 5 disrupted the activity of FRS2α to mediated FGF signaling, embryonic fibroblasts were isolated from homozygous *Frs2α*^{flox} embryos at 14.5 day post copulation as described in Material and Methods. The activity of FGF2 in stimulating expression of the FiRE (FGF-inducible responsive element from mouse syndecan 1 gene)-luciferase reporter was tested with and without coexpression of the Cre recombinase (Fig. 3). The results showed that activation of the FiRE reporter by FGF2 was diminished where Cre was expressed, indicating that excision of the floxed exon 5 inactivate *Frs2α* alleles, and that the activation signals were mediated by FRS2α.

In summary, here we reported generation of a floxed *Frs2α* allele for condition ablation of FRS2α spatiotemporal specifically during embryonic development and a tissue- or cell type-specific in postnatal stages, which provide a valuable and novel venue for studying the role of the FGF signaling pathway in mice.

Materials and Methods

Generation of the *Frs2*$\alpha^{flox/neo}$ allele. *Frs2*α genomic DNA fragments were PCR amplified from genomic DNA purified from AK7 mouse ES cells derived from 129/S mouse with high fidelity enzymes from Roche Allie Science. Briefly, the 1.6 kb fragment for the 5' homology recombination arm in the targeting vector was generated by PCR with primer S1 (CACTGTGCCCTTAAACCGATTCTGTGG) and S2 (CTGTGTACTCGAGGCTAGCATCAAACTAGA). The 1.9 kb floxed fragment was PCR amplified with primer S3 (TGATGGTACCCTGGACTACACAGTAAGACC) and S4 (TAAGATGCTATCTAGACACGCCCTTCAGAT). The 4 kb fragment for the 3' homology recombination arm in the targeting vector was generated by ligation of two PCR fragments generated with primer S5 (TAGCATCTTAATTAAAGTTAGGATGGGCTTAGGAGT) and S6 (GTGGCACATAGCTGGGAAATGATGAAC), and S7 (GGGTGTGCACAGCATATAAAATGTACC) and S8 (AATGTATATTAATTAACACAGTATACGTTCACTTTT), respectively. All oligonucleotides were customer ordered from Integrated DNA Technology, Inc. (Coralville, IA). All PCR fragments were fully sequence verified through Lone Star Lab (Houston, TX) before being cloned into the targeting vector. Sequences across the cloning sites were also verified before linearized with Pme1 for electroporation.

Electroporation of ES cells and Generation of Chimeric Mice. The ES cells were transfected with the linearized targeting vector by electroporation and selected in G418 containing medium as described (Lu *et al.*, 1999). The genotypes of selected clones

were analyzed by Southern blot using the 5' external probe with EcoR1 digested DNAs, which was PCR amplified from the ES cells genomic DNA with primer S9 (CCCAGTGTGAATTCGTCTCAGTCT) and S10 (TCTCTGTGGATCCCAGGCCAGCCA) and cloned in pBluescript SK vector. The positive clones were verified by Southern blot using the same 5' external probe with EcoRV and PacI and Bgl II digested DNA, as illustrated in Fig. 1. Four out of 768 clones were targeted and were microinjected into blastocysts derived from C57BL/6 mice. The chimeric males were bred to C57BL/6 females, and F1 agouti offspring were analyzed by Southern blot for the presence of *Frs2*$\alpha^{flox/neo}$ allele.

Genotyping Analysis. Genotypes of the mice bearing the *Frs2*α^{flox}, *Frs2*$\alpha^{flox/neo}$, *Frs2*α^{null}, and wildtype *Frs2*α allele were determined by Southern blot with the 5' external probe as well as with PCR analyses as illustrated in Figure 1-3. The primer sequences are P1 (GAGTGTGCTGTGATTGGAAGGCAG), P2 (GGCACGAGTGTCTGCAGACACATG), P3 (CGTGGTCAGCTGACTTCCTGATGG), P4 (GATACTGGTCATGTCAATTCATTC), and P5 (TGCTCGCTCGATGCGATGTTT). Primer Flp1 and Flp2 were used for detecting the FLp transgene (Lin *et al.*, 2006), and pcre1 and pcre2 were used for detecting the Cre transgene as described (Jin *et al.*, 2003).

Establishing mouse embryonic fibroblast (MEF) cultures and the FiRE assay. Mouse embryonic fibroblast (MEF) cells were prepared from E14.5 embryos carrying homozygous LoxP-flanked *Frs2*α (*Frs2*α^{flox}) alleles. The cells were cotransfected with the pCMV-Cre plasmid to excise the LoxP flanked FRS2α sequences, the FiRE reporter with Lipofectamine-Plus reagents (Invitrogen, Carlsbad, CA) according to

manufacturer's suggestions. Disruption of the *Frs2*α^{flox} alleles was evaluated with the FiRE-luciferase reporter analyses (Wang *et al.*, 2002).

We thank Dr. James F. Martin for reagents and support, and Dr. Wallace L. McKeehan and Mary L. Cole for critical reading of the manuscript. The work was supported by Public Health Service Grants DAMD17-03-0014 from the U.S. Department of Defense, CA96824 and CA84296 from the National Cancer Institute, and ES09106-07 from the National Institute of Environmental Health Sciences.

References

Farley FW, Soriano P, Steffen LS, Dymecki SM. 2000. Widespread recombinase expression using FLPeR (flipper) mice. Genesis 28:106-110.

Gotoh N, Ito M, Yamamoto S, Yoshino I, Song N, Wang Y, Lax I, Schlessinger J, Shibuya M, Lang RA. 2004a. Tyrosine phosphorylation sites on FRS2alpha responsible for Shp2 recruitment are critical for induction of lens and retina. Proc Natl Acad Sci U S A 101:17144-17149.

Gotoh N, Laks S, Nakashima M, Lax I, Schlessinger J. 2004b. FRS2 family docking proteins with overlapping roles in activation of MAP kinase have distinct spatial-temporal patterns of expression of their transcripts. FEBS Lett 564:14-18.

Hadari YR, Gotoh N, Kouhara H, Lax I, Schlessinger J. 2001. Critical role for the docking-protein FRS2 alpha in FGF receptor-mediated signal transduction pathways. Proc Natl Acad Sci U S A 98:8578-8583.

Jin C, McKeehan K, Wang F. 2003. Transgenic mouse with high Cre recombinase activity in all prostate lobes, seminal vesicle, and ductus deferens. Prostate 57:160-164.

Kouhara H, Hadari YR, Spivak-Kroizman T, Schilling J, Bar-Sagi D, Lax I, Schlessinger J. 1997. A lipid-anchored Grb2-binding protein that links FGF-receptor activation to the Ras/MAPK signaling pathway. Cell 89:693-702.

Lin Y, Liu G, Wang F. 2006. Generation of an Fgf9 conditional null allele. Genesis 44:150-154.

Lu MF, Cheng HT, Kern MJ, Potter SS, Tran B, Diekwisch TG, Martin JF. 1999. prx-1 functions cooperatively with another paired-related homeobox gene, prx-2, to

maintain cell fates within the craniofacial mesenchyme. Development 126:495-504.

McDougall K, Kubu C, Verdi JM, Meakin SO. 2001. Developmental expression patterns of the signaling adapters FRS-2 and FRS-3 during early embryogenesis. Mech Dev 103:145-148.

McKeehan WL, Wang F, Kan M. 1998. The heparan sulfate-fibroblast growth factor family: diversity of structure and function. Prog Nucleic Acid Res Mol Biol 59:135-176.

Trumpp A, Depew MJ, Rubenstein JL, Bishop JM, Martin GR. 1999. Cre-mediated gene inactivation demonstrates that FGF8 is required for cell survival and patterning of the first branchial arch. Genes Dev 13:3136-3148.

Wang F. 2002. Cell- and receptor isotype-specific phosphorylation of SNT1 by fibroblast growth factor receptor tyrosine kinases. In Vitro Cell Dev Biol Anim 38:178-183.

Wang F, McKeehan K, Yu C, McKeehan WL. 2002. Fibroblast growth factor receptor 1 phosphotyrosine 766: molecular target for prevention of progression of prostate tumors to malignancy. Cancer Res 62:1898-1903.

Wang F, McKeehan WL. 2003. The fibroblast growth factor (FGF) signaling complex. Handbook of Cell Signaling, 1st ed. New York: Academic/Elsevier Press. 265-270 p.

Zhou L, McDougall K, Kubu CJ, Verdi JM, Meakin SO. 2003. Genomic organization and comparative sequence analysis of the mouse and human FRS2, FRS3 genes. Mol Biol Rep 30:15-25.

Figure Legends.

Fig. 1. Strategy for generating and genotyping the *Frs2α* conditional null allele. A. *Frs2α* genomic structure contains five coding exons, as depicted in boxes. Solid boxes represent coding sequence; empty box represents non coding sequence, and straight lines represent introns. The PCR fragments generated as described in the text were inserted to the targeting vector at the indicated cloning sites, which contained two LoxP sites (>), one Flp (solid triangles) flanked PGK-neo cassette for positive selection, and one MC1-TK for negative selection. **B-E.** The genomic DNA extracted from targeted ES cells (**B,C**) or mouse tails (**D,E**) were digested with EcoR1 or EcoRV (**B, D**), or BglII and Pac1 (**C,E**), as indicated, for hybridization with the 5'-external probe indicated by thick lines in (**A**). The predicted length of Southern fragments was indicated with double arrow lines and the size of the wildtype (WT) and $Frs2\alpha^{flox/neo}$ (flox/neo) bands were labeled. Note that the 9.6 kb band representing the $Frs2\alpha^{flox/neo}$ allele was not eliminated in **E** due to the mosaic expression pattern of Nestin Cre.

Fig. 2. PCR strategies and genotyping for the *Frs2α* alleles. A. Genotyping for excision of the neo cassette. Primers P1 and P2 amplify fragments of 319 bp from the $Frs2\alpha^{flox}$ and 224 bp from the wildtype *Frs2α* alleles. P3 and P4 amplify fragments of 400 bp from the wild type and 589 bp from the $Frs2\alpha^{flox}$ alleles, no amplification from the $Frs2\alpha^{flox/neo}$ allele. **B.** Genotyping for *Frs2α* null alleles. Primer P5 and P2 amplify a fragment of 261 bp from the null allele of *Frs2α*; no amplification for the wildtype and

Frs2α$^{flox/neo}$ alleles. Primer Cre1 and Cre2 amplify a fragment of 767 bp from the Cre transgene (Jin *et al.*, 2003)

Fig. 3. Inactivation of *Frs2α*^{flox} *alleles in* MEF cells. *Frs2α*$^{flox/flox}$ MEF cells were cotransfected with PCMV-Cre and FiRE-luciferase reporter plasmids for 48 hours and cultured in the presence and absence of 2 ng/ml FGF2. The cells were then lysed and the luciferase activity was analyzed as described elsewhere (Wang *et al.*, 2002). The data were means of triplicate samples.

Fig. 1

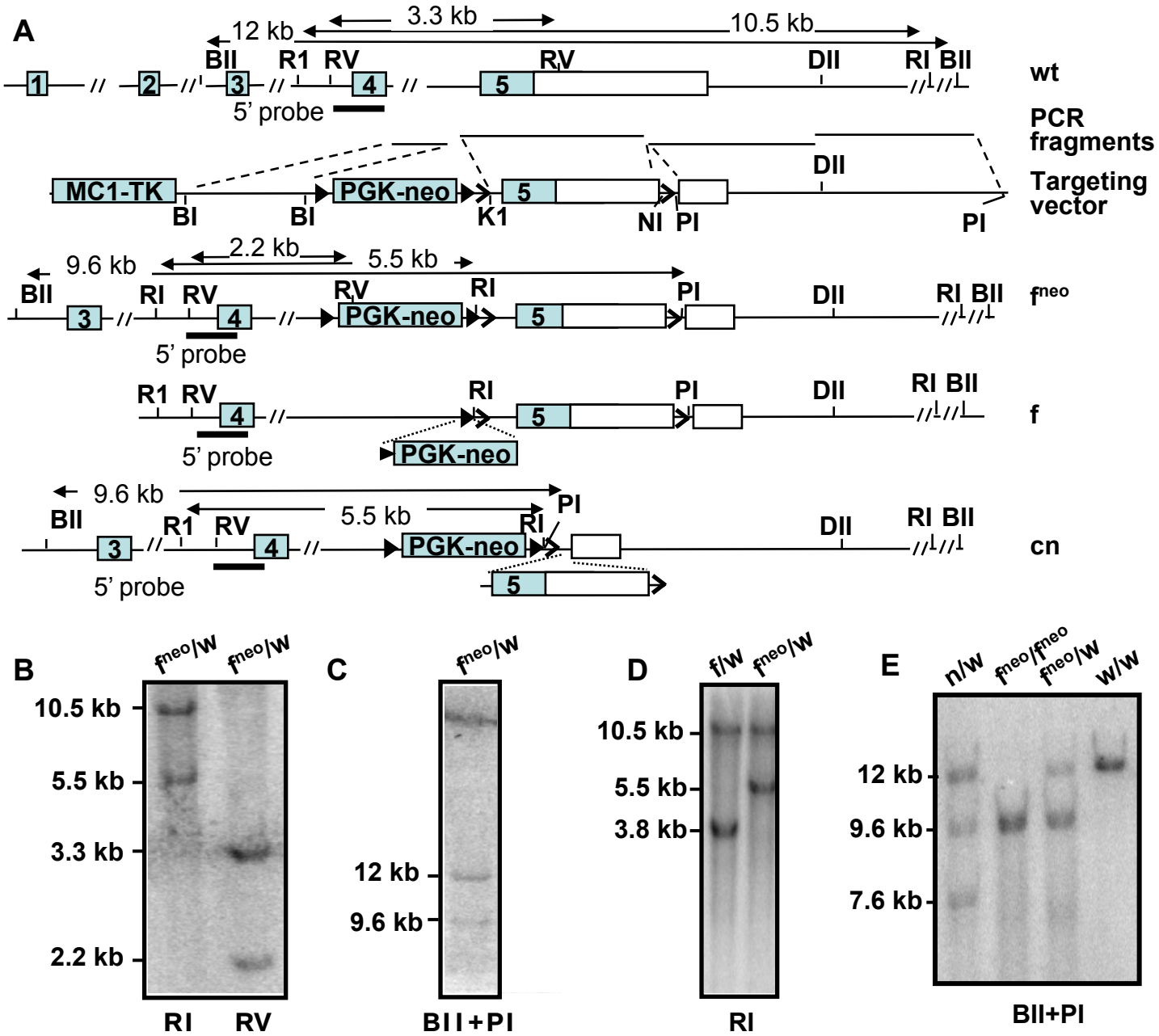
A
12 kb
3.3 kb
10.5 kb
BII
R1
RV
RV
DII
RI
BII
wt
1
2
3
4
5
5' probe
PCR fragments
MC1-TK
PGK-neo
5
DII
Targeting vector
BI
BI
K1
NI
PI
PI
9.6 kb
2.2 kb
5.5 kb
BII
RI
RV
RV
RI
PI
DII
RI
BII
fneo
3
4
PGK-neo
5
5' probe
R1
RV
RI
PI
DII
RI
BII
f
4
5
5' probe
PGK-neo
9.6 kb
5.5 kb
PI
BII
R1
RV
RI
DII
RI
BII
cn
3
4
PGK-neo
5' probe
5
B
fneo/w
fneo/w
10.5 kb
5.5 kb
3.3 kb
2.2 kb
RI
RV
C
fneo/w
12 kb
9.6 kb
BII+PI
D
f/w
fneo/w
10.5 kb
5.5 kb
3.8 kb
RI
E
n/w
fneo/fneo
fneo/w
w/w
12 kb
9.6 kb
7.6 kb
BII+PI

Fig. 2

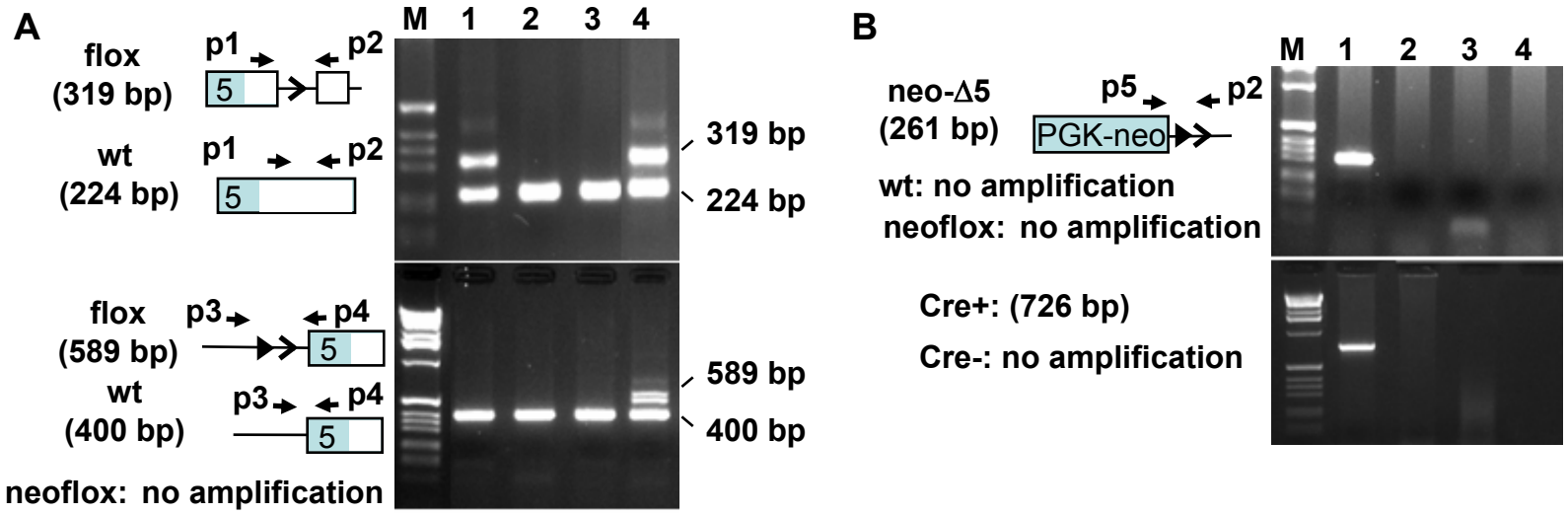
A
flox
(319 bp)
p1
p2
5
wt
(224 bp)
p1
p2
5
M 1 2 3 4
319 bp
224 bp
flox
(589 bp)
p3
p4
5
wt
(400 bp)
p3
p4
5
neoflox: no amplification
589 bp
400 bp
B
neo-Δ5
(261 bp)
p5
p2
PGK-neo
wt: no amplification
neoflox: no amplification
Cre+: (726 bp)
Cre-: no amplification
M 1 2 3 4

Fig. 3

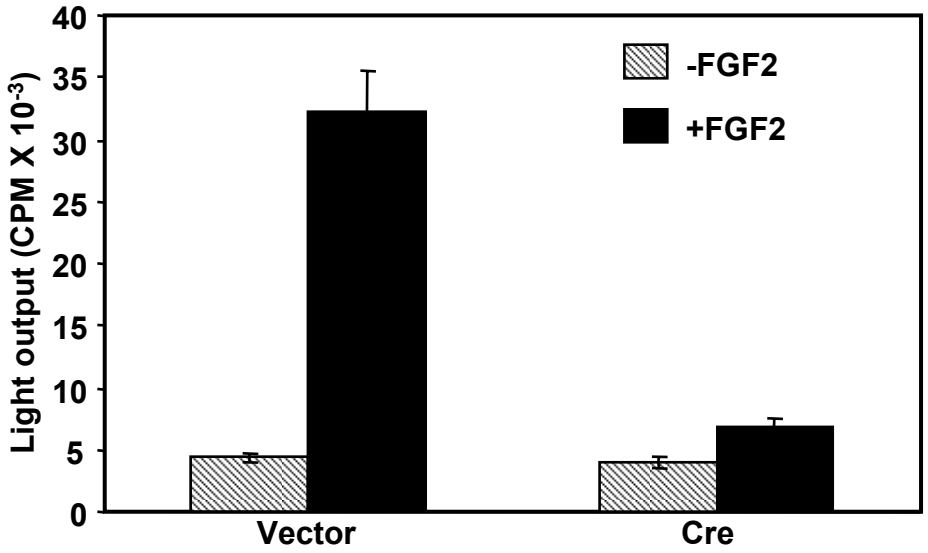
Light output (CPM X 10-3)
40
35
30
25
20
15
10
5
0
-FGF2
+FGF2
Vector
Cre